Chem Soc Rev

# Multicomponent Peptide Assemblies



| | |
|---|---|
| Journal: | *Chemical Society Reviews* |
| Manuscript ID | CS-REV-02-2018-000115.R1 |
| Article Type: | Review Article |
| Date Submitted by the Author: | 21-Mar-2018 |
| Complete List of Authors: | Raymond, Danielle; University of Rochester, Chemistry<br>Nilsson, Bradley; University of Rochester, Chemistry |
| | |

# Multicomponent Peptide Assemblies

*Danielle M. Raymond and Bradley L. Nilsson**

Department of Chemistry, University of Rochester, Rochester, NY, 14627-0216, USA.

E-mail: nilsson@chem.rochester.edu

Fax: +1 585 276-0205; Tel. +1 585 276-3053

**Abstract**

Self-assembled peptide nanostructures have been increasingly exploited as functional materials for applications in biomedicine and energy. The emergent properties of these nanomaterials determine the applications for which they can be exploited. It has recently been appreciated that nanomaterials composed of multicomponent coassembled peptides often display unique emergent properties that have the potential to dramatically expand the functional utility of peptide-based materials. This review presents recent efforts in the development of multicomponent peptide assemblies. The discussion includes multicomponent assemblies derived from short low molecular weight peptides, peptide amphiphiles, coiled coil peptides, collagen, and $\beta$-sheet peptides. The design, structure, emergent properties, and applications for these multicomponent assemblies are presented in order to illustrate the potential of these formulations as sophisticated next-generation bio-inspired materials.

## 1. Introduction

Materials composed of self-assembled peptides and proteins play critical roles in biological function and dysfunction.[1–16] The cytoskeleton and extracellular matrix are composed of dynamic assembled proteins that regulate structure in cells and tissues.[17–20] The abnormal self-assembly of peptides and proteins into amyloid aggregates is characteristic of protein folding disorders,[16,21,22] although the regulated self-assembly of amyloid also gives rise to functional biomaterials.[23–29] These naturally occurring systems have inspired the exploitation of self-assembled peptides and proteins as functional materials, including one- and two-dimensional fibrils and sheets as well as spherical micelles.[30–33] These assembled nano- and microstructures often exhibit emergent properties, such as hydrogelation, that enable these materials to be used for biological applications that include drug delivery,[34–41] regenerative medicine,[42–46] tissue engineering,[47–53] and self-adjuvanting vaccines.[54–60] While the inherent biocompatibility of self-assembled peptides has prompted their development as biomedical materials, recent work has also focused on adapting these materials for applications in energy.[33,61–68]

The inherent emergent properties of self-assembled peptides dictate the potential applications of the materials. For example, one-dimensional fibrils may form entangled hydrogel networks that can be used for drug delivery or tissue engineering if the mechanical properties of the gel are appropriate.[26,69–71] Two-dimensional sheets are unlikely to elicit bulk hydrogelation, but can be engineered for molecular recognition of biological molecules over large surface areas.[72–75] There are now many examples of functional self-assembled peptide materials that have been successfully used in an impressive array of applications. However, the emergent properties of these materials have sometimes limited the potential applications to which they can be applied.[76–78]

It has been found that coassembly of multiple peptidic components can result in supramolecular materials that overcome these limitations in specific instances and enable a broader range of applications for the multicomponent material compared to the self-assembled materials derived from either component.[79–87] Coassembly in these multicomponent supramolecular materials can take several forms. One common form of coassembled peptide material involves the coassembly of a self-assembling peptide with a modified form of the same assembly motif.[56,79,80,88–92] For example, peptides that self-assemble into one-dimensional fibrils have been synthetically modified with biological signal peptides. The modified and unmodified peptide can then be coassembled in varying ratios to provide fibrils that affect multivalent display of the signal peptide at a density that is statistically controlled by the ratio of modified to unmodified peptide. Coassembled systems in which a single self-assembled peptide structure acts as a template for the assembly of a second peptide at the surface of the initial assembly have also been developed.[93–98] In most cases, the multicomponent coassembled systems have enhanced functionality relative to the parent self-assembled structures.

While the same noncovalent interactions govern the formation of single component self-assembled peptide nanostructures and multicomponent coassembled nanostructures,[99–102] the kinetic and thermodynamic parameters that influence these processes are of special interest in the controlled coassembly of multicomponent materials.[102,103] Environmental factors such as temperature,[104,105] pH,[104–106] salt effects,[107–109] and solvent interactions[110–115] have been shown to influence the kinetics and thermodynamics peptide self-assembly in ways that dictate the ultimate supramolecular materials that are formed. When considering coassembly of multiple peptides, the kinetics and thermodynamics of both self-assembly and coassembly of the various components must be accounted for in order to selectively form the desired multicomponent

materials. While dissecting these elements of self- and coassembly pathways is complex, the manipulation of kinetics and thermodynamics can lead to greater hierarchical control over the formation of complex, synthetic biomaterials.

This review will present a discursive overview of efforts to develop multicomponent peptide coassembled materials. It will include peptides of varying secondary and tertiary structures, including $\beta$-sheet fibrils, collagen triple helices, $\alpha$-helical coiled coils, and unstructured peptides. Systems in which the components coassemble in either a statistical manner or in a controlled manner with precise spatial arrangements between the various components will both be examined. The rationale, design, analysis, and application of the various multicomponent coassemblies will be discussed. It is our objective to illustrate the great potential of multicomponent peptide assemblies as sophisticated next-generation materials that are truly greater than the sum of their parts.

## Section 2. $\beta$-Sheet Peptides

$\beta$-Sheet peptides have a high propensity to self-assemble in aqueous solutions and have thus been the focus of intense study as supramolecular materials.[27,116–118] Amyloid aggregates are an example of $\beta$-sheet assemblies that have been of special interest due to their relevance to protein folding disorders.[2,119,120] These materials have inspired the development of engineered $\beta$-sheet aggregates, which tend to be one-dimensional fibrils or nanoribbons that lack functional cytotoxicity and exhibit useful emergent properties that notably include the formation of entangled hydrogel networks.[26,48,117] The abundant research conducted on self-assembled $\beta$-sheet

materials has made them an early target for the development of coassembled multicomponent materials. These materials will be discussed in this section.

### 2.1 Amyloid

Amyloid proteins are of great interest based on their role in protein misfolding diseases including Alzheimer's disease (amyloid-$\beta$ (A$\beta$) and tau), Huntington's disease (huntingtin), Parkinson's disease ($\alpha$-synuclein), type II diabetes (islet amyloid polypeptide (hIAPP)), and others.[2,16,121–123] Each of these disorders is characterized by the presence of $\beta$-sheet-rich aggregates of the relevant proteins. These so-called amyloid aggregates are one-dimensional fibrils with similar peptide packing architecture that consists of $\beta$-sheet structures in which the amide bonds are oriented parallel to the fibril axis, forming an intermolecular hydrogen bond network between the constituent peptides, with the side chain groups oriented perpendicular to the fibril axis.[124,125] This fundamental "cross-$\beta$" packing architecture is preserved among all amyloid aggregates, regardless of sequence similarity. It has also been observed that the formation of non-fibril oligomeric aggregates precedes the appearance of oligomers in most amyloid self-assembly processes; these oligomer species have been hypothesized to be the main toxic congeners in many amyloid disorders.

The Alzheimer's disease amyloid-$\beta$ peptide (A$\beta$) has been the focus of particularly intense study due to the hypothesis that formation of A$\beta$ aggregates is potentially causative to the disorder. Characterization of the mechanism(s) of A$\beta$ self-assembly and the structure of the self-assembled materials has been carried out to gain insight into the relationships between aggregate structure and functional cytotoxicity at the molecular level.[121,126–134] Figure 1 shows two

structures of A$\beta$ fibrils, illustrating that the parallel, cross-$\beta$ packing arrangement can adopt different forms depending on the conditions under which the fibrils are formed.[134–136] A$\beta$ has been the focus of coassembly studies with the primary goal of moderating the formation of toxic aggregates.[137–141] There is a vast body of literature devoted to the development of peptide[142–152] and small molecule agents[153–167] that perturb amyloid aggregation. While many of these studies are technically examples of coassembly, they fall outside the scope of research that will be discussed herein. The coassembly studies discussed herein will instead illustrate examples of peptides, including fragments of A$\beta$, that form unique coassembled structures with the full-length peptide. These coassembled structures are either structurally or functionally distinct from self-assembled A$\beta$ fibrils.

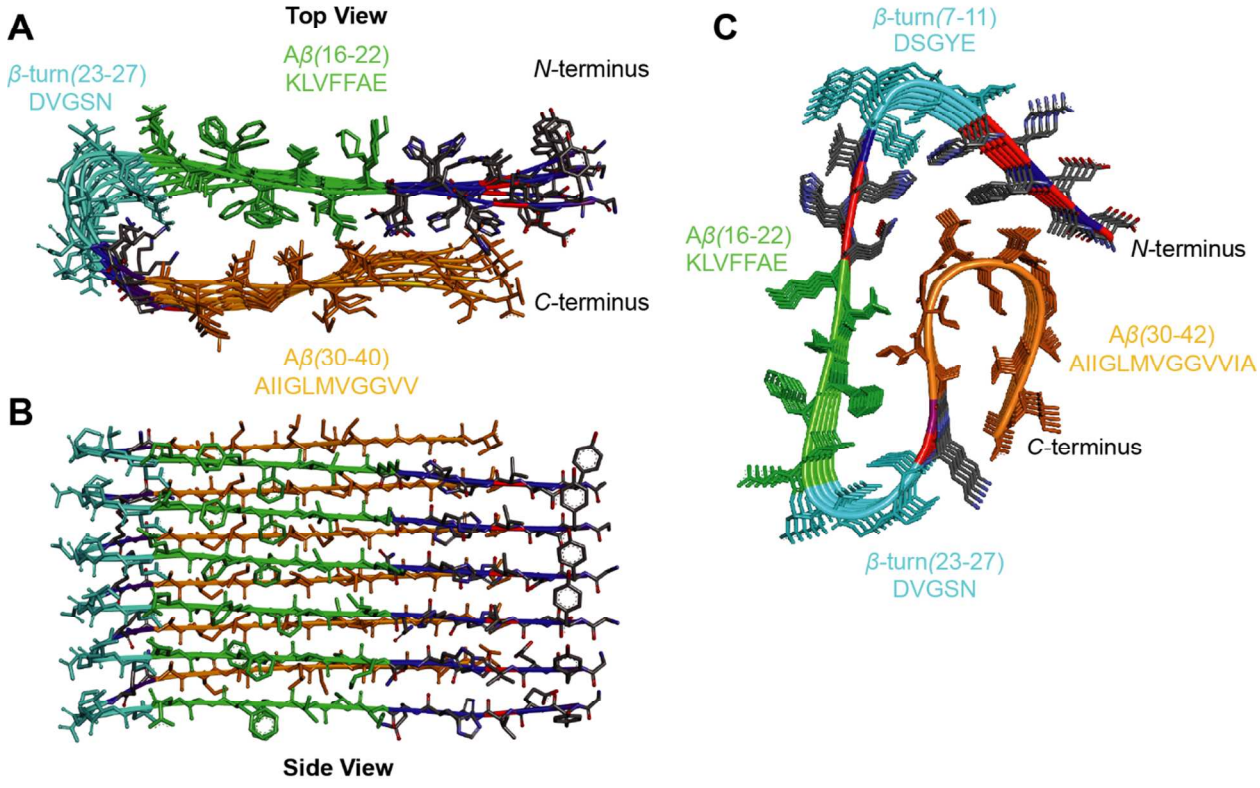


**Figure 1.** Two structural models of A$\beta$40 and A$\beta$42 that illustrate the packing structure of A$\beta$ in the context of protofilaments that are the fundamental constituents of A$\beta$ fibrils. Top (A) and side (B) view

models of the cross-$\beta$ amyloid architecture of A$\beta$40 fibrils indicating $C_{2z}$ symmetry.[130] PDB coordinates were kindly provided by Dr. Robert Tycko. (C) An alternative structural model of A$\beta$42 fibrils determined by cryo-EM analysis showing an in-register, cross-$\beta$ architecture with additional turn motifs.[134]

Barth and coworkers examined the functional consequences of coassembly of A$\beta$40 with A$\beta$42, two common isoforms of the A$\beta$ peptide.[168] A$\beta$42 is found in higher proportions in individuals with Alzheimer's dementia, although both peptides are typically produced and both are able to assemble into aggregate structures that exhibit neurotoxicity,[169] although little was known about the extent of formation of mixed A$\beta$40 and A$\beta$42 multicomponent aggregates. Barth *et al*. interrogated coassembly of these peptides using a site-selective $^{13}$C-carbonyl labeling strategy that enabled isotope edited infrared (IR) spectroscopy to monitor aggregation.[168] They observed that mixtures of these peptides formed pre-fibril oligomer aggregates that were morphologically distinct from those formed by self-assembly of either peptide alone. The coassembled oligomers were composed of $\beta$-sheet aggregates in which A$\beta$40 and A$\beta$42 were interspersed in a nearly random fashion. These coassembly studies strengthened the idea that heterogeneous oligomer formation could be relevant in the onset of Alzheimer's disease.

Several groups have also investigated the coassembly of short A$\beta$ fragment peptides with full length A$\beta$ as a strategy to disrupt natural amyloid self-assembly and mitigate the toxicity of the resulting aggregates.[139,142,170,171] For example, Bitan and coworkers found that two peptides dubbed "*C*-terminal fragments" (CTFs) derived from the *C*-terminus of A$\beta$42 (A$\beta$(31-42) and A$\beta$(39-42)) had a neuroprotective effect toward mouse hippocampal neurons *in vitro* when these peptides were mixed in varying ratios with full length A$\beta$42.[139] Coassembly of the CTFs with

A$\beta$42 had a neuroprotective effect due to the formation of multicomponent hetero-oligomeric structures that lacked the functional cytotoxicity exhibited by self-assembled A$\beta$42 aggregates.

The coassembly of distinct amyloidogenic peptides has also provided insight into the inherent heterogenic nature of natural amyloid systems.[172–175] The precise molecular mechanism of formation of heterogeneous amyloid peptides and their effect on the progression of amyloidogenic diseases is not well understood. Ashcroft and Radford *et al*. investigated the coassembly of hIAPP with A$\beta$40 to this end. Formation of prefibril hetero-oligomeric species was observed in 1:1 mixtures of the two peptides.[172] Amyloid self-assembly is a nucleation dependent process and fibril formation is typically preceded by a concentration-dependent lag phase.[176,177] Under the conditions used in this study the lag phases for A$\beta$40 and hIAPP fibril self-assembly were 9 h and 2 h respectively. A single transition was observed for fibril formation in a 1:1 mixture of the two peptides with a lag phase of 3.5 h and the resulting fibrils contained both A$\beta$40 and hIAPP. A single type of morphologically distinct fibril was generated in the coassembled mixture, although the details of the extent of hIAPP and A$\beta$40 mixing in these fibrils were not determined. These studies provide insight into the role that cross-seeding by disparate amyloid systems can have on the development of amyloid disorders.

The coassembly of amyloid peptides with fluorophore-labeled sequences has been used to visualize the nucleation and elongation processes of amyloid assembly.[96] Lynn and coworkers accomplished this objective using A$\beta$(16-22), a strongly amyloidogenic fragment from the central hydrophobic region of A$\beta$. A$\beta$(16-22) (Ac-KLVFFAE-$NH_2$) was mixed with a rhodamine-labeled variant, Rh-A$\beta$(17-22), in which the lysine residue was replaced with a rhodamine fluorophore (**Figure 2A**). The peptides were mixed at a 250:1 molar ratio of A$\beta$(16-

22): Rh-A$\beta$(17-22). Rh-A$\beta$(17-22) was readily incorporated into the A$\beta$(16-22) fibril assemblies. These fluorescent coassembled structures enabled the use of optical microscopy to directly observe the nucleation and elongation processes. Nucleation occurred by initial hydrophobic collapse of the peptides into an intermolecular molten globule from which fibril structures extended over time. These fibril extensions were elongated by addition of monomeric peptide to the fibril ends at an observed growth rate of 0.15 μm $min^{-1}$. The new growth observed at the ends of preformed mature assemblies was consistent with previous findings and the widely accepted amyloid-seeded model for fibril assembly. This example of the coassembly of a peptide with a fluorophore-modified derivative of the same sequence provides a significant illustration of the power of multicomponent assembly to afford insight into the mechanisms of amyloid aggregation.

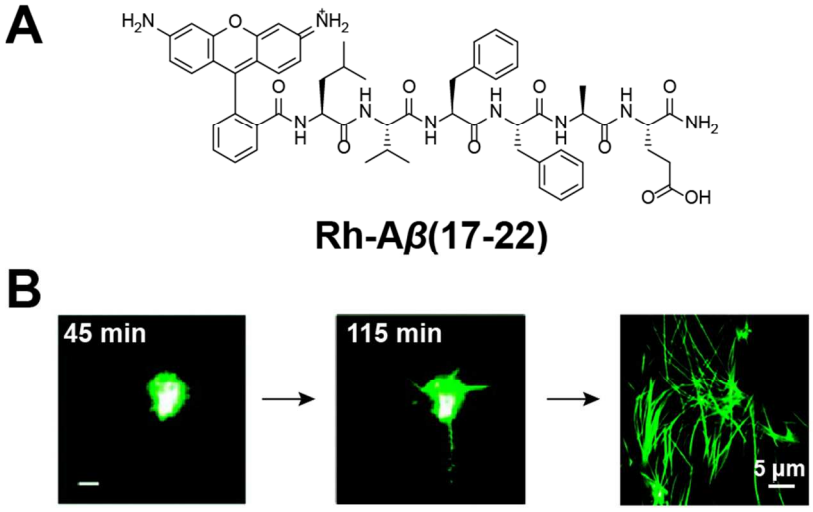


**Figure 2.** (A) Chemical structure of Rh-A$\beta$(17-22). (B) Time lapse fluorescent images of nucleation and growth of A$\beta$(16-22):Rh-A$\beta$(17-22) (0.6 mM:4 μM) over 70 minutes from micelle-like oligomers into one dimensional fibrils. Nanotubes began to form 40 minutes after the peptides were dissolved and disseminated from the center of the initial micellar aggregates. Figure adapted with permission from Y. Liang, D. G. Lynn and K. M. Berland, *J. Am. Chem. Soc.*, 2010, **132**, 6306–6308.[96] © 2010 American Chemical Society.

Nowick and coworkers have utilized macrocylic $\beta$-hairpin peptides to examine coassembled interactions between fragments of A$\beta$ that give insight into how these segments may interact in the context of A$\beta$ assemblies.[174,175] Nowick's macrocyclic $\beta$-hairpin peptides are composed of short hairpin peptides with an unnatural Hao template and δ-linked ornithine turn mimics that close the macrocycle (**Figure 3**). These hairpin mimetics are designed to minimize extended $\beta$-sheet formation by blocking hydrogen bonding to the external face of the template strand while reinforcing hairpin structure by enabling hydrogen bonding within the macrocycle. Hydrogen bonding is also possible on the exterior face of the templated $\beta$-strand peptide. Nowick *et al*. sought to understand possible inter- and intramolecular interactions that may occur during A$\beta$ fibril and oligomer aggregation processes. To this end, they prepared two synthetic macrocyclic $\beta$-hairpin peptides that incorporate fragments of A$\beta$,[178] peptide A (residues 17-23, LVFFAED) and peptide B (residues 30–36, AIIGLMV) (**Figure 3A**).[174,175] In previous work, they observed that each of these peptide macrocycles assembled into stable homotetramers.[174] They subsequently found that mixtures of peptides A and B coassembled into an assortment of multicomponent structures that included each macrocycle in 3:1, 2:2, and 1:3 stoichiometries. The 2:2 heterotetramer was the dominant species observed.[175] NMR analysis revealed that the structure was an $A_2B_2$ tetramer composed of hydrogen-bonded homodimers that laminate face-to-face with the opposite homodimer (**Figure 3B**). This work suggests that the central and *C*-terminal regions of A$\beta$ can self-segregate within $\beta$-sheet hydrogen bond networks and also that these regions of the hydrogen-bonded $\beta$-sheets can further assemble, giving insight into A$\beta$ oligomerization and fibrillization in the biological context.[121,178,179]

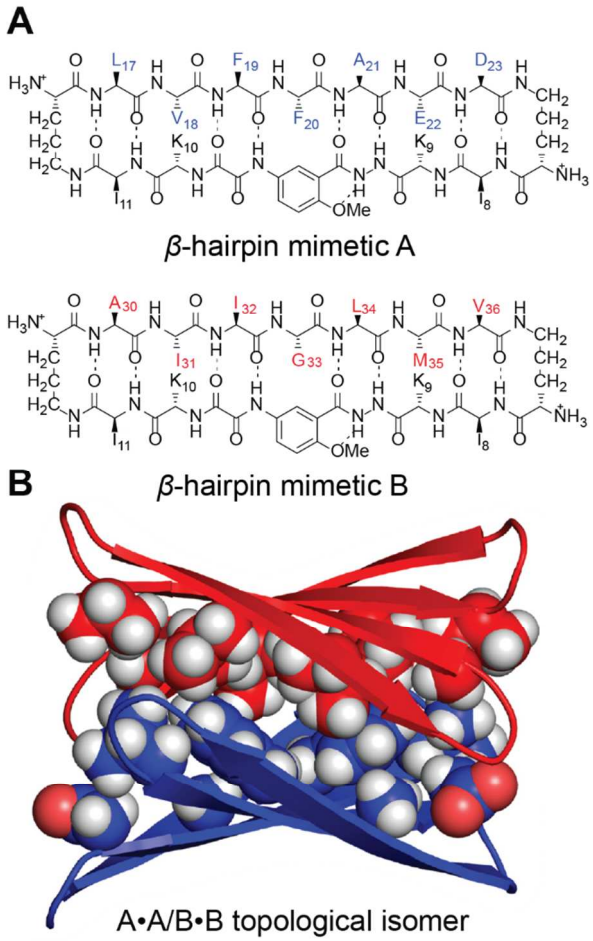


**Figure 3.** (A) Chemical structure of Nowick's macrocyclic *β*-hairpin oligomer mimetics. (B) Energy minimized model of the $A_2B_2$ heterotetramer coassembled structure confirmed by NMR experiments. Figure adapted with permission from N. L. Truex and J. S. Nowick, *J. Am. Chem. Soc.*, 2016, **138**, 13891–13900.[175] © 2016 American Chemical Society.

### 2.2 Amphipathic *β*-Sheet Peptides

*β*-Sheet peptides are among the most widely used self-assembling peptide motifs in synthetic biomaterials.[23,26,27,180,181] Zhang *et al*. pioneered the design of self-assembling amphipathic, ionic complementary peptides with alternating hydrophobic and hydrophilic residues upon discovering the facile self-assembly and hydrogel formation of the EAK16 peptide, which was initially identified in the yeast Zuotin protein (Figure 4).[182,183] It was found that dissolution of EAK16 in water resulted in emergent hydrogelation and that modification of

charge distribution in the sequence resulted in formation of different nanostructures ranging from globular assemblies to long one-dimensional fibrils assemblies using EAK16 varients.[184] Systematic replacement of amino acids in this sequence led to the development of other amphipathic self-assembling peptides that readily self-assemble into fibrils that entangle to form hydrogel networks, including KFE8[185,186] and RADA16,[187,188] Schneider's MAX hairpin peptides,[189–191] Collier's Q11 peptide,[192,193] and others (**Figure 4**).[80,194–198] These self-assembling amphipathic $\beta$-sheet systems have been widely exploited as functional biomaterials for applications ranging from wound-healing to tissue regeneration.[26,36,42,48,63,116,199,200]

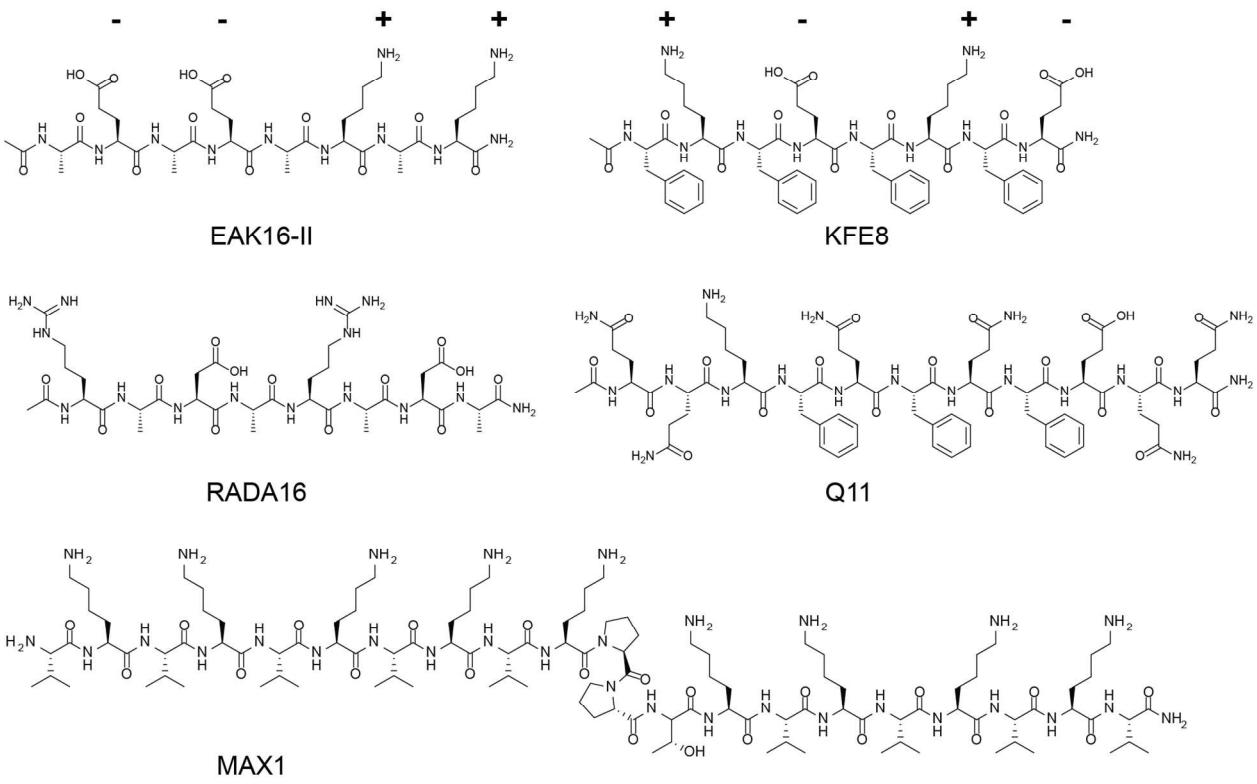


**Figure 4.** Chemical structures of amphipathic $\beta$-sheet peptides: EAK16, KFE8, RADA16, Q11, and MAX1. Alternating charge distribution patterns are shown over the top of alternating hydrophobic/hydrophilic EAK16 and KFE8 peptides.

Amphipathic peptides with alternating hydrophobic and hydrophilic residues are a privileged class of peptide that rapidly self-assemble in aqueous solution.[26,117,187] As illustrated in Figure 5 for the Ac-$(FKFE)_2$-$NH_2$ peptide, these peptides form extended $\beta$-sheets that segregate the hydrophobic side chains and hydrophilic side chains on opposite faces of the sheet, enabling lamination of two sheets into a bilayer architecture that protects hydrophobic functionality from the aqueous environment, leaving the hydrophilic groups exposed to water.[182,185,186] This architecture accounts for the emergent properties of this class of self-assembling peptide that make them appropriate for applications as functional biomaterials.

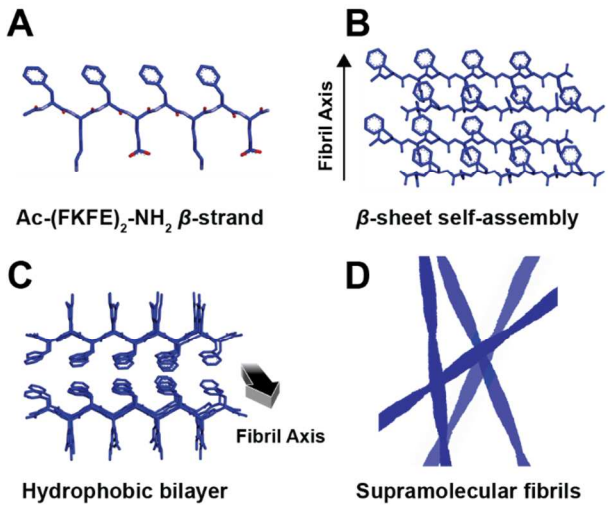


**Figure 5.** (A) Model of the Ac-$(FKFE)_2$-$NH_2$ peptide in an extended $\beta$-strand orientation. (B) $\beta$-strands align in an antiparallel, out-of-register conformation to form $\beta$-sheets. (C) $\beta$-sheets elongate and undergo hydrophobic collapse and bilayer formation between two sheets in aqueous solution. These bilayers segregate the hydrophobic side chains to the bilayer interior and display the hydrophilic side chains on the outer, solvent-exposed surface. (D) Peptide bilayers extend and grow into micrometer long fibers.

Amphipathic peptides with alternating hydrophobic/hydrophilic sequence patterns have been routinely used in multicomponent, coassembled formulations in order to improve compatibility with biological systems.[79,80] Early examples of multicomponent coassembled materials were developed by the statistical mixture of a self-assembling $\beta$-sheet peptide with a functionalized

variant of the assembly motif in which a short peptide or biological molecule was appended to the terminus. Coassembly of the self-assembling peptide with the functionalized peptide in various ratios results in coassembly of the two sequences into fibrils in which the functional sequence is displayed in a multivalent array at the surface of the fibril where it is available for interaction with biological targets.[201–205]

This concept has been illustrated by mixing EAK16-II with functionalized EAK16-II variants to provide multicomponent fibrils for several biological applications.[201–203] The variant peptides were functionalized with sequences that interact with cell surface receptors to provide enhanced biocompatibility. For example, EAK16-II was coassembled with a *C*-terminal hexahistidinylated analogue, EAKIIH6, giving a multicomponent fibril biomaterial in which the hexahistidine ($H_6$) motif is displayed at the fibril surface.[201,203] $H_6$ binds to both Ni and to anti-$H_6$ antibodies, providing a tag for the further functionalization of the $H_6$-bearing fibrils. In initial studies, $H_6$ was verified to be presented on the multicomponent fibrils by showing that a horse radish peroxidase-Ni complex (HRP-Ni) binds selectively to fibrils that have exposed $H_6$.[206] It was then shown that the $H_6$ tag on the multicomponent fibrils could be used to recruit additional proteins for display. Specifically, anti-$H_6$ antibody was incubated with the fibrils, followed by recombinant A/G protein (rpAG), which has multiple sites for binding broadly to all human IgG subclasses. After incubation with rpAG, fluorophore (FITC) labeled IgG was added and it was confirmed by fluorescence imaging that this antibody was confined to the fibril surface. Using this same strategy, anti-CD4 antibodies were also bound to the fibrils and these functionalized fibrils were shown to recruit lymphocytes, both *in vitro* and *in vivo*. These antibody-bearing fibrils were shown to remain biologically active for days.[203]

Multicomponent EAK16-II/EAKIIH6 fibrils were then applied as a mini-thymus complex hydrogel for the anchoring and 3D aggregation of thymic epithelial cells (TECs).[204] The coassembled hydrogels were found to successfully anchor and elicit healthy development of Epcam-expressing TECs through the binding of cells via an adaptor molecule which included anti-His IgG antibodies for binding to the hydrogel matrix displaying $H_6$ as well as rpAG and anti-Epcam IgG antibodies for providing a fibril display that enabled the binding of TECs to the hydrogel matrix. When coassembled hydrogels were implanted into athymic mice, they supported development of functional T-cells *in vivo*. These studies provide an innovative strategy for the multivalent display of functional proteins on multicomponent fibrils for biomedical applications.

The functionalization of RADA16-based hydrogel fibrils by coassembly with modified RADA16 peptides has also been extensively employed to optimize these biomaterials for a range of biological applications.[88,89,207–213] Figure 6 depicts various functionalized RADA16 peptides and their coassembly into a supramolecular fibril structures where the resulting multicomponent RADA $\beta$-sheets display the functional motifs along the fibril in a ratio proportional to the amounts of the various monomers, functionalized and unfunctionalized, used in the coassembly mixture. The functional biological recognition motifs include the integrin-binding RGDS peptide and others derived from various types of collagen,[214,215] laminin,[216] fibrin,[217] fibronectin,[218] and bone marrow homing peptides.[219,220] These coassembled hydrogels have exploited for the attachment and healthy development of cells *in vitro* and *in vivo* by selectively targeting cell surface receptors that promote cell adhesion, proliferation, and other critical processes.

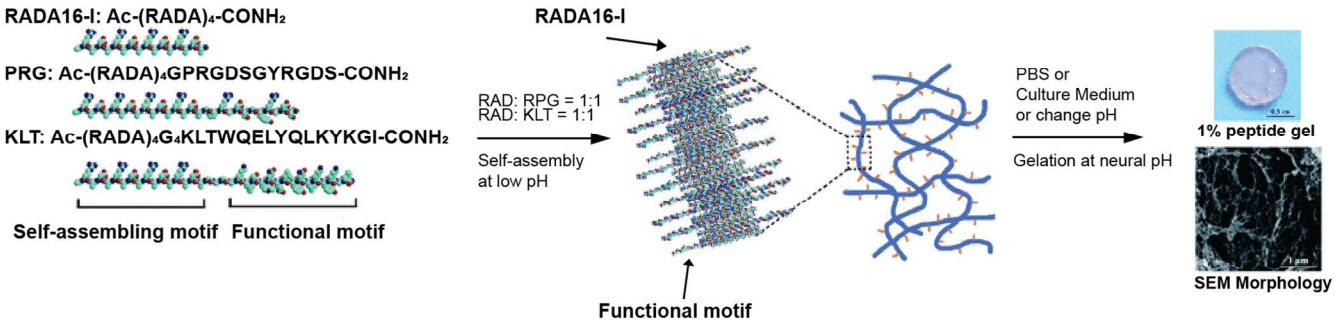


**Figure 6.** Coassembly scheme for mixtures of functionalized and unfunctionalized RADA peptides into fibrils that comprise supramolecular self-supporting hydrogel networks. The PRGDSGYRGDS motif has two integrin-binding RGD sequences and the KLTWQELYQLKYKGI motif acts as a VEGF agonist for inducing cell proliferation. Coassembly of these functionalized RADA sequences with unmodified RADA peptides in various ratios leads to supramolecular $\beta$-sheet fibrils with multivalent display of both integrin- and VEGF-binding motifs along the fibril surfaces. The right hand side of the figure shows a gel image (top) and a scanning electron micrograph (bottom) of the fibrous gel network of coassembled fibrils. Figure adapted from ref 211 (X. Liu, X. Wang, A. Horii, X. Wang, L. Qiao, S. Zhang and F.-Z. Cui, *Nanoscale*, 2012, **4**, 2720–2727)[211] with permission from the Royal Society of Chemistry.

Collier and coworkers have developed multicomponent coassembled materials using the $\beta$-sheet self-assembling Q11 peptide (Ac-QQKFQFQFEQQ-$NH_2$) (**Figure 4**). As with other amphipathic self-assembling peptides, Q11 readily coassembles with modified functionalized Q11 analogs to provide supramolecular fibrils that display the appended functionality. The motivation for much of this work was to create extracellular matrix mimetic materials.[79,80,192,221] Similarly to RADA functionalized hydrogels, the Q11 peptide motif has been functionalized with various cell signaling motifs including fibronectin derived RGDS and laminin derived IKVAV sequences. By mixing these two functionalized components into a single supramolecular hydrogel, significant advantages in human umbilical vein endothelial cell culture were demonstrated with increased binding and cell growth and proliferation with little to no effect on the gel viscoelasticity of the resulting gel.[192] This highlights a significant advantage to using multicomponent systems for the multivalent display of more than one functionalized motif to allow for synergistic effects to improve biological function of the materials developed.

Collier and coworkers also pioneered the use of multicomponent Q11 assemblies to develop self-adjuvanting vaccine materials that elicit innate immune responses *in vivo*.[55,56,193,222,223] Q11 was coassembled with a Q11 peptide coupled to the antigenic $OVA_{322-339}$ peptide sequence via an SGSG spacer (ISQAVHAAHAEINEAGR-SGSG-Q11). Coassembly of these peptides with Q11 into a single multicomponent fibril was investigated for elicitation of immune responses *in vivo*. Mice were subcutaneously injected with hydrogels of these fibrils and immunoglobulin concentrations were measured in collected serum. Interestingly, Q11 hydrogels alone did not raise any detectable IgG and was determined to be non-immunogenic but OVA-Q11 elicited high IgG titers without additional adjuvants.[56] Further studies were conducted to investigate the mechanisms of T cell-dependent immune response against the multicomponent fibrils.[193] When multicomponent OVA-bearing Q11 fibrils were injected into mice, a strong immune response was elicited as evidenced by the appearance of antibodies against OVA. No immune response was seen from self-assembled Q11 fibrils or multicomponent Q11 fibrils bearing the RGD peptide sequence instead of OVA. OVA appended to non-assembling peptides did not raise any significant antibody response *in vivo*. Additional multicomponent Q11 fibrils with alternative epitopes were developed to test the generality of these materials as self-adjuvanting vaccines. Q11 was coassembled with Q11 modified with the malaria $(NANP)_3$ peptide epitope to create materials that raise antibody responses to malaria.[222] As with the OVA-bearing materials, the $(NANP)_3$ fibrils were found to raise anti-malaria antibodies with the addition of adjuvant.

Coassembly of functionalized and unfunctionalized $\beta$-sheet peptides into multicomponent fibrils has also been exploited for the alteration and control of assembly morphology[224–226] and to tailor the emergent properties of the supramolecular coassemblies.[83,227] Nilsson and coworkers have designed multicomponent fibrils of Ac-$(FKFE)_2$-$NH_2$ and peptide nucleic acid (PNA)

modified variants (PNA-$(FKFE)_2$-$NH_2$) to form fibrils that display the PNA nucleotide mimetics.[83] At concentrations at which these fibrils entangle to form hydrogels, the hydrogels can be stiffened in the presence of bridging oligonucleotides that are complementary to the PNA fragments (**Figure 7**). This stiffening of the hydrogel is caused by DNA-mediated cross-linking of the fibril network, which results in stabilization of the network. This stimulus-responsive modification of the emergent properties of a supramolecular hydrogel via biomolecular recognition is a demonstration of the enhanced functionality of multicomponent coassembled materials.

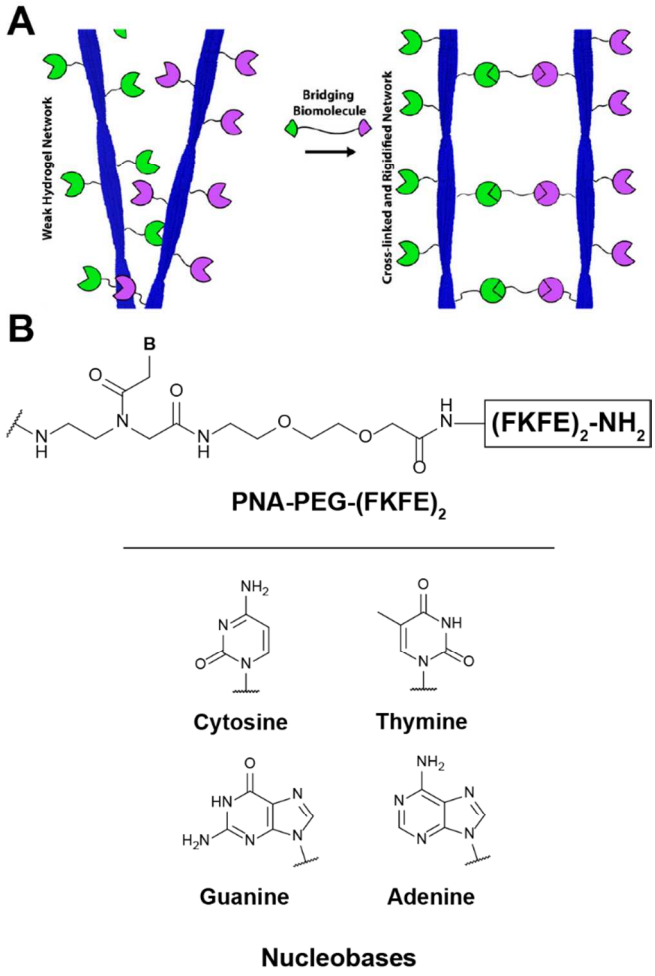


**Figure 7.** (A) Pictorial representation of hydrogel viscoelastic modulation by biomolecular recognition between PNA functionalized $\beta$-sheet peptide fibrils and a bridging complementary DNA sequences. (B) Chemical structure of *N*-terminal PNA modified $(FKFE)_2$ and the structures of PNA nucleobases that

make up the PNA sequences displayed on the supramolecular fibrils. Both *N*-terminal and *C*-terminal PNA modified peptides were mixed in solution and bridging of the supramolecular fibrils occurred after addition of a bridging DNA molecule that was partially complementary to the PNA sequences on both fibrils. Figure adapted with permission from J. T. M. DiMaio, T. M. Doran, D. M. Ryan, D. M. Raymond and B. L. Nilsson, *Biomacromolecules*, 2017, **18**, 3591–3599.[83] © 2017 American Chemical Society.

Statistical coassembly of modified and unmodified self-assembling peptide sequences has also been used to form functionalized multicomponent fibrils that display small molecule biological recognition motifs. The ALEAKLAALEAKLA-$NH_2$ peptide was coassembled with biotin-GG-ALEAKLAALEAKLA-$NH_2$ and the resulting multicomponent fibrils were confirmed to display biotin by interaction with streptavidin-conjugated gold nanoparticles as evidenced by transmission electron microscopy (TEM).[205] Another example by Nilsson *et al*. focused producing peptide fibrils capable of abrogating HIV transmission through multivalent display of aplaviroc, an HIV entry inhibitor that binds to CCR5 (a critical protein receptor that interacts with HIV surface proteins to mediate viral fusion).[228] The $(FKFE)_2$-$NH_2$ $\beta$-sheet self-assembling peptide was synthesized with aplaviroc attached to the *N*-terminus via a PEG linker. The coassembly of aplaviroc bearing peptides in varying ratios with non-functionalized Ac-$(FKFE)_2$-$NH_2$ resulted in fibrils that presented a multivalent display of aplaviroc that targeted these fibrils to CCR5 targets on BC7 cells. While binding of cells by aplaviroc-$PEG_3$-$(FKFE)_2$-$NH_2$ fibrils was observed, the multivalent display did not lead to increased binding compared to aplaviroc alone, presumably due to burial of the hydrophobic aplaviroc molecule in the hydrophobic bilayer of the peptide fibrils. However, this work constitutes proof of principle that multicomponent coassembled fibrils bearing pharmacologic agents that target cell surface receptors have potential for the manipulation of biological systems.

The multivalent display of biological signal molecules on fibril scaffolds is often necessary to tune these materials to elicit specific cellular responses. To this end, there have many

examples of $\beta$-sheet coassembled systems focused on the display of biologically relevant proteins.[91,92,229,230] The multivalent display of short peptides or small molecules on $\beta$-sheet fibrils can be realized trivially by coassembly of the unmodified assembly motif with a functionalized form of the assembly motif. Coassembly of the various components occurs readily when the appended functional group is sterically small, as is seen with small molecules or short peptides. However, when sterically large groups, including functional proteins, are appended to short self-assembling peptides, the steric bulk of the cargo often impedes incorporation of the attached assembly motif into the coassembled fibril. This was demonstrated by Collier *et al*. when they found that Q11 conjugated to green fluorescent protein (GFP) (GFP-Q11) was poorly incorporated into fibrils when mixed with Q11.[92] To solve this problem, Collier *et al*. developed a "$\beta$-tail" technique as one solution to integrating large full-length proteins into supramolecular fibril assemblies. GFP as a model protein was expressed with a 28-residue $\beta$-tail peptide sequence (MALKVELEKLKSELVVLHSELHKLKSEL) that was previously shown to undergo a slow transition from random coil into $\beta$-sheet secondary structures.[231] This $\beta$-tail sequence was also shown to coassemble with the Q11 peptide. When $\beta$-tail-GFP was mixed with Q11, the resulting fibrils showed greater than 80% incorporation of GFP into the multicomponent fibrils, whereas Q11-GFP was incorporated at a much lower ratio (approximately 50%) **Figure 8A** and **8B**). The successful coassembly of $\beta$-tail-GFP with Q11 occurs due to the slow-transitioning $\beta$-sheet propensity of fusion tail incorporation into the supramolecular fibrils. Choice of fusion protein seems to effect integration of protein-functionalization as solutions with nonfolding $\beta$-tail mutant-GFP or lacking Q11 at all show no sedimentation of fluorescently labeled supramolecular fibrils.

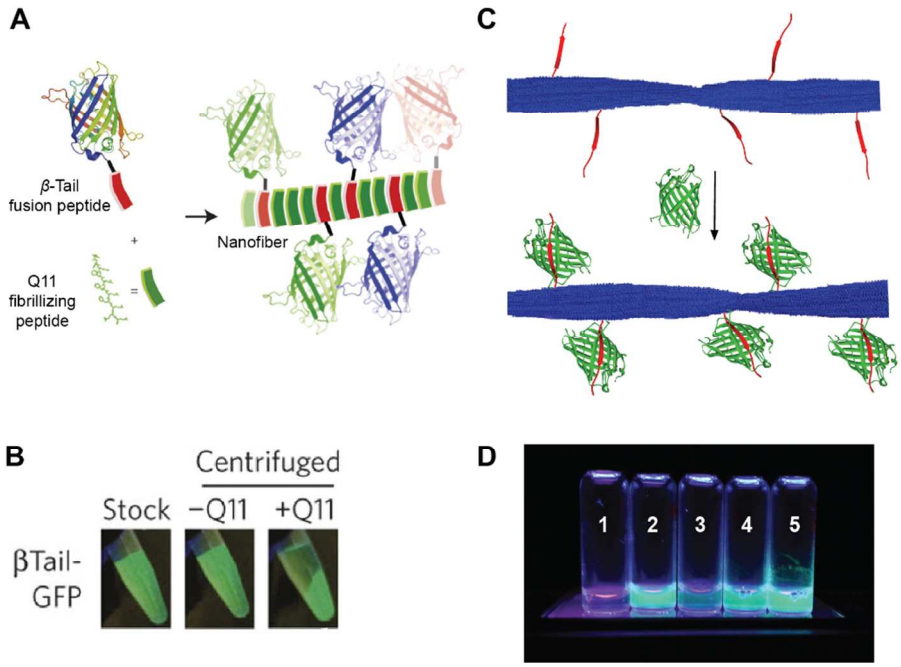


**Figure 8.** (A) $\beta$-tail GFP fusion peptide incorporation into supramolecular fibrils. GFP is expressed with a $\beta$-tail fusion peptide (MALKVELEKLKSELVVLHSELHKLKSEL, red), which undergoes a slow $\alpha$-helix to $\beta$-sheet transition. This $\beta$-tail GFP was mixed in varying ratios with unfunctionalized Q11 (green) in order to produce functionalized Q11 supramolecular fibrils displaying fully folded GFP. (B) Fluorescent images of a stock solution of $\beta$-tail-GFP peptide and the same solution either with or without the Q11 $\beta$-sheet peptide (in a ratio of 1000:1 Q11:$\beta$-tail-GFP) followed by centrifugation. Partitioning of the GFP protein into the fibril from solution was only seen in the presence of Q11. (C) Pictorial representation of the noncovalent attachment of split GFP to fibrils that bear the complementary split GFP peptide strand. (D) Fluorescent visualization of negative and positive controls (1 and 2 respectively) compared to increasing percent mole ratio of GFP displayed on Ac-$(FKFE)_2$-$NH_2$ fibrils (3, 4, and 5). Panels A and B adapted with permission from G. A. Hudalla, T. Sun, J. Z. Gasiorowski, H. Han, Y. F. Tian, A. S. Chong and J. H. Collier, *Nat. Mater.*, 2014, **13**, 829–836.[92] © 2014 American Chemical Society. Panels C and D adapted from ref 91 (J. T. M. DiMaio, D. M. Raymond and B. L. Nilsson, *Org. Biomol. Chem.*, 2017, **15**, 5279–5283.)[91] with permission from Royal Society of Chemistry.

Nilsson *et al*. have reported another method for the multivalent display of functional proteins onto supramolecular $\beta$-sheet fibrils via a split protein strategy.[91] This strategy relies on the coassembly of Ac-$(FKFE)_2$-$NH_2$ with $(FKFE)_2$-$NH_2$ peptides modified with a short affinity motif derived from a split protein system (**Figure 8C**). These affinity motifs are sufficiently short that they do not impair incorporation of the attached assembly motif into the multicomponent fibrils. These affinity motifs can be used for noncovalent attachment of the complementary split protein

segment after the fibrils have been assembled to affect multivalent display of the recombined functional proteins. This was demonstrated with two split protein systems, ribonuclease S′ (RNase S′) and split green fluorescent protein (GFP). Ac-$(FKFE)_2$-$NH_2$ was coassembled with $(FKFE)_2$ modified with either the S-peptide from RNase S′ or with the GFP 11 fragment (the $11^{th}$ strand of the GFP $\beta$-barrel protein). These multicomponent fibrils were then mixed with either the RNase S′ S-protein or GFP 1–10 (strands 1-10 of GFP) respectively. In both cases, fibrils with functional protein displayed at the surface resulted. Solutions of the reconstituted GFP fibrils are shown in Figure 8D. This strategy enables multivalent display of proteins on multicomponent fibrils by circumventing the steric bulk of the proteins with short affinity tags that attract the proteins after the fibrils have been assembled.

Collier *et al*. have also developed a covalent capture strategy for the multivalent display of proteins on multicomponent fibrils. Specifically, Q11 peptide fibrils bearing p-nitrophenyl phosphonate groups that provide an electrophilic handle for the covalent attachment of functional proteins to multicomponent Q11/Q11-p-nitrophenyl phosphonate.[55] Nucleophilic groups on proteins can displace the p-nitrophenyl group displayed on these fibrils to promote covalent attachment of the folded proteins to the fibrils. Proof of principle was demonstrated with cutinase-fusion proteins. Incubation of cutinase-GFP fusions with these fibrils resulted in efficient attachment of GFP to the fibrils as evidenced by fluorescence and immunostaining. Incubation of cutinase-GFP with Q11 fibrils that lack the electrophilic p-nitrophenyl phosphonate groups resulted in no effective attachment of protein to the fibrils. The display of fully folded protein antigens is important for vaccine development. Q11 nanofibers displaying cutinase-GFP antigens were shown to act as self-adjuvanting vaccines in mice eliciting robust and durable anti-GFP antibody responses. In contrast, injection of cutinase-GFP fusions with

unmodified Q11 fibers resulted in antibodies primarily against cutinase. In principle this strategy can be used to create vaccines for any protein that can be effectively folded in a cutinase fusion, providing a general strategy for protein display on multicomponent $\beta$-sheet fibrils.

### 2.3. Spatial Control of Biological Signal Motifs in Multicomponent Peptide Materials

While the statistical methods of coassembling peptides discussed in this section provide some minor control over the overall architecture of the coassembled structures, precise spatial control over the display of multivalent biological signal motifs in synthetic peptide supramolecular biomaterials is necessary in some cases. Stevens *et al*. have developed one strategy for spatial control over the presentation of ligands on multicomponent supramolecular peptide materials. They synthetically attached fibronectin derived peptides, RGDS and PHSRN, to variably spaced side chains on a $\beta$-sheet peptide scaffold.[232] Supramolecular fibrils were prepared by coassembly of the unmodified assembly motif with a functionalized variant in which the ligands were arranged in near (0.7 nm), optimal (3.5 nm), or far (6.2 nm) spacings as determined for ideal $\alpha_5\beta_1$ integrin activation (**Figure 9A, 9B**). HUVEC cells were shown to bind and spread at a higher rate over 24 hours and had increased $\alpha_5$ integrin gene expression as determined by PCR analysis when cultured on the hydrogels which incorporated the correct spacing of integrin binding domains as compared to the near or far spacing of ligands. Immunostaining was used to visualize the amount of $\alpha_5\beta_1$ integrin in HUVEC cells cultured in hydrogels with the three differently spaced ligands and the hydrogel with the correct ligand spacing was found to bind cells more effectively than the alternate spacings (**Figure 9C**). This provides a clear

demonstration of the importance of spatial control in the display of biological ligands in the context of multicomponent supramolecular materials.

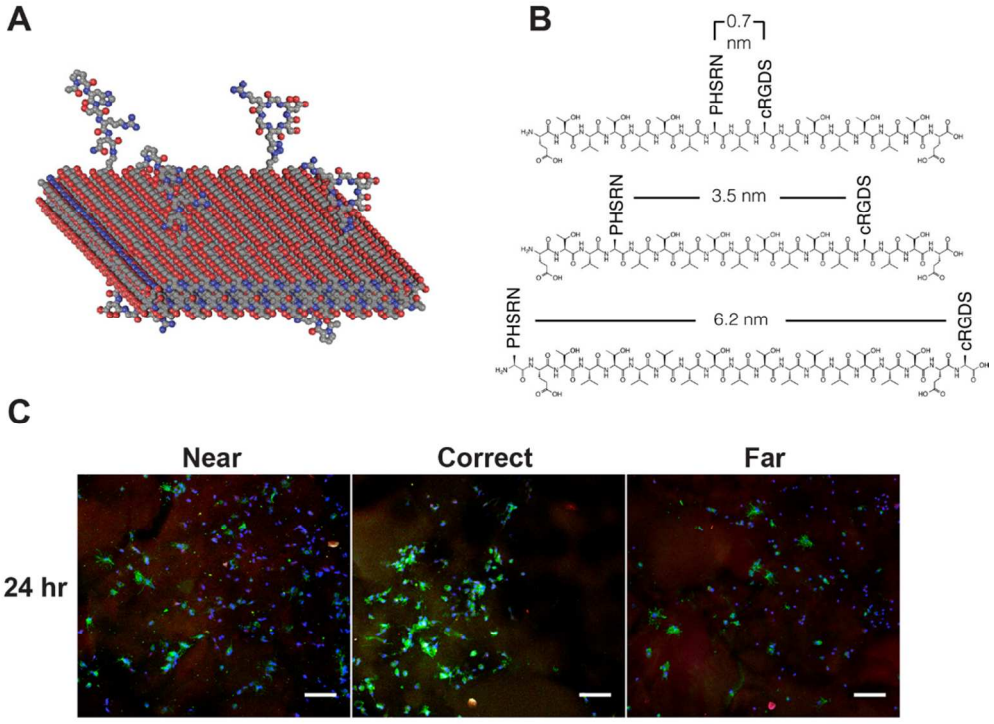


**Figure 9.** Model of supramolecular fibrils with fibronectin derived ligands. (B) Backbone spacing of ligands with "near", "correct", or "far" arrangements for optimal integrin binding on self-assembling amphipathic $\beta$-sheet peptide networks. (C) Immunocytochemistry staining over 24 hours of HUVEC cells cultured with hydrogels displaying differently spaced RGDS and PHSRN ligands. Green color indicates the stained $\alpha_5\beta_1$ integrin. Figure adapted with permission from E. T. Pashuck, B. J. R. Duchet, C. S. Hansel, S. A. Maynard, L. W. Chow and M. M. Stevens, *ACS Nano*, 2016, **10**, 11096–11104.[232] © 2016 American Chemical Society.

### 2.4 Spatially Controlled Coassembly of $\beta$-Sheet Peptides Using Charge

The multicomponent materials described in the previous sections rely on statistical coassembly of peptides to display functional groups on the supramolecular fibrils. This strategy provides supramolecular materials in which the spatial orientation of the components within the assemblies is statistically controlled only as a function of the relative concentrations of the components, resulting in the polydisperse arrangement of functionality on the resulting materials.

While statistical mixtures of functionalized and unfunctionalized peptides are useful for heterogeneous assembled biomaterials, there is little control over the spatial presentation of ligands. An ultimate goal in the preparation of multicomponent, highly functionalized, synthetic biomaterials is the ability to spatially control or direct the mixture of the components that compromise the assembly. Electrostatic or polarity pairing has been exploited as a prominent strategy in efforts to affect more precise spatial control of the components within coassembled $\beta$-sheet peptide materials.[233–240] Mixing oppositely charged short peptides has been shown to be an effective director of coassembly and a method to control the spatial orientation of peptides in the assembled state, the morphology of the assemblies, and even the emergent properties of the resulting coassembled structures.[234,235,238]

Lynn and coworkers have developed coassembled $\beta$-sheet peptide nanotubes in which coassembly is directed between complementary ionic interactions between the constituent peptides.[239] Fragments of A$\beta$(16–22), the positively charged Ac-KLVFFAL-$NH_2$ peptide and the negatively charged Ac-(pY)LVFFAL-$NH_2$ peptide (where pY is a negatively charged phosphotyrosine residue) coassemble into robust bilayer nanotubes with thicknesses mimicking natural phospholipid membranes. It was discovered that equimolar mixtures of these peptides generates a nanotube with a negative outer surface and a positive inner surface, composed of an inner leaflet that consists of antiparallel $\beta$-sheets of the positive peptide and the outer leaflet composed of antiparallel sheets of the negative peptide. The interface of the two leaflets is stabilized by attractive ionic interactions between the positive and negative sheets. Cross seeding experiments were conducted in which the individual peptides were self-assembled into one-component nanotubes. These tubes were sonicated and it was shown that the fragmented tubes could seed tube extension of the opposite polarity peptide. In these cross seeding experiments,

the resulting nanotubes were composed of discrete negative and positive domains. These coassembled materials provide versatile possibilities for the development of biomaterials in which charge direction is desired.

Hudalla and coworkers have also used charge complementarity to design coassembled $\beta$-sheet fibrils.[240] The Hudalla strategy uses "CATCH" peptides (Co-Assembly Tags based on CHarge complementarity) to induce coassembly and hydrogelation of CATCH(+) and CATCH(-) Q11 based peptides with oppositely charged hydrophilic residues that selectively coassemble with the charge complement sequence in aqueous solution. CATCH(+) (Ac-QQKFKFKFKQQ-$NH_2$) and CATCH(-) (Ac-EQEFEFEFEQE-$NH_2$) peptides were designed resist self-assembly due to charge repulsion at neutral pH, but to coassemble when mixed. Recombinant CATCH(-)-GFP was also generated to test the limits of coassembling a fully folded protein into the supramolecular structures produced from this coassembling $\beta$-sheet peptide system. Coassembly CATCH(+)Q11, CATCH(-), and recombinant CATCH(-)Q11-GFP resulted in one dimensional nanofibers that effectively displayed GFP. Interestingly, binary mixtures of CATCH(-)-GFP and CATCH(+) resulted in microparticle formation instead of nanofibers, and the presence of the peptide-GFP fusion protein altered the assembly kinetics for all components by lowering the critical coassembly concentration relative to the parent CATCH peptides individually. Charge-directed coassembly thus has interesting potential not only for directing the spatial arrangement of peptide within binary assemblies, but also in the design of more complicated ternary or even high order supramolecular structures.

### 2.5 Rippled $\beta$-Sheets as Spatially Controlled Coassembled Materials

In 1953, shortly after the initial description of pleated $\beta$-sheet structure, Pauling and Corey predicted that enantiomeric L- and D-$\beta$-sheet peptides would selectively coassemble into unique

$\beta$-sheet arrangements (**Figure 10**).[241] These coassembled $\beta$-sheets were envisaged to adopt an alternating orientation of L- and D-peptides within the sheet structure. They coined the term "rippled $\beta$-sheet" to describe the appearance of these anticipated structures. This prediction suggests the possibility of exploiting chirality to direct the coassembly of $\beta$-sheet peptides into rippled $\beta$-sheet structures as another strategy to produce spatial control in coassembled multicomponent peptide materials.

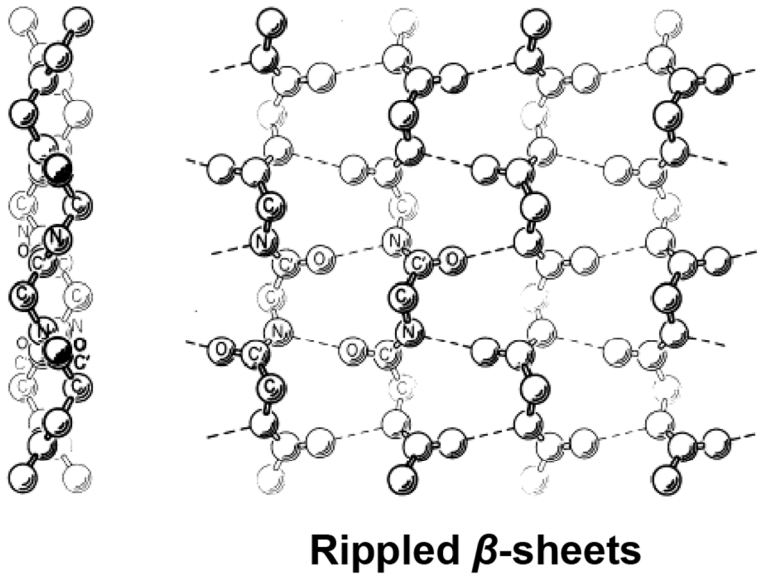


**Figure 10.** Pauling and Corey's predicted model (side and top view) of a parallel-chain alignment of enantiomeric $\beta$-sheet peptides to form rippled $\beta$-sheet fibrils. Figure reproduced with permission from L. Pauling and R. B. Corey, *Proc. Natl. Acad. Sci.*, 1953, **39**, 253–256.[241]

The use of D-amino acids in self-assembling peptide structures has previously been exploited to alter the structural morphology of the materials or to prolong stability of the materials against enzymatic degradation.[242–248] In early research, it became evident that mixing enantiomeric peptides provided interesting and structurally unique supramolecular assemblies compared to the corresponding single-enantiomer assemblies although initial understanding of the principles that governed these effects was unclear.[249–251] In 2005, Higashi and Goto separately reported

experiments in which the coassembly of enantiomeric L- and D-$\beta$-sheet peptides was assessed.[250,251] Goto and coworkers reported that the L- and D-enantiomers of the Ser20–Lys41 fragment of $\beta_2$-microglobulin separately self-assembled into fibrils of opposite chirality, but that seeded assembly of either enantiomer by fibrils of opposite chirality did not proceed smoothly. This result led them to conclude that seeded cross-reaction between self-assembling peptides of opposite chirality was precluded by incompatible geometric constraints. Higashi *et al*. conducted similar analyses using enantiomers of the triblock $L_4K_8L_4$ peptide (L-enantiomer is 1L, D-enantiomer is 1D). 1L and 1D separately self-assembled into left-handed and right-handed twisted fibrils respectively. In contrast, equimolar mixtures of 1L and 1D did not form fibrils, but instead formed only globular aggregates. These results also supported the notion that assembly into amyloid-like fibrils required stereochemical compatibility, possibly contradicting Pauling and Corey's prediction of rippled $\beta$-sheet formation. It should be noted, however, that neither of these studies explicitly predicted or searched for rippled $\beta$-sheets.

More recently, Schneider *et al*. reported that mixing equimolar ratios of L- and D-$\beta$-sheet peptides produced supramolecular hydrogels with enhanced viscoelasticity.[85] This work was conducted using the designed self-assembling $\beta$-hairpin peptide, MAX1 (**Figure 4**). MAX1 undergoes directed hydrogelation at high salt concentrations, which masks the positive lysine charges and triggers hairpin folding with concurrent fibril self-assembly and entanglement into hydrogel networks. Enantiomeric mixtures of MAX1 and DMAX1 in 3:1, 1:3, and 1:1 ratios resulted in hydrogels that were more rigid than the single enantiomer materials. Rheological analysis of the hydrogels revealed that the storage modulus of the hydrogel formed from 1:1 MAX1:DMAX1 was more than four times those of either of the pure enantiomeric peptides and approximately two times that of the 1:3 and 3:1 enantiomeric ratios (which were approximately

equivalent to one another). They confirmed that the mixtures formed coassembled fibrils that contained both enantiomers. These studies provided clear evidence for coassembly enantiomeric $\beta$-strand peptides with alternating hydrophobic/hydrophilic sequence patterns although the structural basis for the enhanced emergent properties was not immediately evident.

Concurrently, Nilsson *et al*. reported a similar phenomenon occurring with equimolar mixtures of enantiomeric Ac-$(FKFE)_2$-$NH_2$ peptides.[252] Equimolar mixtures of this self-assembling peptide formed supramolecular structures that were distinct from those formed by single enantiomers. TEM characterization of the assembled structures revealed that the enantiomeric coassembly formed morphologically distinct fibrils that were approximately half the width of the single enantiomer peptide fibrils and that also lacked the distinctive helical tape morphology seen with self-assembly of single enantiomers (**Figure 11A**). Isotope edited IR and FRET experiments confirmed that the enantiomeric Ac-$(FKFE)_2$-$NH_2$ peptides were arranged in an alternating L/D fashion as predicted by Pauling and Corey for rippled $\beta$-sheets (**Figure 11B**). Isothermal titration calorimetry experiments showed a 9.3 kcal $mol^{-1}$ enthalpic advantage for coassembly of D-Ac-$(FKFK)_2$-$NH_2$ and L-Ac-$(FEFE)_2$-$NH_2$ compared to the same titration experiment using only L- peptides. It was also demonstrated that rippled $\beta$-sheet fibrils of L- and D-Ac-$(FKFE)_2$-$NH_2$ peptides had enhanced hydrogel viscoelasticity, similar to Schneider's observations, and increased proteolytic stability against chymotrypsin, trypsin, and proteinase K compared to the all-L- pleated $\beta$-sheet fibrils.[84]

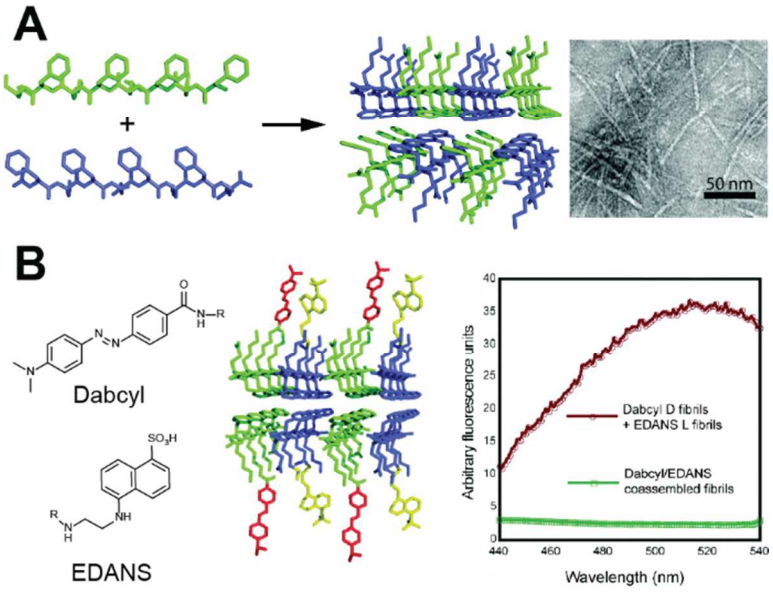


**Figure 11.** (A) Proposed structure of amphipathic L- and D- Ac-$(FKFE)_2$-$NH_2$ rippled $\beta$-sheet fibrils. TEM image indicates rippled $\beta$-sheet peptide fibrils half the width of either enantiopure peptide individually. (B) Structures and model of coassembly of donor/acceptor fluorophores attached to enantiomeric strands of Ac-$(FKFE)_2$-$NH_2$. FRET measurement of coassembled mixtures shows quenching (green line) indicating close packing structure of L- and D- strands compared to FRET measurements of preassembled fibrils (red line) which shows minimal quenching. Figure adapted with permission from R. J. Swanekamp, J. T. M. Dimaio, C. J. Bowerman and B. L. Nilsson, *J. Am. Chem. Soc.*, 2012, **134**, 5556–5559.[252] © 2012 American Chemical Society.

Wetzel and coworkers have shown that rippled $\beta$-sheet formation is not confined only to self-assembling peptides with alternating sequences of hydrophobic and hydrophilic amino acids.[253] Polyglutamine peptides self-assemble into amyloid fibrils and are characteristic features of Huntingtin aggregation in Huntington's disease.[254–256] Wetzel *et al.* reported that aggregates of both L- and D-polyQ peptides were equally cytotoxic to cells in culture and that seeds from fibrils of either enantiomer could indiscriminately seed aggregation of either enantiomer without stereospecificity. This suggests that polyQ peptides are competent to form chirally cross-seeded rippled $\beta$-sheet structures.

Raskatov *et al*. subsequently explored the coassembly of L- and D-A$\beta$42 peptides to investigate how potential rippled $\beta$-sheet formation might influence the functional toxicity of amyloid fibrils.[257] A binary mixture of enantiomeric A$\beta$42 peptides showed accelerated formation of fibrils without any lag phase compared to single enantiomer assembly. Prefibril oligomer formation was suppressed in the enantiomeric mixture, resulting in reduced toxicity against two different neuronal cell lines. Racemic rippled $\beta$-sheet coassembly was also corroborated by fluorescently labeling each enantiomer; equimolar racemic mixtures of A$\beta$42 were imaged by confocal microscopy confirming significant colocalization of fluorophores in the coassembled materials. Thus, rippled $\beta$-sheet formation appears to be general for a variety of $\beta$-sheet peptides and not just a feature of amphipathic peptides with alternating hydrophobic and hydrophilic residues.

Recently Schneider and Tycko structurally confirmed coassembly of MAX1 and DMAX1 into rippled $\beta$-sheet fibrils and developed an explanation for the enhanced hydrogel rigidity of the coassembled fibrils.[86] Using the previously mentioned MAX1 peptide conjugated to an azide group and its enantiomer, DMAX1 conjugated to biotin, they were able to observe colocalization of dibenzylcyclooctyne (DBCO)-conjugated 10 nm gold nanoparticles and streptavidin-conjugated 5 nm gold nanoparticles to a single fibril by TEM imaging (**Figure 12A**). Solid state NMR was employed to elucidate the structure of the enantiomeric peptide fibrils. The NMR analysis clearly shows coassembled rippled $\beta$-sheets with distinctive packing architectures compared to pleated $\beta$-sheets (**Figure 12B**). The enhanced hydrogel rigidity of the rippled $\beta$-sheets can be explained by small angle neutron scattering and diffusing wave spectroscopy data that indicate the racemic fibrils are themselves more rigid lending to a stiffer gel network. The enthalpic and kinetic preference for coassembly of enantiomeric $\beta$-sheet peptides into rippled $\beta$-

sheets provides an additional avenue for the design of spatially controlled multicomponent supramolecular materials.

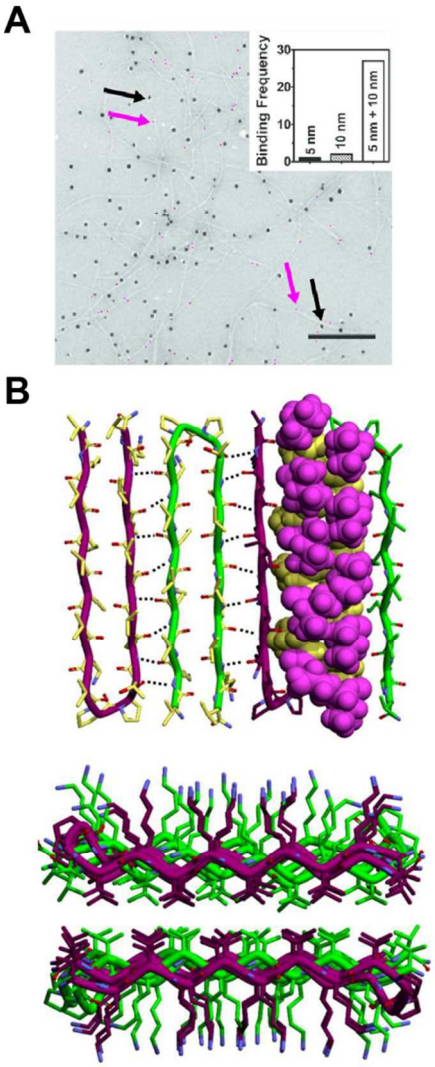


**Figure 12.** (A) TEM image of MAX1-azide and DMAX1-biotin coassembly after incubation with DBCO-conjugated 10 nm gold nanoparticles and streptavidin-conjugated 5 nm gold nanoparticles. Co-localization of 5 nm (magenta color) and 10 nm (black color) gold nanoparticles were found within a single fibril as opposed to self-sorting into individual fibrils with individual nanoparticles. (B) Top and side packing model for rippled $\beta$-sheet coassembled mixtures of 1:1 MAX1: DMAX1 based on solid state NMR correlations. Figure adapted with permission from K. Nagy-Smith, P. J. Beltramo, E. Moore, R. Tycko, E. M. Furst and J. P. Schneider, *ACS Cent. Sci.*, 2017, **3**, 586–597.[86] © 2017 American Chemical Society.

## Section 3. Coassembly of Low Molecular Weight Peptides

Low molecular weight (LMW) modified amino acids and peptides have been developed that self-assemble into functional supramolecular materials.[35,258–266] These include di- and tripeptides that self-assemble into structures with similar emergent properties, including hydrogelation, as longer peptide sequences. LMW supramolecular peptide materials have been particularly attractive as cheaper alternatives to those derived from synthetic peptides and proteins. However, the limited chemical space accessible by LMW peptides sometimes limits the robustness of the emergent properties of the resulting supramolecular materials. Coassembly of multiple LMW peptides has often provided multicomponent materials that have drastically improved properties.[82,267–272] While appropriately modified single amino acid derivatives have also been found to self- and coassemble into supramolecular structures,[87,273–283] the discussion in this section will be limited to materials formed from peptides that are at least two amino acids in length.

### 3.1 Diphenylalanine Derived Coassembled Materials

Diphenylalanine (FF) and its derivatives are the most widely used minimalistic peptide building blocks for self-assembled materials.[61,284] FF is the minimal fragment of the Alzheimer's disease A$\beta$ peptide that undergoes spontaneous self-assembly.[30,285–292] The self-assembly of FF into discrete nanotubes was first reported by Gazit and coworkers.[285] FF nanotubes have remarkable mechanical,[293–295] photophysical,[296–298] and electrical[299,300] properties that have inspired intense investigation of these materials.[293–304] Structural analysis of FF nanotubes suggests that aromatic π-π stacking of the Phe side chains and hydrogen bonding mediate self-assembly (**Figure 13**).[285,286,290] FF derivatives, including the cationic *C*-terminal amide (FF-

$NH_2$),[305,306] *N*-terminal acetate (Ac-FF),[307] and carbamate-modified Fmoc-FF and Boc-FF,[115,308,309] also self-assemble into diverse structures, including nanotubes, vesicles, and fibrils, depending on the structure of the chemical modifying group and the solvent conditions.[115,305–312] The supramolecular assemblies of FF derivatives often display unique properties relative to the parent dipeptide, dramatically expanding the possible applications of the resulting materials.[284,313]

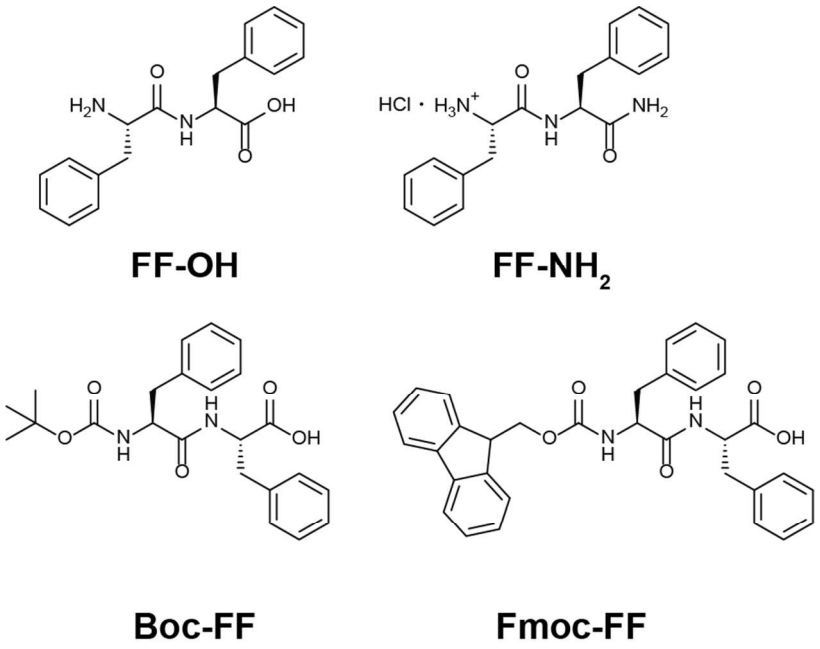


**Figure 13.** Chemical structures of Phe-Phe (FF) and FF derivatives that have been shown to form self-assembled supramolecular structures.

It has been found that coassembly of FF with modified FF derivatives or other short peptides provides unique multicomponent supramolecular materials (**Figure 14**).[82,293,314–319] For example, Reches *et al*. showed that the coassembly of FF with Boc-FF in 50% ethanol in various ratios produced a variety of supramolecular structures ranging from spheres to elongated fibers that resembled biomolecular necklaces (**Figure 15B**).[316] Later, Gazit *et al*. hypothesized that coassembly of FF with Boc-FF could alter the elongation kinetics of FF in the multicomponent

mixture, possibly affecting the properties of the resulting materials.[293,314] Accordingly, they examined the coassembly of FF with Boc-FF at FF:Boc-FF ratios ranging from 20:1 to 5:1. It was observed that the length distribution of the coassembled nanotubes decreased as the ratio of Boc-FF increased. The random integration of Boc-FF into the FF structures was found to elicit length control by perturbation of the kinetics of coassembly. Thus, Boc-FF/FF coassembly enabled fine-tuning of the assembly process and the resulting supramolecular structures.

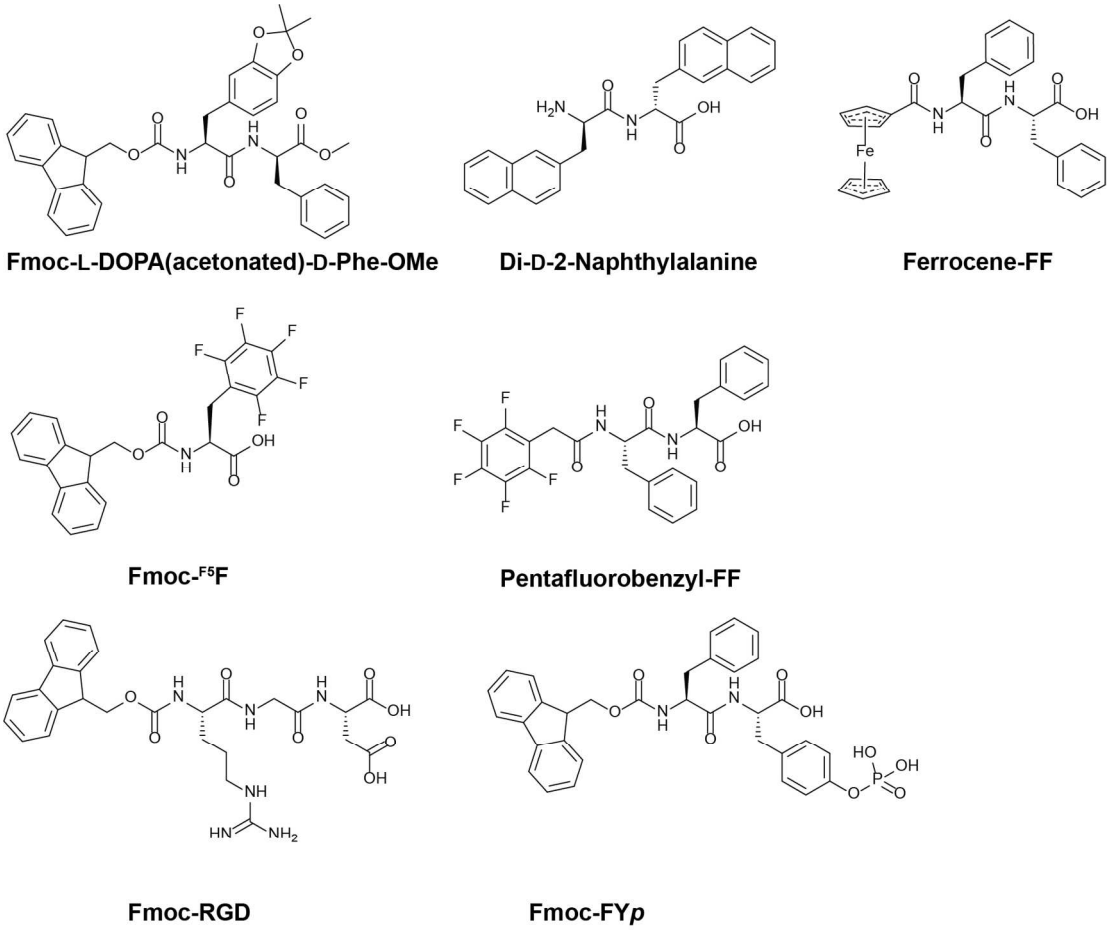


**Figure 14.** Chemical structures of low molecular weight molecules that have been investigated in coassembled mixtures with FF or FF derivatives discussed in sections 3.1, 3.2, and 3.3.

In addition to FF/Boc-FF coassembly, Reches *et al*. also examined FF coassembly with other aromatic dipeptides to explore structural diversity in coassembled peptide materials.[317,319] Coassembly of FF with Fmoc-L-DOPA(acetonated)-D-Phe-OMe (**Figure 14**) produced varied nanostructures including spheres (0.5 mg/mL$^{-1}$ equimolar peptide concentrations), bi-concave disks similar to red blood cells (RBCs) (1 mg/mL$^{-1}$ equimolar peptide concentrations), and spherical assemblies with bulges similar in morphology to white blood cells (WBCs) (2 mg/mL$^{-1}$ equimolar peptide concentrations) (**Figure 15C**).[319] These materials were assessed for drug encapsulation and release. FF/L-DOPA-D-Phe coassemblies were formed in buffered solutions containing the anti-cancer drug doxorubicin, which was encapsulated within or adsorbed onto the coassembled peptide microstructures. Doxorubicin was released into solution over 24 hours concomitant with the structural collapse of the multicomponent RBC-like structures. This work again highlights the tunability of the physical properties of coassembled supramolecular structures to produce functional biomaterials.

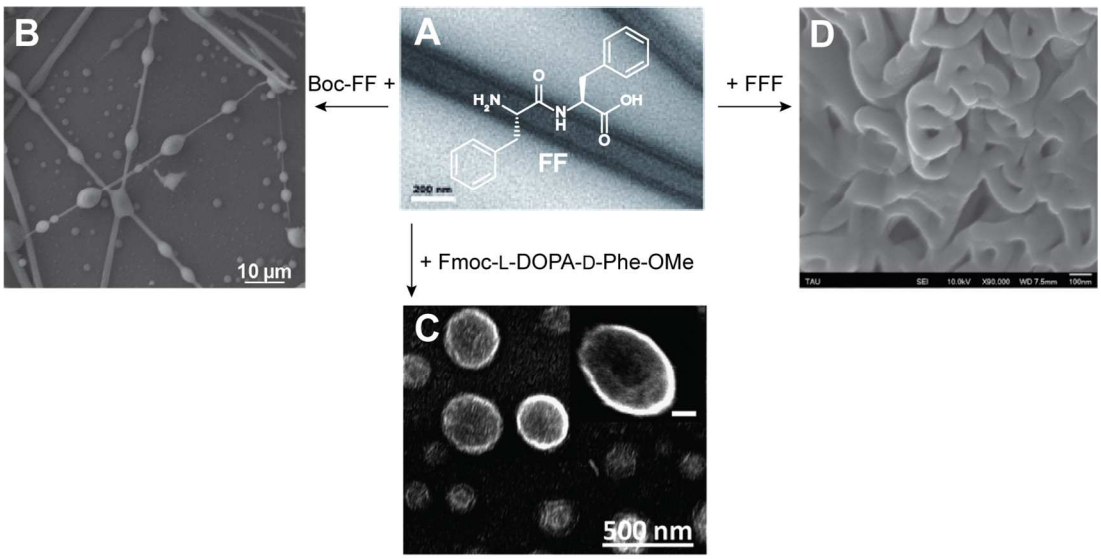


**Figure 15.** (A) Chemical structure of FF and TEM image of nanotubes formed from the self-assembly of cationic FF.[320] Panels B-D show various supramolecular structures formed from the coassembly of FF

with (B) Boc-FF to produce biomolecular necklaces,[316] (C) Fmoc-L-DOPA(acetonated)-D-Phe-OMe to produce red blood cell like nanostructures (shown in inset with 100 nm scale bar),[319] and (D) FFF to produce nano-toroidal structures.[317] Panel A adapted with permission from X. Yan, Q. He, K. Wang, L. Duan, Y. Cui and J. Li, *Angew. Chemie Int. Ed.*, 2007, **46**, 2431–2434. © 2007 Wiley-VCH Verlag GmbH & Co. Panel B adapted with permission from S. Yuran, Y. Razvag and M. Reches, *ACS Nano*, 2012, **6**, 9559–9566. © 2012 American Chemical Society. Panel C adapted with permission from ref 319 (S. Maity, S. Nir and M. Reches, *J. Mater. Chem. B*, 2014, **2**, 2583–2591) with permission from the Royal Society of Chemistry. Panel D reproduced with permission from C. Guo, Z. A. Arnon, R. Qi, Q. Zhang, L. Adler-Abramovich, E. Gazit and G. Wei, *ACS Nano*, 2016, **10**, 8316–8324. © 2016 American Chemical Society.

Tendler *et al*. also illustrated tuning the properties of a supramolecular peptide materials by coassembly of FF with the aromatic di-D-2-napthylalanine (di-D-Nal, **Figure 14**) dipeptide.[82] The rationale of this study was to investigate the structural and mechanical properties that arise from the coassembly of the well-characterized FF and di-D-Nal self-assembled materials. Each of these dipeptides self-assembles into unique nano- and microstructures. While FF assembles into highly rigid nanotubes 500–2000 nm in diameter with persistence lengths greater than 10 μm, di-D-Nal self-assembles into flexible nanotubes with narrower 50–1000 nm diameters and shorter persistence lengths (< 1 μm).[321] Coassembly of FF with di-D-Nal in various ratios (20-80% di-D-Nal) gave rise to multicomponent assemblies with altered structural and mechanical properties. At lower ratios of di-D-Nal (20%, 40%, and 60%), two distinct nanotube populations were observed, with the 20% nanotube formulations matching closely to those observed with the corresponding self-assembled materials. The 40% and 60% di-D-Nal formulations also displayed nanotubes with bimodal diameters, although these were approximately 50 nm and 450 nm in diameter. At 80% di-D-Nal, the nanotubes were generally observed to be of the smaller diameter size. The variable size distributions were attributed to nonhomogenous coassembly of the components within individual tubes. This conclusion was supported by thermal stability analyses, which suggested that individual tubes were most likely composed of phase-separated

FF and di-D-Nal assemblies. Interrogation of the mechanical stiffness of the nanotubes showed a reduction in stiffness as a function of increasing di-D-Nal concentration, indicating that mechanical strength can be tuned by a coassembly strategy. These studies illustrate that structural compatibility, including stereochemical compatibility, strongly influences the homogeneity of coassembled materials. In this system, the FF and di-D-Nal peptides are not intimately and homogenously coassembled, but are rather largely arranged in self-assembled phase-separated patterns within the resulting nanostructures.

Hierarchical coassembly of FF derivatives into complex microstructures under dynamic conditions has also been explored. In one example, He and coworkers studied the coassembly of FF and ferrocene-FF (Fc-FF, **Figure 14**).[318] Individually, under conditions where each derivative is diluted from hexafluoroisopropanol (HFIP)/methanol into water, FF self-assembles into crystalline microtubes whereas Fc-FF self-assembles into nanospheres or nanofibers as a function of water content.[318] Coassembly of FF and Fc-FF was then examined by dissolving the two materials in HFIP/methanol cosolvent at 5 wt% Fc-FF relative to FF. When water was added, FF rapidly self-assembled into microtubes in a gel-like network. The wetted microtube networks, which were surrounded by Fc-FF in solution, were then placed on glass surfaces where the solvent was allowed to evaporate under conditions of controlled humidity. Capillary force on the solution of Fc-FF wetting the FF microtubes resulted in subsequent assembly of Fc-FF at the FF microtube ends, providing multicomponent structures with a dandelion-like appearance. This hierarchical coassembly in which one component first assembles and then acts as a template for the assembly of the second component is a simple strategy to control the formation of multicomponent nano- and microstructures under conditions in which the components have differential assembly properties.

In an attempt to expand the structural diversity of nanostructures formed via the self-assembly of minimalistic phenylalanine-based peptides, Gazit, Wei, and Zhang investigated the coassembly of FF with the FFF tripeptide.[317] While FF self-assembles into nanotubes, FFF self-assembles into solid nanoplates[322] and nanospheres.[323] Computational molecular dynamics simulations predicted that these peptides are capable of coassembly and that the multicomponent structures would form unique nanotoroid architectures (**Figure 15D**). These theoretical predictions were experimentally confirmed by the demonstration that FF and FFF indeed undergo coassembly into a variety of nanostructures that transition from hollow toroidal to solid structures dependent on the ratios of FF to FFF. These unique structures were explained based on FFF favoring structures with negative curvature, which facilitates facial clustering of the hydrophobic benzyl side chains, altering FF- and FFF-water interactions which directs the coassembly mechanisms.[317] This work illustrates the important co-application of theoretical and experimental methodologies to predict and explain complex coassembly phenomena.

These examples provide compelling early demonstrations of the unique properties exhibited by coassembled LMW peptides. It is clear that the packing architecture of the peptides within the multicomponent assemblies accounts for the distinct supramolecular morphologies and the resulting emergent properties. Imaging techniques including atomic force microscopy (AFM),[324,325] transmission electron microscopy (TEM),[326,327] scanning electron microscopy (SEM);[328,329] thermal analysis techniques like differential scanning calorimetry (DSC);[330,331] and the observation of amyloid like properties of coassemblies via fluorescence techniques like thioflavin T staining[332–334] can provide information about the morphology and stability of these structures. However, these techniques do not provide atomic scale resolution to decipher the molecular arrangements of the components within the assemblies. An important avenue of future

research will be the application of advanced structural analysis to correlate the molecular packing structures of the components in coassembled formulations with the observed properties in order to further understand these materials.

### 3.2 Multicomponent Low Molecular Weight Hydrogels For Tissue Engineering

Much research on the coassembly of LMW peptides has been motivated by efforts to develop next-generation hydrogel materials for tissue engineering and other biomedical applications.[90,335–338] Self-assembled supramolecular hydrogels of peptides have proven to be versatile biomaterials.[34,339–342] The corresponding LMW materials are less expensive alternatives to longer peptides, but often are often deficient in the requisite emergent properties.[274] For example, hydrogels for tissue engineering must have appropriate viscoelastic rigidity, stability, and shear responsiveness.[47,343,344] LMW peptide-based gels are often unstable to mechanical agitation, which can result in precipitation of the gel network.[345–348] Coassembly of various LMW peptides has been explored as a method to engineer the needed emergent properties into the resultant hydrogels. Coassembled LMW hydrogel materials, as discussed for $\beta$-sheet materials in the previous section, are often tuned for cell culture applications by immobilization of cell receptor ligands onto the gel network to facilitate the growth and proliferation of cells *in vitro*. In addition, the fundamental viscoelastic properties of coassembled LMW peptide gels are often drastically improved compared to the corresponding self-assembled materials. In this section we will discuss notable example of coassembled LMW peptide hydrogels.

Adler-Abramovich *et al*. demonstrated the ability to functionalize multicomponent LMW peptide hydrogels with hydroxyapatite (HAP, $Ca_5(PO_4)_3(OH)$) for bone tissue engineering

applications.[349] HAP has been shown to support cell growth of human osteoblast cells and is important for bone mineralization and regeneration in bone tissue engineering scaffolds.[350–353] In addition, biomimetic hydrogels for bone tissue engineering must have adequate mechanical strength.[37,354] Coassembly of Fmoc-FF and Fmoc-R in varying molar ratios provided hydrogels with tunable physical characteristics. Fmoc-FF provided a mechanically rigid network, while the positive charge provided by the Fmoc-R guanidine group enabled binding of HAP to the surface of the network fibrils. Interestingly, the inclusion of HAP increased the mechanical rigidity of all ratios of Fmoc-FF:Fmoc-R coassembled hydrogels, increasing the storage modulus by as much as 24-fold for the 3:1 tri-component gel. Cell viability assays of NIH 3T3 mouse fibroblasts on the 3:1 Fmoc-FF:Fmoc-R/HAP hydrogels indicated a high number of both live and adherent cells compared to cells cultured on control Fmoc-FF/HAP hydrogels. These multicomponent Fmoc-FF/Fmoc-R inorganic HAP hydrogels illlustrate both the mechanical advantages of coassembled hydrogel systems as well as the ability of individual components to recruit other biofunctional entities to the matrix to improve the overall biochemical properties of the material.

Another example of mechanical modulation of cell culture hydrogels by multicomponent coassembly was demonstrated by Adler-Abramovich using Fmoc-FF and Fmoc-pentafluorophenylalanine (Fmoc-$^{F5}$F) (**Figure 16**).[355] Fmoc-pentafluorophenylalanine (Fmoc-$^{F5}$F) has been shown to independently form supramolecular hydrogels, due in part to enhancement of the types of side chain interactions that are possible based on electronic perturbation of the quadrupole moment of the perfluoronated phenyl ring.[87,273,277] Hydrogels of mixtures of Fmoc-$^{F5}$F and Fmoc-FF tended to form more rapidly than those of either individual component alone and the resulting hybrid hydrogels were more mechanically rigid. The 1:1 Fmoc-$^{F5}$F:Fmoc-FF hydrogel was the most mechanically rigid, with a storage modulus nearly

twenty times greater than that of Fmoc-FF hydrogels and sixty times greater than Fmoc-$^{F5}$F gels. Thus, the multicomponent hydrogels result in synergistic improvement of the overall mechanical properties of the materials compared to the self-assembled gels of the individual components.

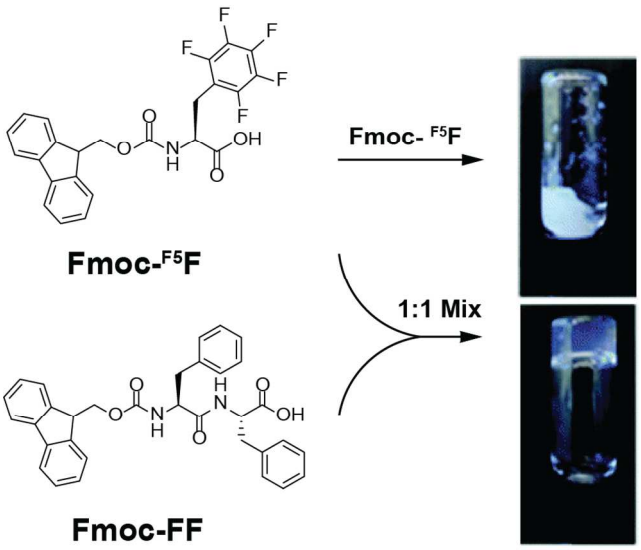


**Figure 16.** Enhanced viscoelastic hydrogels of coassembled Fmoc-$^{F5}$F and Fmoc-FF as indicated by a visual vial inversion test. Figure reproduced from ref 355 (M. Halperin-Sternfeld, M. Ghosh, R. Sevostianov, I. Grigoriants and L. Adler-Abramovich, *Chem. Commun.*, 2017, **53**, 9586–9589)[355] with permission from the Royal Society of Chemistry.

Similarly, Lin *et al*. studied multicomponent hydrogels of *N*-terminal pentafluorobenzyl (PFB) modified FF (PFB-FF, **Figure 14**) coassembled with PFB-F.[356] Hydrogel mixtures at varying gelator ratios (1 wt% total gelator) were assessed to determine the effects of coassembly on time to gelation and hydrogel viscoelasticity. Generally, increasing the ratio of PFB-FF was found to result in increasing hydrogel storage moduli. The 1:1 PFB-FF:PFB-F hydrogel was noteworthy in that it formed a semi-translucent gel with an average storage modulus of 3 kPa at neutral pH, making it well-suited for application as a cell culture scaffold. Based on these emergent properties, this hydrogel was assessed for compatibility with CTX TNA2 astrocytes and MCF-7 breast cancer cells. Cell survival rates over 72 hours were 50% and 80% respectively

when seeded on the 1:1 PFB-FF:PFB-F gels. This work illustrates the cooperative effects of coassembly to tune hydrogel gelation at physiologic pH with emergent properties that support cell culture applications.

Several groups have utilized the fibronectin-derived RGD motif in coassembled di- and tripeptide supramolecular assemblies for the formation of synthetic cell responsive biomaterials. Since RGD and other cell signaling motifs facilitate cell adhesion, multivalent display of these ligands throughout a hydrogel provides a scaffold that more closely mimics natural extracellular matrix.[218,357–361] Nisbet *et al*. investigated the coassembly and hydrogelation of two short Fmoc-derivatized peptides in which the assembly motif was modified with either the fibronectin RGD or laminin IKVAV sequences.[362] Each of these ligands are common components of mammalian extracellular matrix (ECM)[18,363] and incorporation into a multicomponent hydrogel was hypothesized to provide a synergistic effect to improve the material as a cell culture scaffold. Coassembled hydrogels of Fmoc-FRGDF and Fmoc-DIKVAV supported the *in vitro* growth and viability of C212 myoblast cells more effectively than either of the self-assembled hydrogels of the individual components, or hydrogels in which the components were pre-assembled separately and then mixed (**Figure 17**).

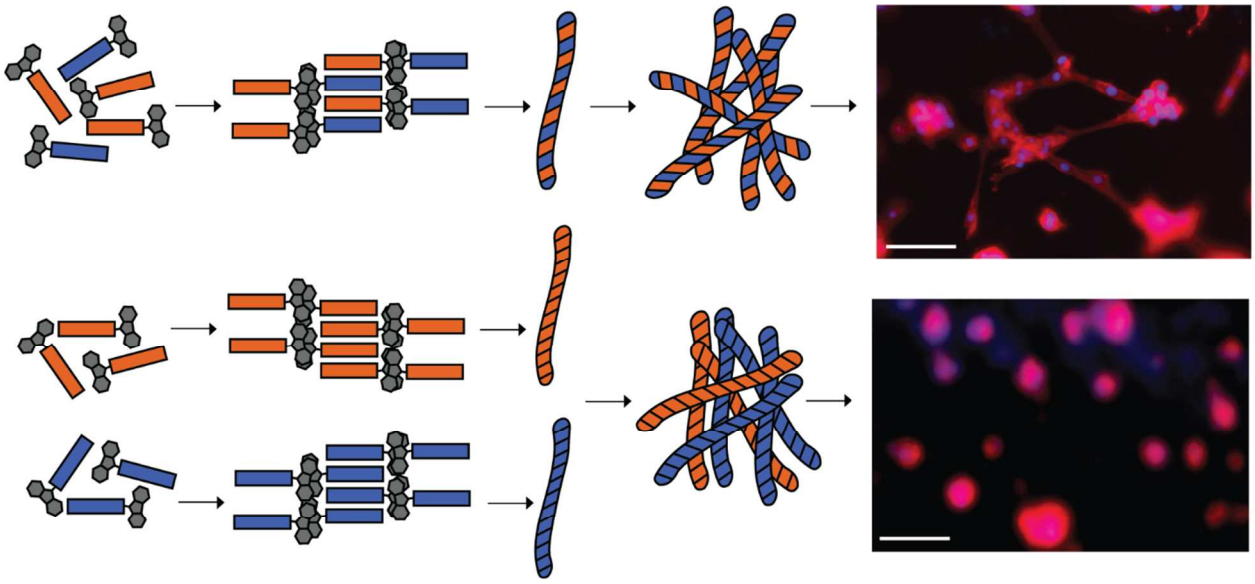

**Figure 17.** C212 myoblast cell culture on coassembled hydrogels displaying RGD and IKVAV peptides (depicted by orange and blue rectangles respectively) (top image). Cell culture did not produce as many healthy cells when cultured on hydrogels that were formed where the peptide components were pre-assembled separately and then mixed together (bottom image). Figure reprinted from C. C. Horgan, A. L. Rodriguez, R. Li, K. F. Bruggeman, N. Stupka, J. K. Raynes, L. Day, J. W. White, R. J. Williams and D. R. Nisbet, *Acta Biomater.*, 2016, **38**, 11–22,[362] © (2016) with permission from Elsevier.

Ulijn and coworkers also developed coassembled Fmoc-RGD-containing LMW hydrogels to mimic extracellular matrix for improved tissue engineering applications.[364,365] Multicomponent hydrogels of coassembled Fmoc-FF and Fmoc-RGD peptides provided a network that effectively displayed the fibronectin RGD motif to improve cell adhesion. These coassembled hydrogels were tested in a three-dimensional cell culture system using human adult dermal fibroblasts. After 14 days, cells remained viable and had deposited their own dense networks of fibronectin and collagen within the artificial Fmoc-FF/Fmoc-RGD hydrogel network. Comparison of cell viability on Fmoc-FF/Fmoc-RGD gels with Fmoc-FF/Fmoc-RGE (an analogue of RGD) gels showed preferential adhesion and viability for the native RGD-presenting hydrogel fibrils. These systems utilize the Fmoc-FF assembly motif to provide the

mechanical stability of the gel while the Fmoc-RGD assembly partner tunes the cellular biocompatibility of the gel.

Nilsson *et al*. have designed coassembled gels of Fmoc-fluorinated phenylalanine derivatives, Fmoc-3F-FR and Fmoc-3F-FD dipeptides in an attempt to spatially control presentation of the R and D side chains to mimic fibronectin in cell culture applications.[361] Based on structural models of self-assembled fibrils of Fmoc-F derivatives, it was hypothesized that the side chains of the appended R and D residues would be presented at the surface of the coassembled Fmoc-3F-FR/Fmoc-3F-FD hydrogels (**Figure 18**). At neutral pH, the complementary positive and negative charges of the R and D residues respectively would assist in imposing a supramolecular structure in which the R and D residues alternate at the fibril surface. Based on this hypothetical packing structure, it was expected that the spatial presentation of R and D would mimic that in the RGD motif in fibronectin and facilitate cellular adhesion to the gel by integrin-binding. This hypothesis was confirmed based on the observation that NIH 3T3 fibroblasts adhered to gel fibers and were viable over 5 days in systems in which Fmoc-3F-FR and Fmoc-3F-FD were coassembled in near equimolar ratios. Integrin-binding assays further confirmed that interactions of cellular integrins with the gel network were crucial hydrogel biocompatibility. This work is an example of structure-based design in the development of coassembled multicomponent peptide materials.

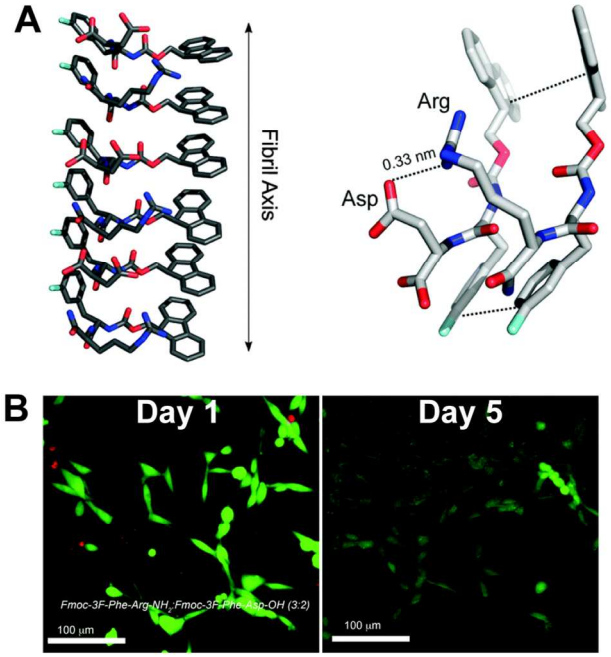


**Figure 18.** (A) Molecular model of the proposed packing architecture of Fmoc-3F-FR and Fmoc-3F-FD into multicomponent fibrils (left) and expanded model of a possible orientation and contacts between Arg and Asp residues. (B) Confocal microscopy images of NIH 3T3 fibroblast cells cultured on hydrogels of Fmoc-3F-FR: Fmoc-3F-FD (3:2) over the course of 5 days. Live/dead stained images indicate live cells in green and dead cells in red. Figure reproduced from ref 361 (W. Liyanage, K. Vats, A. Rajbhandary, D. S. W. Benoit and B. L. Nilsson, *Chem. Commun.*, 2015, **51**, 11260–11263)[361] with permission from the Royal Society of Chemistry.

Following early work identifying the structurally diverse supramolecular assemblies formed from aromatic dipeptides and their *N*-terminal Fmoc-modified variants, Ulijn *et al.* surveyed a range of Fmoc-dipeptides as potential supramolecular gelators for cell culture scaffolds.[366] They postulated that spontaneous self-assembly of Fmoc-dipeptides could be tailored to form fibrous networks that formed self-supporting hydrogels at neutral pH. Investigation of the self-assembly of various Fmoc-dipeptides led to the discovery of a number of morphologically distinct fibrous networks that varied in fibril diameter and pH initiation. Three formulations were found to form stable, self-supporting hydrogels at neutral pH: Fmoc-FF, Fmoc-FF/Fmoc-Gly-Gly, and Fmoc-FF/Fmoc-Lys. All three gels were found to

support proliferation and retention of phenotype in both two- and three-dimensional bovine chondrocyte cell culture experiments with the positively charged Fmoc-FF/Fmoc-Lys gel facilitating more effective cell growth.

These experiments led to further investigation of the displayed chemical functionality that is best suited for *in vitro* cell culture.[367] It is known that tuning hydrogel properties for specific cell types is possible by altering the either the surface charge of the gel material or by altering the mechanical properties of the gel.[368–370] Chemical functionality was introduced into Fmoc-FF hydrogel networks by coassembling with Fmoc-Lys, Fmoc-Ser, or Fmoc-Asp to modify the surface charge on the resulting fibrous network. The hydrogels formed from all mixtures were composed of densely packed fibers of varying thickness that correlated to the coassembly partner. The average fibril diameters were 32, 51, and 58 nm for Fmoc-FF/Fmoc–Lys, Fmoc-FF/Fmoc-Ser, and Fmoc-FF/Fmoc–Asp gels respectively. The mechanical rigidity of each gel was determined by rheological analysis and revealed a range of storage moduli from 0.5–21 kPa where Fmoc-FF/Fmoc-Asp << Fmoc-FF/Fmoc-Ser < FmocFF/Fmoc-Lys < Fmoc-FF. Each gel type was investigated for the ability to support cell culture of three different cell types (chondrocytes, mouse fibroblasts, and human fibroblasts). Each of the gels were reasonable cell culture scaffolds for specific cell types, but only the Fmoc-FF/Fmoc-S hydrogel supported the general growth and proliferation of all three cell types over at least three, and up to seven days. This work demonstrates the utility of multicomponent coassembly to tailor the emergent viscoelastic and biochemical properties of supramolecular hydrogels.

These studies prompted further investigation of the Fmoc-FF/Fmoc-Ser supramolecular hydrogels.[371,372] The structure of the Fmoc-FF/Fmoc-S coassembled hydrogels was determined

to be a core/shell arrangement in which the fibril interior was stabilized by hydrophobic interactions while the polar side chains of the surfactant-like Fmoc-Ser molecules were displayed at the surface of the nanofibers. These core/shell nanofibers are noncovalently cross-linked in the presence of cell culture media to result in hydrogelation via dense fibrous network formation. The display of the serine hydroxyl group at the fibril surface provides beneficial interactions with both the medium and cell surfaces. Stem cell differentiation is strongly influenced by the mechanical properties of surrounding tissues or scaffolds.[373,374] In order to apply these hydrogels to stem cell culture, efforts to tune the viscoelasticity of the gel were pursued. Varying the relative concentrations of Fmoc-FF and Fmoc-Ser in the binary mixtures led to highly tunable gel stiffness ranging from 0.1 kPa to 32 kPa, which enabled stiffness-directed mesenchymal stem cell differentiation.[372] The available polar functionality and tunable mechanical properties of these hydrogels makes them suitable candidates for the chondrogenic induction of pericytes (perivascular stem cells). These cells are highly abundant in adipose tissue and therefore a better candidate for cartilage tissue engineering than the more costly and time consuming method of isolating mature chondrocytes from the differentiation of mesenchymal stem cells.[375] To this end, MSCs and pericytes were cultured on Fmoc-FF/Fmoc-Ser hydrogels containing dilute concentrations of molecules (including lysophosphatidic acid and cholesterol sulfate) that direct stem cell differentiation. The combination of tunable gel stiffness and bioactive molecule additives was found to stimulate individual metabolic pathways for targeted cell differentiation starting from both autologous MSCs and pericytes.

With this foundation, a more focused study on the differentiation of pericytes was conducted by altering the mechanical and chemical properties of the cell culture peptide hydrogels.[376] Pericytes were monitored over a long-term (five weeks) 3D cell culture experiment

on an Fmoc-FF/Fmoc-Ser hydrogel tuned to a storage modulus of 15.5 kPa, similar to that found in chondrons. Cellular expression levels were assessed for four different cartilage biomarkers up to 35 days and all biomarker levels were highest for cells cultured in Fmoc-FF/Fmoc-S gels in the presence of chondrogenic induction medium. Interestingly, collagen X biomarkers were present in significantly higher amounts than collagen II biomarkers in the cells cultured on these gels with the chondrogenic induction medium, suggesting a greater population of hypertrophic chondrocytes. This versatile system highlights the advantages of adaptable coassembled LMW peptide properties for fostering growth and specific cell differentiation.

### 3.3 Other Coassembled Low Molecular Weight Peptide Systems

In addition to cell culture and tissue engineering, coassembled materials produced from LMW peptides have been used in other applications over the last 10 years. These applications include artificial hydrolase mimetics;[377] immobilization of gold nanoparticles onto FF derived hydrogels for catalytic reduction of 4-nitrophenol;[378] formation of "sticky tubes" and magnetic hydrogels through coassembly of FF with melanin-derived polydopamine (PDA) spheres or core-shell PDA-$Fe_3O_4$ magnetic spheres;[379] and synthesis of two-component charge transfer organogels via coassembly of p-type tetrathiafulvalene-FF and various electron acceptor molecules.[380] In this section we will present representative examples of multicomponent coassembled LMW hydrogelators for biocatalysis and energy transfer applications.

A coassembly strategy has been used for the development of biocatalytic microspheres.[381] In order to produce multicomponent gel microparticles to immobilize biocatalytic enzymes, Ulijn and coworkers developed a combined coassembly/Pickering emulsion strategy. Pickering liquid-

liquid emulsions are emulsions that are stabilized by solid particles confined to the liquid-liquid interface.[382] Ulijn *et al*. found that Fmoc-amino acids (Fmoc-S, D, K, or Y) coassembled with Fmoc-FF formed functionalized peptide microgel spheres 120 nm in diameter when emulsified by hydrophobic $SiO_2$ nanoparticles (**Figure 19**). This is in contrast to the nanotubes and tapes formed from Fmoc-FF/Fmoc-S, D, K, or Y coassemblies formed without $SiO_2$ present. Lipase B, an esterase, was immobilized into the microgel particles. Catalytic esterification of octanol and octanoic acid in heptane by these microspheres was observed. The polarity of the functional groups of the Fmoc-X derivative in the coassembled microgels had an effect on the catalytic activity of the immobilized enzyme. This was evidenced by decreasing esterification reaction rates exhibited by increasing hydrophobicity of the emulsified gels in the order Fmoc-FF/Fmoc-S gels < Fmoc-FF/Fmoc-D < Fmoc-FF/Fmoc-K < Fmoc-FF/Fmoc-Y. This strategy enables the design of microgel particles that mimic natural biocatalytic systems.

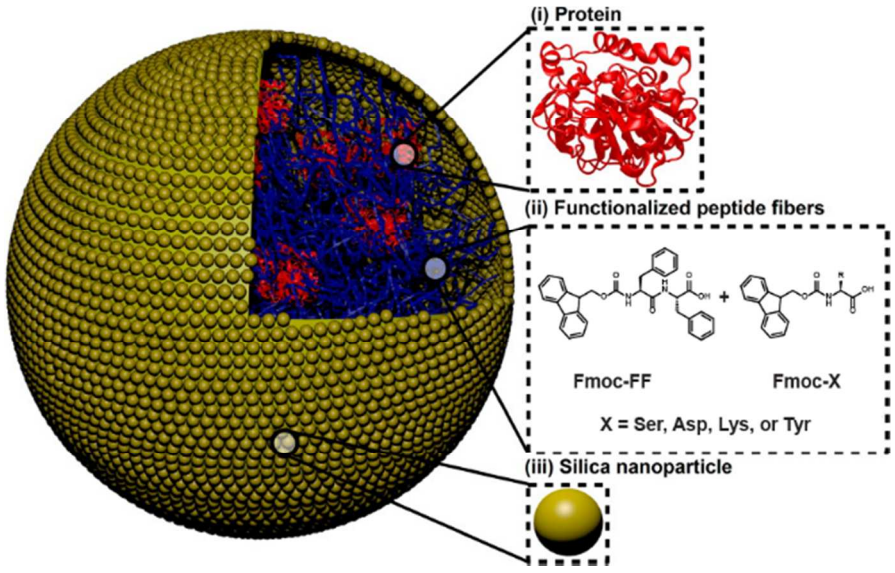


**Figure 19.** Structural model of immobilized Lipase B (red) in coassembled Fmoc-FF/Fmoc-X microgels (blue) stabilized in a Pickering emulsion via solid silica nanoparticles (gold). Figure adapted with permission from G. Scott, S. Roy, Y. M. Abul-Haija, S. Fleming, S. Bai and R. V. Ulijn, *Langmuir*, 2013, **29**, 14321–14327.[381] © 2013 American Chemical Society.

Ulijn and coworkers have also conducted studies to exploit biocatalysis to direct the coassembly of Fmoc-diaromatic peptides.[383–385] Peptides containing phosphorylated Tyr (Y*p*) have been shown to undergo self-assembly and hydrogelation upon dephosphorylation by phosphatases.[386–390] Ulijn showed that phosphatase treatment of mixtures of Fmoc-FY*p* with Fmoc-S, Fmoc-T, or Fmoc-RGD provided a multicomponent fibrous hydrogel network under physiological conditions upon conversion of Fmoc-FY*p* to Fmoc-FY.[383] The mechanical properties of the resulting gels could be controlled by modifying the concentrations of enzyme used. Higher enzyme concentrations led to faster dephosphorylation kinetics and more elastic gels for Fmoc-FY*p*/Fmoc-T and Fmoc-FY*p*/Fmoc-RGD coassemblies. The opposite effect was seen with Fmoc-FY*p*/Fmoc-S coassembled gels. These studies highlight the complexity of the correlation between dephosphorylation kinetic rates and coassembly/gel formation in these multicomponent coassemblies. This complexity warrants further investigation to more completely explain how these factors influence the emergent properties of the resulting materials.

Ulijn has also investigated the enzyme-promoted coassembly of LMW peptides appended to organic donor and acceptor molecules to create novel charge-transfer assemblies.[391] Specifically, coassembly of diaromatic peptides conjugated to semiconducting naphthalenediimide (NDI-XY) acceptor molecules with various π-electron rich donors such as dialkoxy/hydroxyl/amino-naphthalene or pyrene derivatives (**Figure 20**) was explored. It is often challenging to predict the ideal dipeptide sequences that will provide the most stable coassembled structures. To address this challenge, Ulijn *et al*. employed an enzyme-modulated dynamic combinatorial library approach to form thermodynamically stable dipeptide/acceptor molecule combinations *in situ* from a pool of amino acids. Dipeptides formed in the presence of

amide-bond forming enzymes that can undergo coassembly with partner molecules in solution will be removed from the pool as they spontaneously coassemble under the reaction conditions. The reversible formation of dipeptides conjugated to acceptor molecules was accomplished by mixing NDI-Tyr with a pool of X-$NH_2$ amino acid amides (X= Tyr, Phe, Leu, Val, Ala, and Gly) in the presence of thermolysin. Thermolysin reversibly forms amide bonds in a promiscuous manner. The resulting dipeptide-acceptor monomers that can coassemble with various electron rich donor molecules, including dialkoxy and hydroxyl/amino naphthalenes, are selected for by removal from solution upon coassembly. The most stable charge transfer combinations of donor/acceptor-peptide assemblies were then identified. It was discovered that NDI-YF and NDI-YL derivatives effectively coassembled with 1,5-diaminonaphthalene to form multicomponent one-dimensional charge-transfer fibers in aqueous solutions. This study illustrates the potential of library-based methodologies to create functional multicomponent materials.

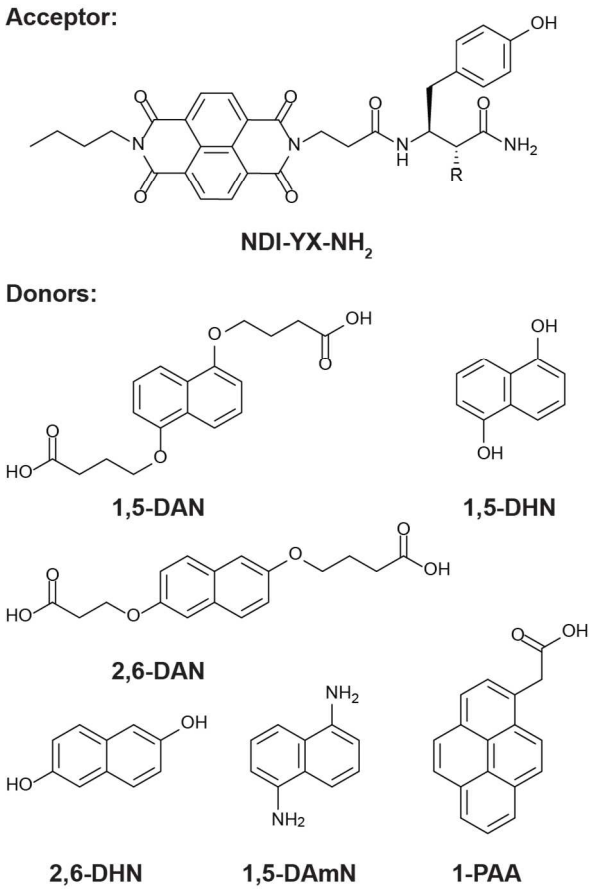


**Figure 20.** Chemical structures of a π-electron acceptor thermolysin-catalyzed products between NDI-Y and X-$NH_2$ where X = Tyr, Phe, Leu, Val, Ala, or Gly. Chemical structures of partner donor molecules 1,5- and 2,6-dialkoxy naphthalenes (1,5- and 2,6-DAN), 1,5-diamino naphthalene (1,5-DAmN), 1,5- and 2,6-dihydroxy naphthalenes (1,5- and 2,5-DHN), and pyrene acetic acid (1-PAA) that were mixed with NDI-YX-$NH_2$ derivatives to create stable coassembled charge transfer peptide libraries.[391]

Unmodified tripeptides have also been developed that undergo multicomponent coassembly.[392–394] Ulijn and Tuttle have leveraged combined theoretical and experimental methods to identify tripeptides that effectively self-assemble into supramolecular hydrogels. They have subsequently used this approach to identify tripeptides that undergo cooperative coassembly to provide copper-binding structures that undergo gelation in the presence of copper ions.[394] Specifically, they sought conditions under which FFD, a previously identified self-assembling peptide, would coassemble with GHK, a non-self-assembling, copper-binding

peptide derived from extracellular matrix proteins.[394] They found that equimolar mixtures of GHK and FFD formed homogenous, clear solutions, but that spontaneous hydrogelation occurred in the presence of stoichiometric amounts of $CuCl_2$. The hydrogelation was found to be specific to copper-binding as hydrogelation was not observed in the presence of zinc or cobalt ions. In addition, these multicomponent tape-like assemblies were distinct from the random aggregates formed by GHK alone and the nanotubes formed by FFD alone. Computational modeling of the coassembly mechanisms suggests that FFD forms a bilayer structure with the negatively charged aspartate groups at the surface. The positively charged GHK peptides are then organized at the surface of this FFD bilayer due to complementary charge effects. Copper-binding is facilitated by the G and H residues of GHK. These materials have potential for application in cosmetics and skin treatments based on prior observations that GHK-copper complexes facilitates cellular uptake of copper and subsequent angiogenesis. This cooperative coassembly that is promoted by specific solution ions is an interesting illustration of combined theoretical and experimental strategies in the design and evaluation of functional multicomponent peptide-based materials.

In addition to the studies discussed above in this section, LMW peptide hydrogel materials are also often investigated as nanocarrier systems to bind and/or encapsulate drugs[395–404] or organic dye molecules.[405–409] Technically, LMW hydrogels impregnated with small molecules are multicomponent materials. However, the small molecules in these systems are often not intimately associated with the supramolecular hydrogel scaffold but are merely suspended within the network. As such, we will not include a detailed discussion of these types of hydrogel delivery systems herein and direct the reader to other articles that focus specifically on these systems.[34,38,410–417] Instead, we have limited our discussion to multicomponent systems

in which the various components are shown to be co-integrated into the assembled structure in a manner that accounts for the properties of the material.

### 3.4 Multicomponent Materials of Coassembled Low Molecular Weight Peptides and Proteins

The coassembly of LMW peptides with macromolecules has been shown to influence the supramolecular properties of the resulting materials through cooperative assembly.[418–420] This cooperative binding can strengthen or diversify ubiquitous supramolecular network formation during LMW peptide assembly. Often, natural macromolecular systems can form compartmentalized architectures through self-assembly and phase-separation of dissimilar molecular components.[421–423] Some examples have been reported of controlled phase separations via the mixture of peptidic components with various macromolecular systems, including perfluorinated phospholipids,[424,425] surfactants,[426] or polymeric molecules.[427] While these systems show great potential in the generation of novel multicomponent materials, in this section we will limit our discussion specifically to coassembled, cooperative structure formation through interaction between LMW peptides and proteins as a method for modifying the mechanical properties of the resulting materials.

Ulijn and Sefcik examined protein templating and binding effects on the assembly of Fmoc-dipeptides.[428] These studies were conducted with dilute $\beta$-lactoglobulin and bovine serum albumin (BSA) protein clusters at lower protein concentrations than would normally exert crowding effects in the context of assembly phenomena. The assembly behavior of a collection of self-assembling Fmoc-protected dipeptides (Fmoc-YN, Fmoc-YS, Fmoc-YL, and Fmoc-VL)

having a range of charge and hydrophobic character was assessed in the presence of either β-lactoglobulin or BSA. Cooperative effects of the proteins Fmoc-dipeptide assembly was manifested by a change in chirality of the resulting supramolecular assemblies. This effect was dependent on the amount of protein added. For example, increasing concentrations of β-lactoglobulin induced a change in Fmoc-YL supramolecular structures from right-handed to left-handed twisted fibrils. Similar, though less pronounced, results were seen with the BSA protein. Changing the terminal amino acid of the dipeptide to Asn or Ser (Fmoc-YN or Fmoc-YS) to introduce additional hydrogen bonding capability and reduce hydrophobicity resulted in changes further changes in the chirality of the assembled structures in response to proteins. Fmoc-YN self-assembles into left-handed twisted fibrils, but this handedness switches to right-handed in the presence of β-lactoglobulin or BSA. Similar effects were seen for all dipeptides examined, but the extent of inversion varied from peptide to peptide. In addition, the emergent viscoelasticity of the resulting gels was also altered, although the effects varied as a function of protein identity and peptide sequence. This work gives insight into the complex nature of cooperative assembly in multicomponent environments. All aspects of the environment affect the assembly pathways of supramolecular peptide-based materials, and this investigation illustrates the need for further research to better understand these effects.

Li and coworkers have also examined the assembly of LMW peptides in the presence of proteins.[429] Hydrogels were produced through the assembly of FF in the presence of a range of proteins, including hemoglobin, myoglobin, bovine serum albumin, human serum albumin, and fibrinogen. These studies were also conducted in the presence of glutaraldehyde, which can form dynamic covalent imine bonds to further cross-link the FF/protein network. Gelation occurred in all peptide/protein mixtures over varying times with FF-hemoglobin (FF-Hb) forming most

readily in 4 hours and resulted in a hydrogel with the highest degree of pH-responsiveness. It was found that all three components at nearly neutral pH were required for dynamic bond formation and hydrogelation to occur. FF-Hb hydrogels were found to be pH responsive in that the proteins were released from the hydrogel upon gel-sol transition without secondary structure interruption of the native proteins. Upon changes in pH from neutral to acidic, the Schiff base dynamic bonds were disrupted and the protein-peptide gels gradually degraded, whereas changes to basic pH resulted in deprotonation the carboxylic acids of the peptides and led to quicker gel collapse. These pH adaptive hydrogels could also encapsulate small molecules such as CdTe quantum dots, citrate-modified gold nanoparticles, and water soluble dyes without disruption of the gel network demonstrating their versatility as a hydrogel system and adaptive guest molecule incorporation. A hydrogel was also formed via the coassembly of glucose oxidase into the FF-Hb hydrogel network to effectively produce a hydrogel capable of oxidizing glucose into gluconic acid and $H_2O_2$. This resulted in protonation events from the released gluconic acid and subsequent hydrogel collapse demonstrating formation of a bioresponsive hydrogel. These hydrogels formed between LMW peptides and proteins further illustrate the effect of cooperative environmental effects on supramolecular assembly.

While many self-supporting hydrogels of FF-containing multicomponent mixtures have been reported, many yet lack the ideal mechanical and rheological properties for *in vivo* applications.[274] One such property is shear-responsive behavior, which enables injection of the hydrogels into living organisms for applications such as drug delivery. Yan *et al*. have addressed this problem using a multicomponent supramolecular hydrogel composed of Fmoc-FF with positively charged poly(L-lysine) (PLL) polymers.[54] The coassembly of these oppositely charged components produced a shear-thinning, injectable hydrogel that maintains the helical nanofiber

structure of self-assembled Fmoc-FF. The coassembled hydrogels displayed tunable mechanical properties in response to varying the molecular weight of PLL. Often, protein and peptide immunomodulatory agents can bind and affect antigen-specific T-cell surface receptors to elicit autoimmune responses.[430–432] These hydrogels were investigated for their effectiveness as vaccines in mice due to their similar helical structure to fimbrial antigens that elicit T-cell response. Injections of Fmoc-FF/PLL hydrogels were found to activate auto-immune responses through T-cell recognition of specific geometrically defined fibers raising antitumor activity *in vivo* in tumor-bearing mice. Increased ratios of CD4+/CD8+ T-cells were observed in mice injected with the hydrogels which is often an indication of antigen-specific T-cell response. Mixing Fmoc-FF with poly(L-lysine) provided hydrogels with improved shear-thinning properties as a function of highly ordered, fibrous structure formation between electrostatically charged components, further illustrating the advantages of multicomponent peptide systems as next-generation materials and possible vaccines.

### 3.5 Coassembly of LMW Peptides with Organic Molecules: Peptide/Porphyrin Multicomponent Assemblies

Peptides have also been coassembled with nonpeptidic organic molecules. For example, the coassembly of peptides with photosensitizer molecules has emerged for a number of applications, including light harvesting and photocatalysis,[433–436] DNA sensing,[437] biomimetic materials,[438–440] and drug delivery and anti-tumor therapy.[441–443] Porphyrins are macrocyclic tetrapyrrole photosensitizers found in biological catalytic and light-harvesting systems[444,445] that have been exploited in these types of multicomponent systems due to their inherent photophysical properties.[446,447] While the self-assembly of molecules consisting of a porphyrin

conjugated to a peptidic component has been studied for various applications,[433,440,443,448,449] this section will focus on a the coassembly of low molecular weight peptides and porphyrins into hybrid supramolecular structures.

Yan and Möhwald *et al.* have taken advantage of the inherent self-assembly of cationic dipeptides in order to design coassembled systems for the organization of porphyrin molecules to form structures for light-harvesting and photocatalysis.[434–436] They envisioned the coassembly of the cationic dipeptides FF and KK with a sulfonated porphyrin, tetrakis(4-sulfonatophenyl)porphine ($H_2$TPPS) (**Scheme 1**), based on Coulombic attraction between the negatively charged sulfonic acid groups on the porphyrin and the cationic amines of the dipeptides. In aqueous solutions at pH 2 FF is net cationic at the *N*-terminus and $H_2$TPPS is dianionic due to negatively charged sulfonic acid groups and positively charged pyrrole nitrogens.[450] Coassembly of FF-$NH_2$:$H_2$TPPS into one-dimensional nanorods was observed at 2.3:1 stoichiometric ratios of peptide to porphyrin.[434] UV-vis spectroscopy was used to identify the presence of J-aggregates formed from stacking of the $H_2$TPPS porphyrin groups. These experiments indicated that the porphyrin groups stack into core fibrils that are then encased in an FF assembly that forms a shell around the J-aggregates to give elongated nanorods (**Scheme 1**). These nanorods subsequently associate to form microporous spheres 3-5 μm in diameter (**Scheme 1**).

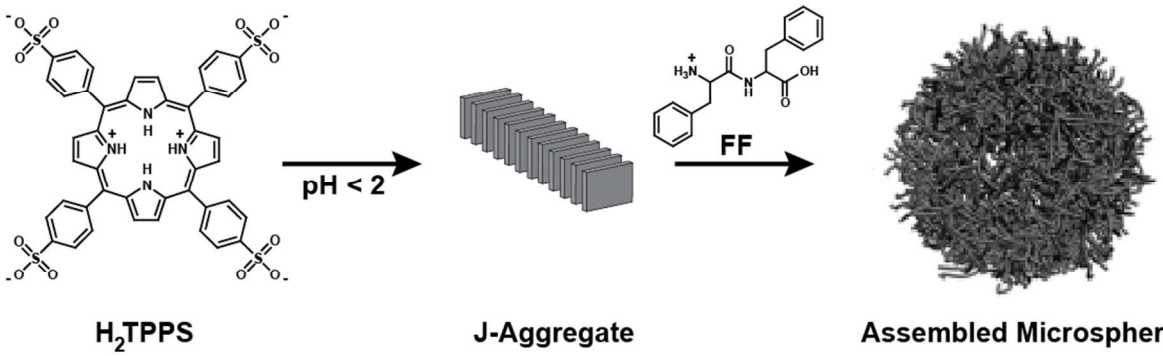

**Scheme 1.** $H_2$TPPS assembles into J-aggregates in aqueous solutions below pH 2. In the presence of cationic FF, electrostatic interactions and π-stacking allow for the formation of core-shell nanorods with $H_2$TPPS forming the core and FF forming the shell layer. These nanorods further aggregate into microporous spheres. Scheme adapted with permission from Q. Zou, L. Zhang, X. Yan, A. Wang, G. Ma, J. Li, H. Möhwald and S. Mann, *Angew. Chemie Int. Ed.*, 2014, **53**, 2366–2370.[434] 

The coassembly of the $H_2$TPPS porphyrin system with the KK dipeptide was also examined.[435] KK and $H_2$TPPS coassembled into long fiber bundles several μm in width and tens–hundreds of μm in length. These KK/$H_2$TPPS aggregates were distinct from the 20–30 nm wide nanorods formed from self-assembled $H_2$TPPS J-aggregates.[451] Both KK/$H_2$TPPS and FF/$H_2$TPPS coassembled systems were investigated as light-harvesting photocatalytic materials. The FF/$H_2$TPPS and KK/$H_2$TPPS coassembled structures effectively captured visible light and facilitated the photocatalytic synthesis of Pt nanoparticles in the presence of ascorbic acid as an electron donor. These coassembled peptide-porphyrin systems enhance the control and stability of porphyrin J-aggregates for photocatalytic activity.

Porphyrins are proposed prebiotic precursors to early life and photosynthetic organisms.[452,453] As such, Yan and Möhwald proposed that multicomponent hydrogen-producing materials may have arisen under prebiotic conditions. To test this hypothesis, KK and $H_2$TPPS were mixed under simulated prebiotic conditions (pH 2, 70 ºC, in the presence of $Na^+$, $Ti^{4+}$, $Pt^{2+}$, etc.).[454] Under these conditions, KK and $H_2$TPPS form core-shell nanorods that underwent extensive fiber bundling which increased with the addition of NaCl to shield like charges and facilitate fiber growth and aggregation. Mineralization of both $TiO_2$ and Pt nanoparticles on the KK/$H_2$TPPS nanofibers was observed. The hybrid fibers capture light and were also shown to enable photoactivated charge separation to interfacial $TiO_2$ and Pt nanoparticles, demonstrating potential for these materials to act as reaction centers. Light-generated $H_2$ production was also

observed in the presence of the KK/$H_2$TPPS/$TiO_2$/Pt biomineralized fibers. This peptide-porphyrin coassembly is an interesting example of a photobacteria-like biomimetic system similar to one that may have evolved under prebiotic conditions.

## Section 4. Organopeptide Hybrids

Supramolecular materials composed of organopeptide hybrids composed of self-assembling peptides conjugated to nonnatural organic functionality have also been developed. In these materials, the organic components tethered to peptide elements either assist in directing assembly or elicit novel emergent properties in the resulting materials. The unique emergent properties of self-assembled organic peptide hybrids that are instilled by the organic components include novel photophysical properties and charge transfer capability. Notable examples of supramolecular organopeptide hybrid materials include Stupp's peptide amphiphiles,[43,105,455–458] discotic peptides,[459–461] and polyaromatic peptide hybrids.[67,462,463] As with previously discussed materials, multicomponent coassembly of organopeptide hybrids can lead to novel materials with unique properties. Some of the coassembled materials discussed in section three also fit the technical description of organopeptide hybrids; this section will focus on specifically on longer organopeptides with specifically defined secondary structure and the influence that the organic components have on the resulting multicomponent materials.

### 4.1 Peptide Amphiphiles

Stupp's peptide amphiphiles (PAs) are a prominent and versatile class of self-assembling organopeptide hybrids.[43,105,455–458] PAs are typically composed of a $\beta$-strand peptide segment bound to a hydrophobic modifier, often a long chain alkyl group (**Figure 21A**). PA self-assembly

is promoted by hydrophobic collapse of the alkyl group in aqueous solution to provide a micelle-like hydrophobic core, which facilitates one-dimensional $\beta$-sheet formation by the appended peptides to give supramolecular nanofibers with high aspect ratios (**Figure 21B**). When biological signal motifs are included as elements in the design of PAs, the resulting self-assembled structures can be used as scaffolds for an impressive array of biomedical applications, including progenitor cell differentiation,[464] regenerative tissue engineering,[465] hydrogel platforms for neurite outgrowth and cell migration,[466] and injectable anti-hemorrhagic nanofiber networks.[467] As discussed with $\beta$-sheet coassembled peptides, these materials are sometimes self-assembled structures, but are often multicomponent statistical mixtures of functionalized and unfunctionalized PAs that enable the multivalent surface display of bioactive motifs on PA nanofibers. This section will discuss efforts to utilize mixtures of PAs in coassembly strategies to impart desired function to the resulting materials.

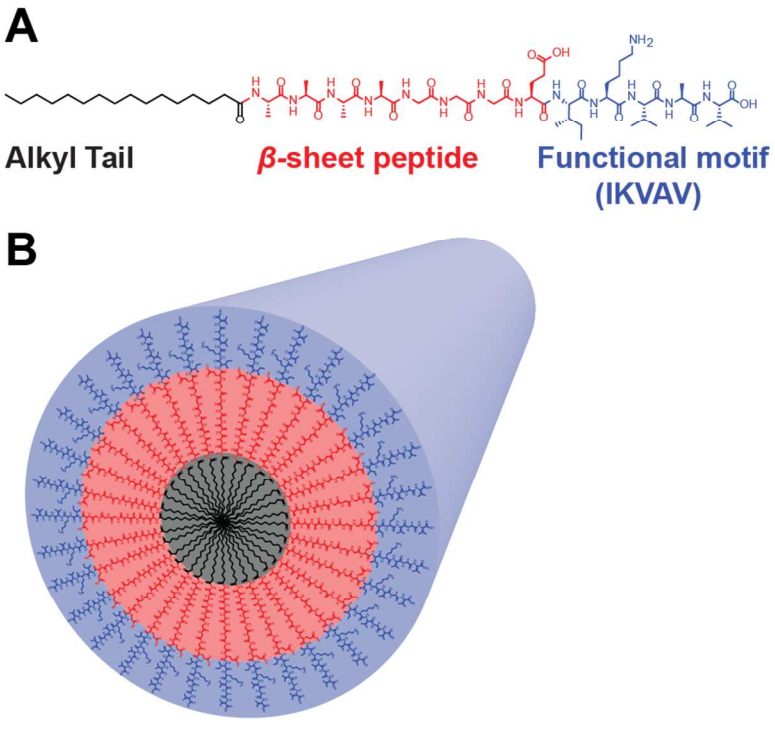


**Figure 21.** (A) Chemical structure of Stupp's peptide amphiphile containing a hydrophobic segment (black), a $\beta$-strand peptide (red), and biological signal motif (laminin derived –IKVAV sequence)

(blue).[464] (B) Pictorial representation of the self-assembly of functionalized peptide amphiphiles into high aspect ratio nanotubes with the functional groups displayed on the outer surface.

An example of the statistical coassembly of PA sequences displaying biologically relevant recognition motifs was demonstrated in the creation of materials for cartilage regeneration. Specifically, supramolecular fibers displaying the HSNGLPL peptide that is a binding epitope for transforming growth factor β-1 (TGFβ-1) were expected to promote the chondrogenic differentiation of human mesenchymal stem cells (MSCs) (**Figure 22**).[457] Supramolecular coassemblies were constructed with mixtures of TGF-ligand-bearing PA and unmodified PA to produce nanofibers that display HSNGLPL at the surface in ratios that correlate to the amount of modified PA included in the mixture. These materials were assessed for cell signaling activity that ultimately supported MSC viability and differentiation *in vitro*. Release of the TGFβ-1 growth factor was to occur significantly more slowly from multicomponent PA nanofiber scaffolds with 10% HSNGLPL than from self-assembled PA nanofibers composed only of the unmodified assembly motif. MSCs cultured on HSNGLPL PA coassembled hydrogels indicated enhanced cell viability a period of four weeks. The multicomponent HSNGLPL-bearing fibers were found to effectively promote healing of microfracture chondral defects in rabbits *in vivo*. Self-assembled PA hydrogels without the TGFβ-1 ligand while the presence of filler PA gels did not impede healing, but a significant increase in cartilage matrix regeneration at the wound site was observed when the coassembled TGFβ-1 ligand gels were applied.

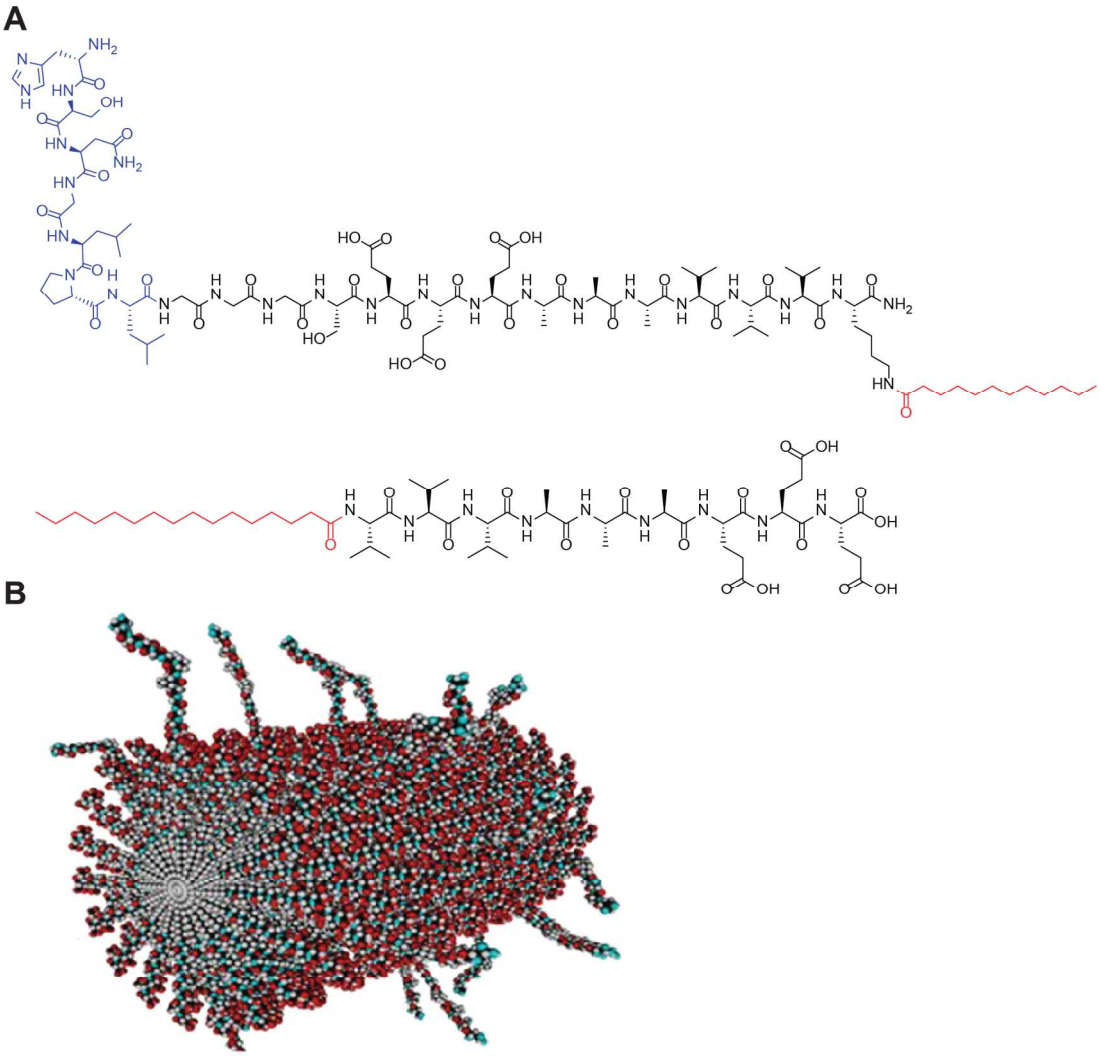


**Figure 22.** (A) Chemical structure of TGF-binding peptide amphiphile (TGF binding sequence in blue, top) and peptide amphiphile filler (bottom) with hydrophobic chains shown in red. (B) Coassembly of peptide amphiphiles into supramolecular nanofibers decorated with the TGF motif. Figure reproduced with permission from R. N. Shah, N. A. Shah, M. M. Del Rosario Lim, C. Hsieh, G. Nuber and S. I. Stupp, *Proc. Natl. Acad. Sci.*, 2010, **107**, 3293–3298.[457]

Multicomponent antitumor PAs were prepared by coassembly of cytotoxic PAs with pegylated PAs.[4] PAs bearing the cationic membrane-lytic $(KLAKLAK)_2$ peptide at the *C*-terminus were mixed with *C*-terminal PEG-bearing PAs. Multicomponent fibrils in with 50% pegylated PA were found to impart a protective effect on proteolytic degradation of the $(KLAKLAK)_2$ sequence on the partner PA without reducing the cytotoxicity of the lytic

peptides. This resulted in coassembled fibrils that were highly serum-stable and that exhibited significant reduction in tumor growth and tumor cell proliferation in tumor-bearing mice. This work demonstrates the great potential of multifunctional coassembled PA nanostructures as versatile materials for *in vivo* biomedical applications.

Stupp *et al*. have also designed multicomponent PA materials in which ordered coassembly is directed by selective interactions between the constituent PAs instead of merely statistically controlled coassembly. One strategy to accomplish this objective has been the use of "reverse" PAs, in which PAs with inverse polarity selectively coassemble (**Figure 23**).[468] Typically, self-assembling PA design places the hydrophobic alkyl chain at the *N*-terminus of the peptide due, in part, to the ease of solid phase synthesis on resin. Self-assembly of these PAs gives parallel *β*-sheet structures within the *β*-sheet segments of the assembled nanofibers. By designing "reverse" PAs in which the alkyl chain is appended to the *C*-terminus of the *β*-sheet peptide, Stupp and coworkers create the possibility for formation of antiparallel *β*-sheets when the "reverse" *C*- and *N*-terminal PAs are mixed. One advantage of this coassembled system is that the *N*-terminus of the reverse peptide is left exposed at the fibril surface, increasing the design space for attachment of functional peptides to the resulting nanofibrils. In order to test this design strategy, appropriate peptides were prepared in which coassembly was further biased using a charge strategy in which coassembly partners were either net positive ($K_3$ tag) or net negative ($E_3$ tag) (**Figure 23**). "Reverse" peptides with complementary charges did, in fact, effectively coassemble into two-component fibrils in which on PA exposes its *C*-terminus at the fibril service and the partner PA exposes its *N*-terminus. The utility of this design was demonstrated by the *N*-terminal display of peptides that bind either bone morphogenetic protein-2 (BMP-2) or TGFβ-1 (both important for stem cell differentiation) on "reverse" PAs and

demonstrating the effective display of these ligands on coassembled PA fibrils. This work illustrates the versatility of multicomponent PAs systems with directed coassembly for diversification of the orientation of epitopes display at the nanofibril surface, expanding their potential utility as functional biomaterials.

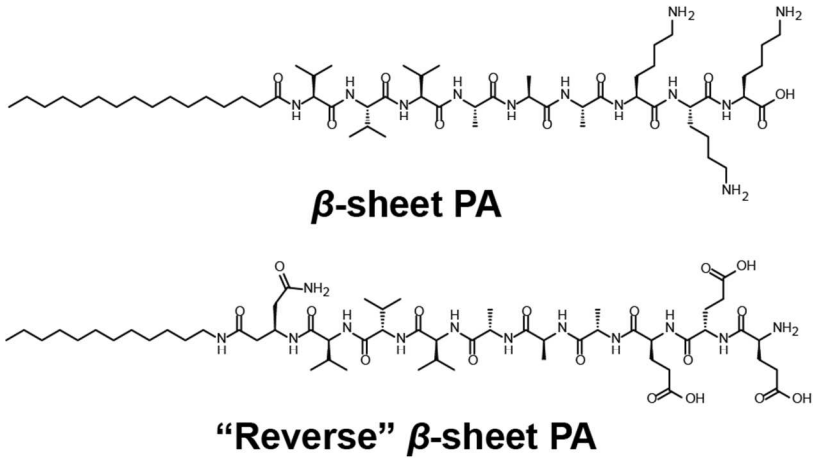


**Figure 23.** Chemical structures of opposite polarity peptide amphiphiles. The top structure represents a traditional PA with a free *C*- terminus and the bottom structure represents a "reverse" PA with a free *N*-terminus.[468]

Stupp and coworkers used a similar charge-based complementarity strategy to induce coassembly of PAs to modulate the fluorescence of an attached chromophore.[469] PAs were synthesized that had either a negatively charged $E_3$ motif or a positively charged $K_3$ motif along with a hydrophilic branched stilbene fluorophore (**Figure 24**). The complementary charge on these peptides induced efficient coassembly into two-component one-dimensional nanofibrils in which the fluorophore was displayed on the hydrophilic exterior. Coassembly was examined at varying ratios of each of the PAs. At equimolar ratios of PAs, the displayed fluorophores were in close proximity, resulting in fluorescence quenching; the characteristic β-sheet structure was also disrupted in comparison to the self-assembled fluorophore-PA. This suggests that intermolecular π-π interactions between fluorophores at the fibril surface are enhanced in these

coassembled materials relative to the self-assembled fibrils. When the fluorophore-PA was included in diluted ratios in binary mixtures, the fluorescence of the fluorophores on the nanofibrils was amplified. In addition, when the non-labeled PA was tagged with a heparin-binding motif, resonance energy transfer was observed between the nanofibril fluorophores and a complementary acceptor on heparin. This demonstrates that coassembly is a highly effective strategy to modulate the photophysical properties of fluorescent multicomponent nanofibrils.

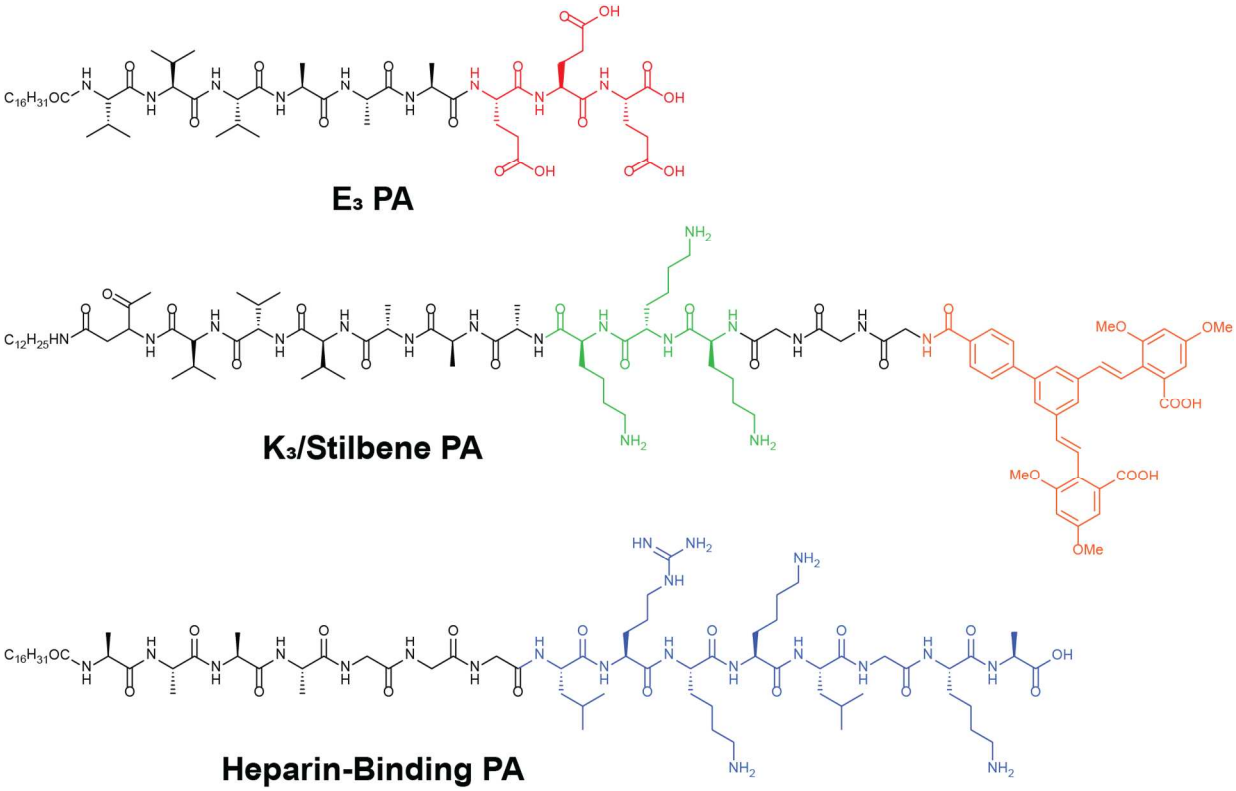


**Figure 24.** Chemical structures of Stupp's $E_3$ PA (Glu residues in red), $K_3$/branched stilbene PA (Lys residues in green, stilbene fluorophore in orange), and heparin-binding PA (heparin binding sequence in blue).[469]

Coassembled PA systems have also been developed which are aimed at affording electroactive fibers through the conjugation and display of organic chromophores on the multicomponent fibrils. Guler *et al*. coassembled both n- and p-type *β*-sheet organopeptide

chromophore hybrids into a single, n/p, electroactive nanowire.[470] Pyrene coupled to the cationic $\beta$-sheet VVAGKK peptide (pPC) was coassembled in various ratios with the anionic VVAGEE conjugated to naphthalenediimide (nPC) (**Figure 25A**). The resulting coassembled n/p nanowires exhibited an increase in fluorescence quenching with increasing amounts of nPC (**Figure 25B**). Electrical measurements also showed that the coassembled structures were significantly more conductive than self-assembled n- or p-type nanowires individually. In this case, coassembly provided PA materials with enhanced emergent photophysical properties.

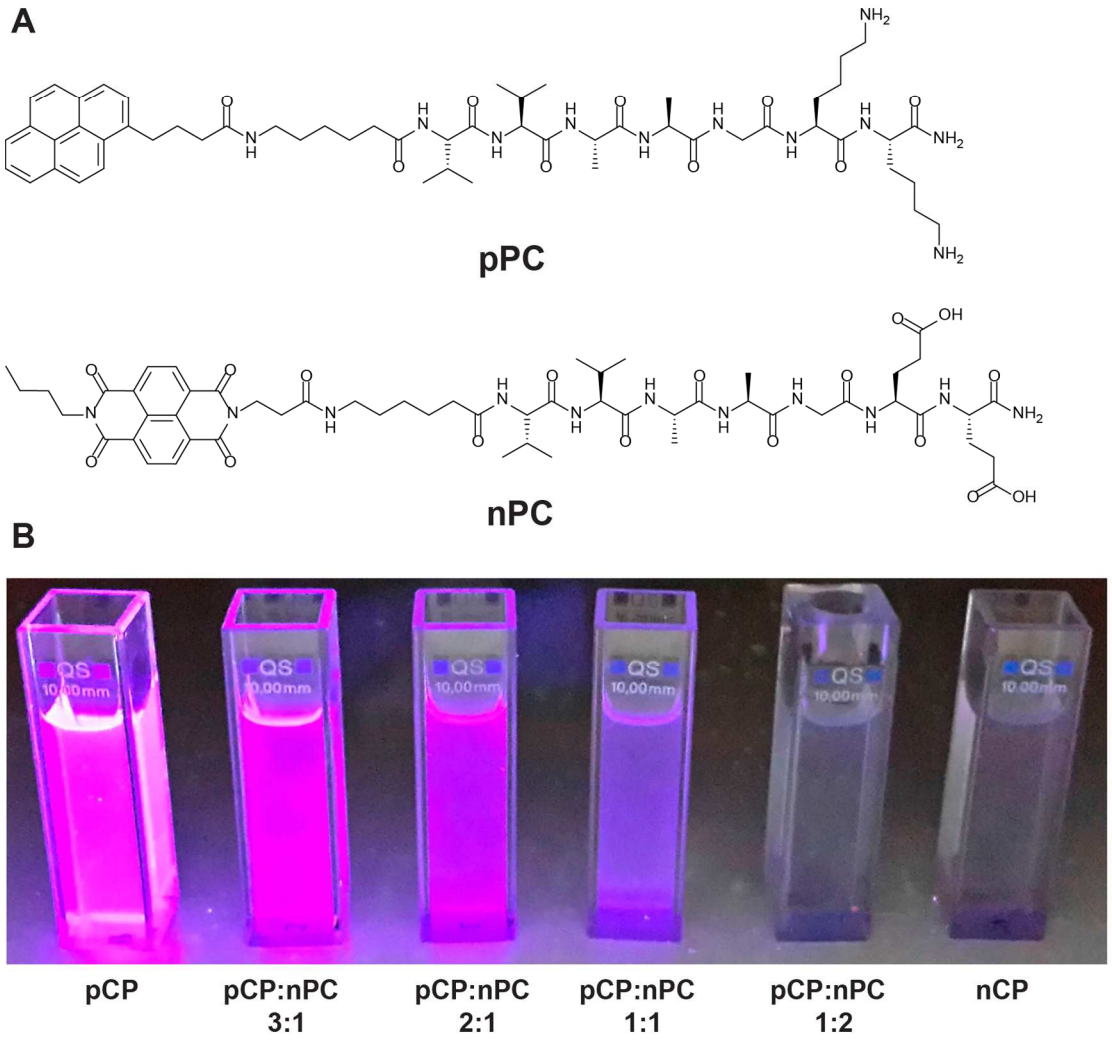


**Figure 25.** (A) Structures of pyrene (pPC) and naphthalenediimide (nPC) conjugated peptides. (B) Increasing ratios of nPC mixed with pCP show higher degree of fluorescence quenching when illuminated under 254 nm light. Figure adapted with permission from M. A. Khalily, G. Bakan, B. Kucukoz, A. E.

Topal, A. Karatay, H. G. Yaglioglu, A. Dana and M. O. Guler, *ACS Nano*, 2017, **11**, 6881–6892.[470] © 2017 American Chemical Society.

Hamley and coworkers have also investigated directed coassembly of PAs using complementary electrostatic interactions.[471,472] The $C_{16}$-KTTKS sequence is a self-assembly PA in which the KTTKS pentapeptide stimulates collagen.[473] The self-assembly of this PA occurs in relatively dilute or basic aqueous solutions. Coassembly of this PA was explored with the oppositely charged $C_{16}$-ETTES PA. Mixtures of these PAs formed slightly opaque hydrogels composed of a network of partially soluble β-sheet nanofibrils. Coassembly was most efficient in aqueous solutions at pH ≈ 5 and proceeded without the addition of salt, which is typically required to induce self-assembly of charged PAs. Calculations predicted that under these conditions, the net charge for $C_{16}$-KTTKS should be +1 and -3 for $C_{16}$-ETTES at pH 5.4, suggesting that a ratio of 3:1 $C_{16}$-KTTKS:$C_{16}$-ETTES may be the most efficient conditions for ideal coassembly. However, it was experimentally determined that ratios of 1:0.5 wt% $C_{16}$-KTTKS:$C_{16}$-ETTES provided the most transparent, stable hydrogel; other binary mixtures formed cloudy solutions due to partial solubility of the β-sheet assemblies. This work illustrates both the advantage of coassembly strategies in modifying the emergent properties of supramolecular materials and also the challenges associated with rational design that must still be addressed using empirical approaches.

Multicomponent binary assemblies of PAs with non-peptide fatty acids have also been developed. Stupp and coworkers exploited attractive anion-π interactions to facilitate coassembly between dodecanoic acid and PAs containing pentafluorophenylalanine ($^{F5}$F).[474] $^{F5}$F has a fluorinated benzyl side chain in which the quadrupole moment is reversed relative to that of the benzyl group in Phe. While the side chains of canonical aromatic amino acids have been shown

to participate in attractive cation-π interactions, it was hypothesized that $^{F5}$F perfluorobenzyl group would instead form anion-π interactions with carboxylate groups. As such, $^{F5}$F groups near the *N*-terminus of the PAs designed for these studies were expected to interact with the terminal carboxylate of dodecanoic acid to promote coassembly of the two materials (**Figure 26**, $^{F5}$F-PA 1). It was hypothesized that the dodecanoic acid group would be buried within the hydrophobic core of the coassembled nanofibers, taking advantage of both hydrophobic and anion-π effects to facilitate coassembly. The position of the $^{F5}$F amino acid was varied within the PA in order to determine how this would effect possible anion-π interactions with the fatty acid carboxylate (**Figure 26**, $^{F5}$F-PA 2, $^{F5}$F-PA 3).

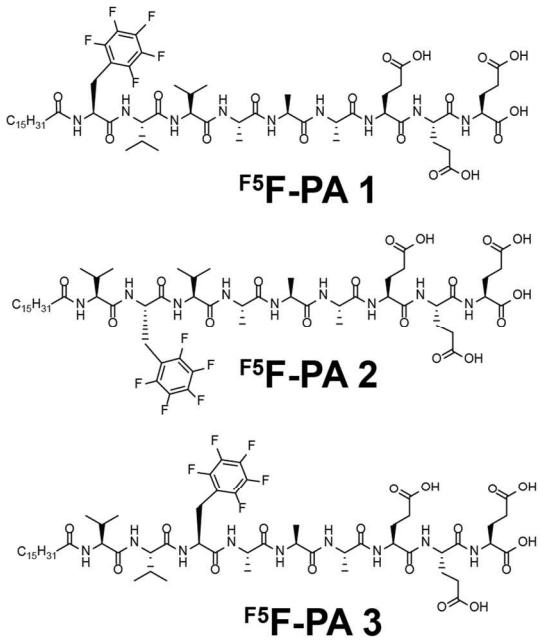


**Figure 26.** Chemical structures of peptide amphiphiles with $^{F5}$F in varying positions for studying anion-π interactions between dodecanoic acid and PAs 1-3.[474]

The coassembly studies provided clear evidence that the design principles that promoted coassembly of the PA with dodecanoic acid were sound. The PAs were each found to undergo self-assembly into high-aspect ratio cylindrical nanofibers consistent with previously observed

PAs. PAs with $^{F5}$F near the *N*-terminus were found to form coassembled nanofibers with dodecanoic acids that retained the one-dimensional, cylindrical morphology. NMR, CD, and atomistic simulations collectively verified that incorporation of dodecanoic acid into the multicomponent nanofibrils occurred on the basis of efficient formation of anion-π interactions. As the position of the $^{F5}$F changed shifted away from the *N*-terminus of the PA, the resulting anion-π interactions were perturbed, resulting in a change in morphology of the resulting coassembled materials. PAs with $^{F5}$F shifted away from the *N*-terminus resulted in formation of ribbon-like assemblies instead of cylinders. Increasing the ratio of dodecanoic acid in the binary mixtures also resulted in a change in assembly morphology from one-dimensional fibers to vesicles. These studies are an elegant demonstration of the selective use of specific interactions in order to modify the fundamental characteristics of multicomponent supramolecular materials.

### 4.2 Discotic Peptides

Another interesting class of amphiphilic peptides includes those that can aggregate to form columnar or porous supramolecular assemblies.[459–461,475] Besenius *et al*. have studied the controlled aggregation of discotic amphiphiles which are $C_3$-symmetric templated oligopeptides (**Figure 27**).[476,477] Central tri-substituted aromatic molecules decorated with three peptides undergo assembly-induced aggregation to form triple β-sheet nanofibrils in aqueous solutions.[23] Attaching amphipathic β-sheet pentapeptides with either positive or negative charges to alternating positions around an aromatic core provides symmetrical discotic monomers (**Figure 27A**) that will only undergo salt-induced self-assembly at neutral pH due to the repulsive effects of the uniform cationic or anionic charge on either system. However, when these discotic

peptides are mixed in equimolar ratios, the complementary charge in each system enables the directed coassembly of these materials into nanorod aggregates at neutral pH where both lysine and glutamic acid residues are charged. Coassembly only occurs via complementary electrostatic interactions between the β-strands since the self-assembly of these materials does not occur under these salt-free conditions due to charge repulsion.

This assembly process is tunable by modifying the pH of the solution. At low or high pH conditions, the charge on either peptide is neutralized and dynamic self-assembly and disassembly processes occurs based on which of the discotic amphiphiles is neutralized (**Figure 27B**). The range of pH-triggered disassembly can be altered from pH 4.2 to pH 5.8 by shortening the *β*-sheet segments, providing a strategy to alter assembly preferences and assembly propensity in the multicomponent mixture. These studies demonstrate interesting supramolecular systems in which electrostatic interactions can be effectively exploited to manipulate dynamic coassembly processes.

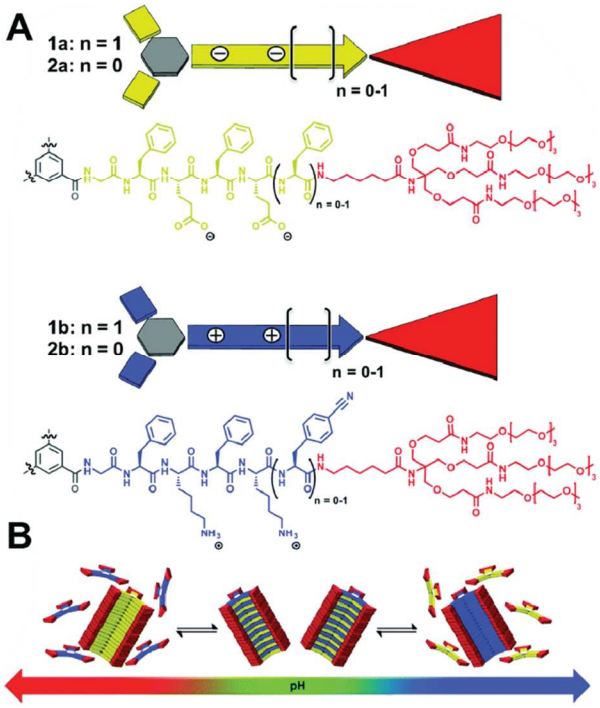

**Figure 27.** (A) Schematic and chemical structure of discotic amphipathic peptide monomers with opposite charges. (B) Tuneable pH profile that allows either self- or coassembly of the discotic amphiphiles based on pKa of the peptide side chains. As pH becomes more acidic or basic, coassembly is disrupted when only one of the monomers remains charged and self-assembly takes place based on the pKa of the lysine or glutamic acid residues in the monomers. Figure reproduced from ref 477 (P. Ahlers, H. Frisch and P. Besenius, *Polym. Chem.*, 2015, **6**, 7245–7250)[477] with permission from the Royal Society of Chemistry.

### 4.3 Aromatic Conjugated π-Organopeptide Hybrids

Several groups have taken advantage of the inherent nature of self-assembled peptide networks for the organization of conjugated-π aromatic molecules in coassembled structures in aqueous solutions.[454,478,479] For example, Tovar *et al*. have harnessed the intrinsic assembly of *β*-sheet peptides to organize supramolecular networks of aromatic conjugated-π molecules into complex donor-acceptor arrays that act of mimics of natural light-harvesting, energy-transfer systems.[462,463] This was accomplished by coassembly of organopeptide hybrids in which the peptides are tethered to either an organic aromatic electron donor or acceptor molecule. The peptides and conjugated-π aromatic groups were organized in a peptide-π-peptide pattern (**Figure 28A**). Specifically, DFAA-1,4-distyrylbenzene-AAFD (electron donor, OPV3) and DFAA-quaterthiophene-AAFD (electron acceptor, 4T) were coassembled in statistical mixtures, providing supramolecular fibrils that elicited efficient energy transfer between the conjugated-π systems via multiple mechanisms, including exciton migration in the OPV3 units and FRET between the OPV3 and 4T units (**Figure 28B**).[462] Interestingly, changes in pH and temperature altered coassembly capability of the constituents and thus affected the energy transfer processes of the coassembled structures. These results are a significant demonstration of biomimetic energy transfer in aqueous media.

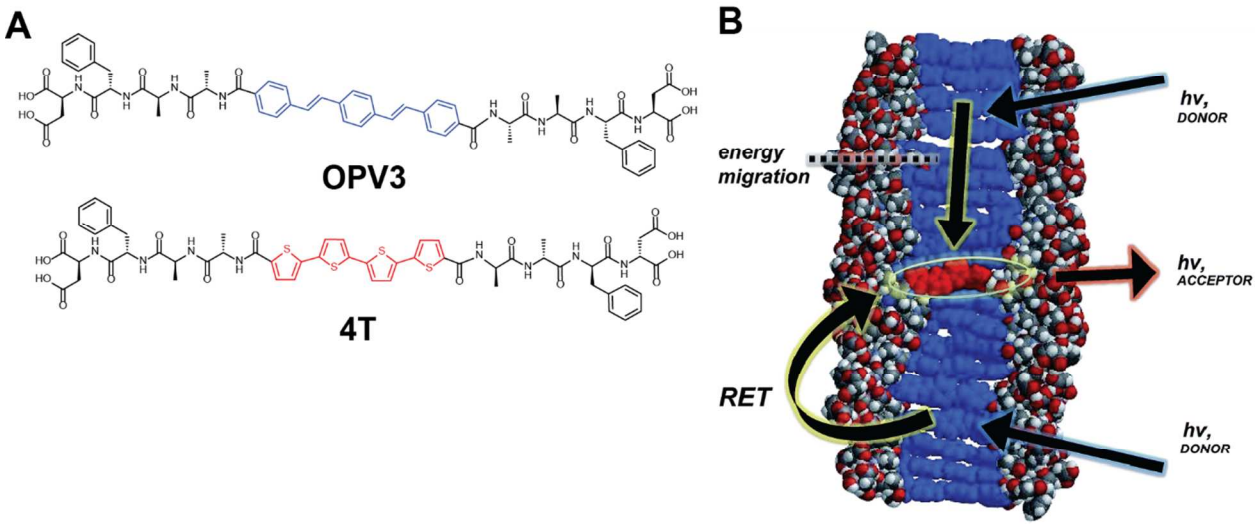


**Figure 28.** (A) Chemical structures of π-conjugated distyrylbenzyl (OPV3) and quarterthiophene (4T) peptide amphiphiles. (B) Packing model of amphiphiles into a supramolecular fibril capable of multiple energy transfer events. Figure reproduced from ref 462 (H. A. M. Ardoña and J. D. Tovar, *Chem. Sci.*, 2015, **6**, 1474–1484)[462] with permission from the Royal Society of Chemistry.

Tovar subsequently extended the study of these coassembly process to investigate the effect of the immediate environment of conjugated-π groups in supramolecular assemblies on the photophysical properties of materials.[463] In this work, the OPV3 π-system was coassembled with a related peptide-core-peptide with an aliphatic, flexible $C_{10}$ n-decyl group as the linking core unit. The aliphatic $C_{10}$ n-decyl component is incapable of interacting in any π-electron transfer events. Coassembly of these materials in various ratios resulted in either dilution/isolation of the OPV3 molecules within the supramolecular architecture or the localized formation of self-associated OPV3 stacks that can interact to elicit electronic delocalization (**Figure 29**). Photoluminescence analysis of the various coassembled arrangements indicated that both arrangements exist and illustrated the nonresonant and local peptide field effects that exist in these system, providing insight into how the optoelectronic properties of the multicomponent materials can be tuned by varying the local environment.

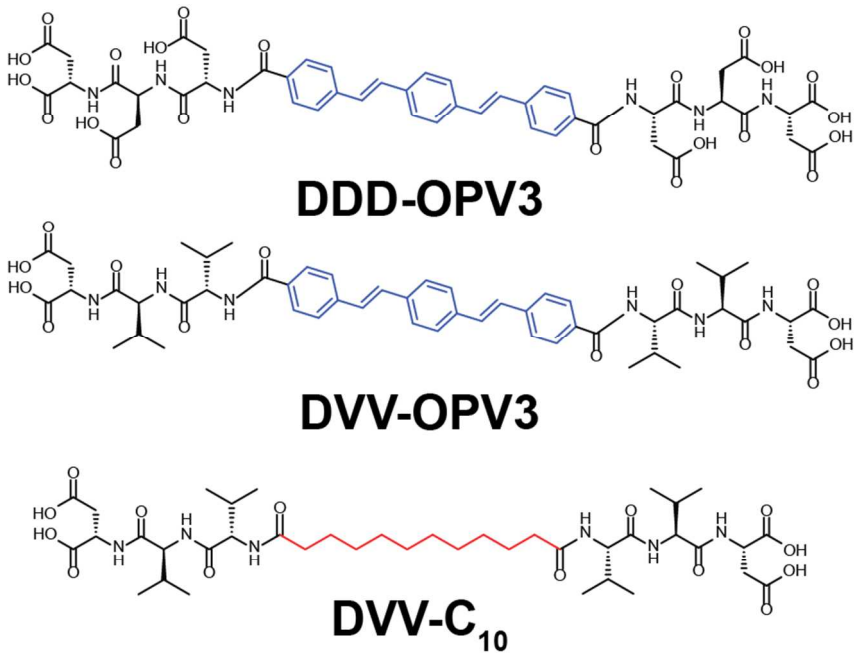


**Figure 29.** Chemical structures of organopeptide hybrids DDD-OPV3 and DVV-OPV3 designed to coassemble with DVV-$C_{10}$ to isolate and study the effects of the π-electron interactions on the assembly.[463]

Tovar *et al*. then employed a kinetic control strategy to produce multicomponent organopeptide π-conjugated hybrids in which the spatial arrangement of the core π-electron units is controlled.[67] Three organopeptide with peptide-core-peptide structures (OPV3, OT4-NDI, and OT4-Ac) were prepared in which each peptide includes arrangements of π-conjugated molecules with distinct photonic and electronic donor-acceptor properties (**Figure 30A**). The peptide segments were designed so that assembly could be variably triggered in response to gradual acidification of pH as a function of subtle p$K_a$ differences between the various peptide components. Oligo-(p-phenylenevinylene) (OPV3) is an electron donor molecule that can funnel energy through exciton migration to a quarterthiophene-appended peptide acceptor if in close enough proximity within coassembled structures. The quarterthiophene serves as an excited state electron donor to the naphthalenediimide (NDI) structures appended to the ends of the OT4-NDI

organopeptide hybrids. Sequential photonic/electronic energy transfer was monitored as coassembly occurred upon either rapid solution acidification (by addition of HCl) or graduate solution acidification (by slow hydrolysis of glucono-δ-lactone, GdL). When the pH was rapidly acidified, all components randomly coassembled into supramolecular structures in which energy transfer between the acceptor-donor functional groups was readily observed within the supramolecular structures (**Figure 30B**). When the pH was gradually acidified, subtle differences in the p$K_a$ of the organopeptide components resulting in stepwise, self-sorted self-assembly of distinct structures in which energy transfer occurred only in an interfibril manner (**Figure 30B**). This method highlighted the ability to control the spatial ordering of the organopeptide monomers by taking advantage of the intrinsic differences in fundamental properties of the self-assembly motifs, in this case the p$K_a$ of the peptide side chains. This work highlights the delicate balance and synergistic effects of electronic effects and peptide self-assembly to form coassembled structures with intrinsic characteristics derived from the interaction of their individual components.

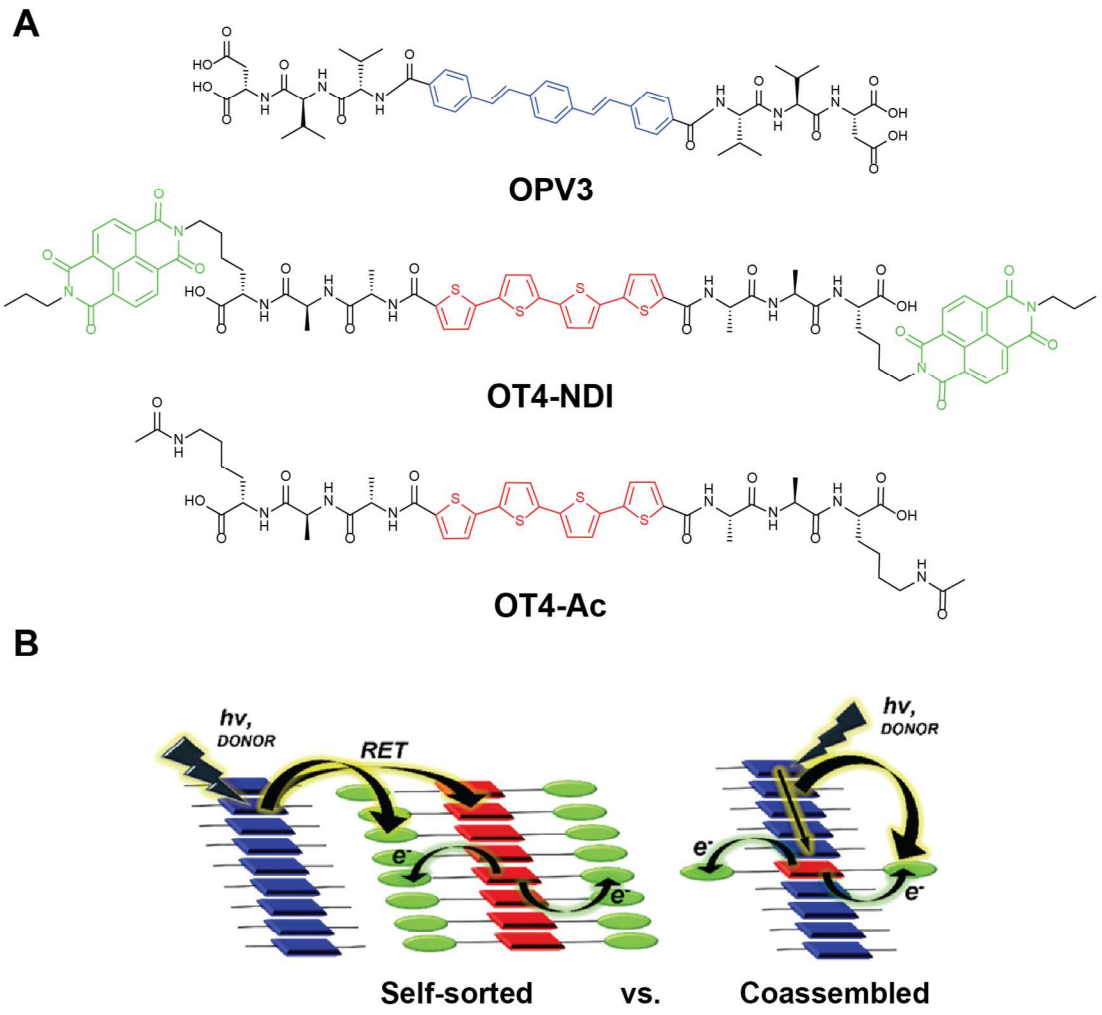


**Figure 30.** (A) Chemical structure of OPV3, OT4-NDI, and OT4-Ac organopeptide hybrids. (B) Pictorial representation of organopeptide hybrids that self-sort into discrete fibrils capable of inter-fibril electron transfer events or coassemble to form multicomponent fibrils containing multiple conjugated organic molecules capable of intra-fibril electron transfer events. This process is controlled by varying the pH either slowly with GdL to produce self-sorted fibrils, or quickly with HCl to coassemble the organopeptide hybrids into a single fibril. Figure adapted with permission from H. A. M. Ardona, E. R. Draper, F. Citossi, M. Wallace, L. C. Serpell, D. J. Adams and J. D. Tovar, *J. Am. Chem. Soc.*, 2017, **139**, 8685–8692.[67] © 2017 American Chemical Society.

## Section 5. Coiled-Coil Peptides

The coiled coil motif is another protein structure that has been exploited in the design of self-assembled, supramolecular peptide materials.[480–483] The $\alpha$-helical secondary structure consists of seven-amino acid repeats that compromise two turns of the standard helix, with each amino acid

in this heptad denoted as ***abcdefg*** (**Figure 31A**). Coiled coils are bundles of two to seven $\alpha$-helices stabilized by hydrophobic knob-in-hole and complementary electrostatic interactions between the constituent $\alpha$-helices.[484,485] The coiled coil motif is abundant in nature, playing roles in protein machinery that mediate biological processes ranging from gene transcription to viral infection.[486–488] Coiled coils have been extensively investigated in the design of self-assembled, one-dimensional nanofibrous materials. Conceptually, extended coiled coil fibrils have been designed using a "sticky-end" approach in which $\alpha$-helical proteins with blocks of positive and negative charges that can interact leaving dangling ends that can nucleate addition of partner $\alpha$-helices at both ends (**Figure 31B** and **31C**). These extended structures form long helical fibers that have been used as functional biomaterials. Both homo- and hetero-coiled coils exist in nature, making coiled coil peptides distinctly appropriate targets for the design of multicomponent coassembled materials.[489–495] This section will highlight the design, assessment, and application of multicomponent materials derived from coassembled coiled coils.[496,497]

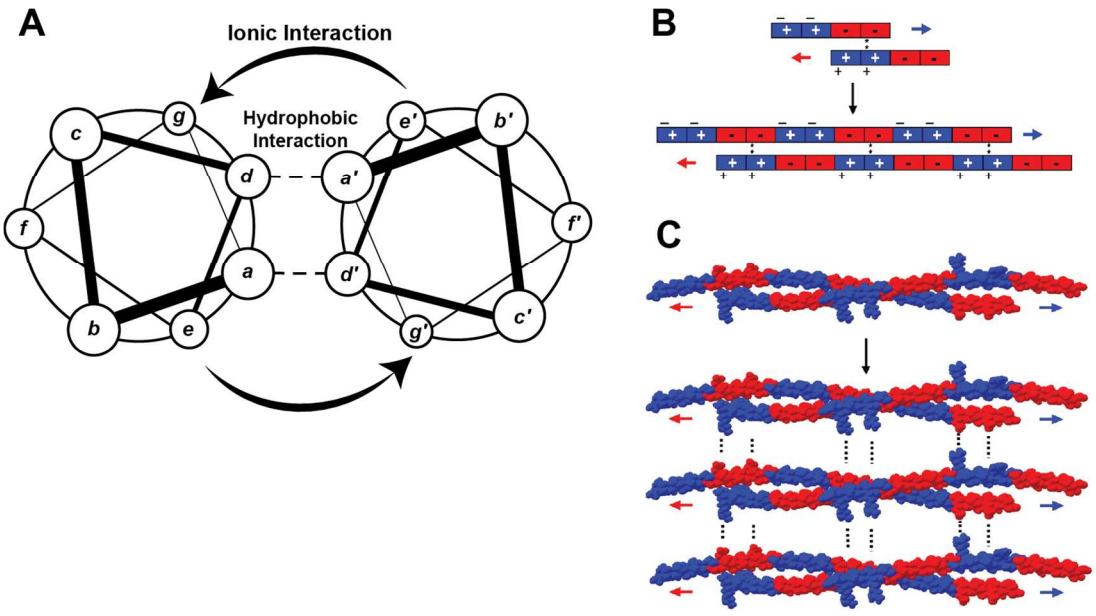

**Figure 31.** (A) Representation of the seven amino acid repeat, ***abcdefg***, that compromises $\alpha$-helical peptides that wrap around each other to form a left-handed helix supercoil. Hydrophobic residues in the ***a*** and ***d*** positions make quaternary contacts to form a hydrophobic core and polar residues in positions ***e*** and ***g*** often form salt bridged contacts further stabilizing the helix. (B) Woolfson's designed block helical peptides with nonpolar residues in helix residue positions ***a*** and ***d***, and alternating ***e*** and ***g*** positions have Lys (blue) or Glu (red) resides that provide a positive or negatively charged overhanging "sticky end". (C) "Sticky ends" promote protofibril-protofibril lamination events and elongation of the helix bundles to form extended fibril networks. Inter-helical electrostatic interactions are shown in dashed lines. Panels B and C reproduced with permission from D. Papapostolou, A. M. Smith, E. D. T. Atkins, S. J. Oliver, M. G. Ryadnov, L. C. Serpell and D. N. Woolfson, *Proc. Natl. Acad. Sci.*, 2007, **104**, 10853–10858.[498]

Self-assembled coiled coil nanofibers have been pioneered by several methods. Woolfson *et al*. have explored synthetic coiled coil self-assembled fiber systems and their subsequent hydrogelation for the formation of biomaterials.[498–500] In the Woolfson strategy, helical peptides were designed with complementary charged blocks in which the ***e*** and ***g*** residues were either Lys (positively charged) or Glu (negatively charged).[498] Electrostatic-driven self-assembly into dimeric coiled coils left terminal "sticky ends" that promoted longitudinal extension of coiled coil bundles, creating fibrils 50 nm × 10 μm or larger (**Figure 31C**). Alteration of the building blocks of these materials can give rise to unique supramolecular morphologies that include linear, waved, kinked, and branched structures.[493,496–499,501] Hartgerink *et al*. also designed self-assembled coiled coils nanofibrils that demonstrated that "sticky ends" were not strictly required to facilitate longitudinal extension of the materials.[501] In this approach, blunt ended coiled coils in which the charge of amino acids in the peripheral ***b***, ***c***, and ***f*** positions is carefully modified were also shown to extend longitudinally and aggregate laterally into one-dimensional fibrils. Collectively, these strategies have been exploited to design functional, supramolecular-coiled coil peptide materials.

Iwata and coworkers have developed coassembled coiled coil systems in the preparation of hydrogels for cell culture applications.[502] They used extracted coiled coil from natural type II

keratin (K14) coassembled with a designed chimeric protein consisting of an $\alpha$-helical K14 fragment fused with the globular domain 3 of the laminin $\alpha$3 chain (LG3K14). This mixture resulted in the formation of K14 centralized coiled coils which entangled to form hydrogels with LG3 domains, which are known to interact with integrins and provide a point of adhesion for neural stem/progenitor cells, exposed at the surface of the hydrogel network. The utility of these coassembled hydrogels was demonstrated with the improved survival rate of neurosphere-forming embryonic rat brain cells, a cell type prone to poor survival, on K14-LG3K14 gels compared to pure keratin gels. Similar to previously discussed $\beta$-sheet, LMW, and organopeptide hybrid hydrogels, these multicomponent coiled coil materials also exhibited enhanced functionality relative to the self-assembled counterparts.

Koksch *et al*. demonstrated that a self-assembling $\alpha$-helical coiled coil peptide were able to coassemble with a $\beta$-sheet self-assembling peptide, and that the coassembled material formed a coiled coil fibrous structure devoid of $\beta$-sheet structure.[503,504] They identified two 26-residue peptides, VW01 and VW19 based on an $\alpha$-helical coiled coil heptad repeat. VW01 was designed with structural elements that favor $\alpha$-helical conformations, while VW19 incorporated Val residues in critical positions of the heptad repeat, which was expected to favor $\beta$-sheet conformations (**Figure 32**).[504] As expected, VW01 self-assembled into a three-helix coiled coil fibril whereas VW19 self-assembled into amyloid-like $\beta$-sheet fibrils. The coassembly of VW01 and VW19 was then assessed in molar ratios (VW19:VW01) of 2:1, 1:1, and 0.5:1. When VW19 was in excess (2:1), $\beta$-sheet amyloid fibrils were observed in the mixture. However, at equimolar concentrations or at an excess of VW01, $\alpha$-helical coiled coil aggregates were instead observed, with two molecules of VW01 and one molecule of VW19. The helical VW01 peptide induces

cooperative helical folding of VW19, suppressing its aggregation into amyloid fibrils and instead forming multicomponent coiled coils. This work has interesting implications for the use of helical peptides to divert dysfunctional amyloid into non-cytotoxic folding pathways.[503]

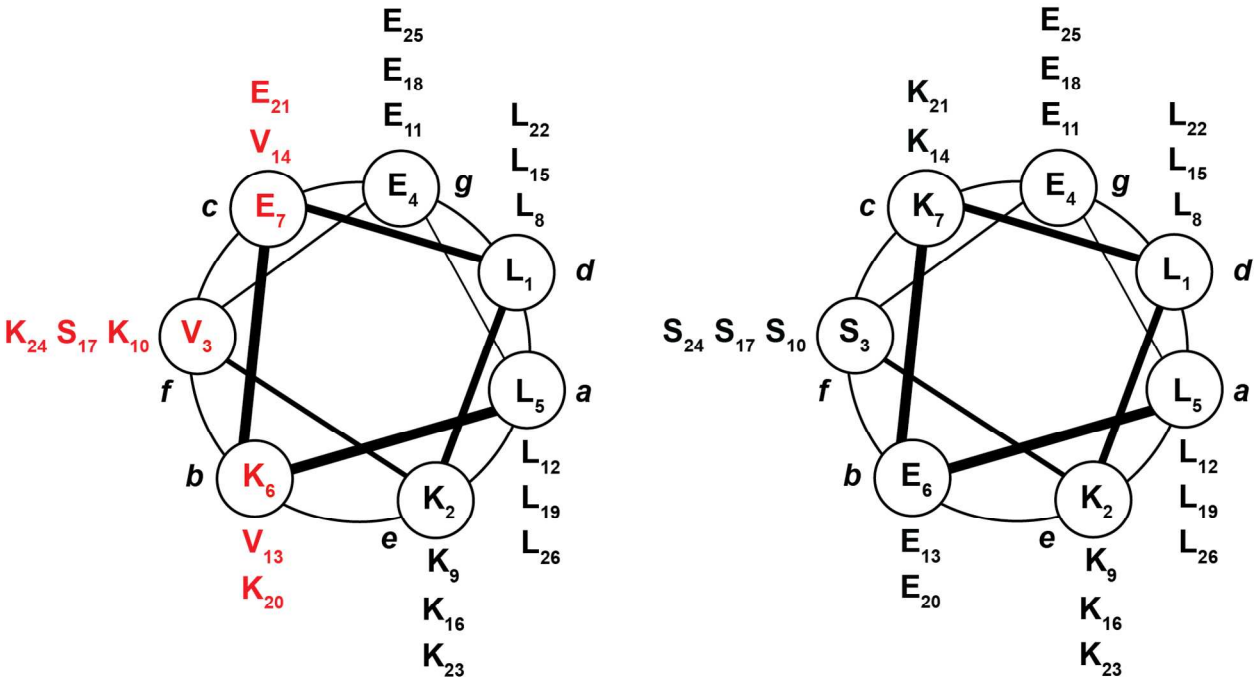


**Figure 32.** Schematic of designed peptides based on the ***abcdefg*** heptad repeat in $\alpha$-helical peptides. The ***b***, ***c***, and ***f*** positions of the sequence on the left have been replaced with amphipathic residues (shown in red) that induce $\beta$-sheet self-assembly between peptides (VW19). The right sequence is the $\alpha$-helical peptide capable of destabilizing the $\beta$-sheets and inducing $\alpha$-helical formation upon coassembly in various ratios (VW01).[504]

In an attempt to prepare more complex supramolecular 3D microstructures using designed coiled coil peptides, Woolfson and coworkers developed self-assembled peptide-based cages (SAGEs) decorated with various proteins to demonstrate the multivalent display and co-localization of proteins onto nanoparticles.[500,505] The foundation of these multicomponent structures was constructed of a homotrimeric coiled coil core (CC, **Figure 33** shown in green in top left panel). To the exterior face of each of the three core strands was attached an additional $\alpha$-helical peptide, covalently attached to the binding partner via a disulfide bond. These exterior

$\alpha$-helical peptides were either acidic (DiA, **Figure 33** shown in red in top left panel) or basic (DiB, **Figure 33** shown in blue in top left panel). These six-helix multicomponent structures (CC-DiA and CC-DiB) were then mixed to form a two-dimensional, hexagonal peptide lattice (SAGE) (**Figure 33**, top right panel) in which the coassembly of CC-DiA and CC-DiB was driven by complementary electrostatic charge interactions. The hexagonal peptide lattice extends two-dimensionally and eventually folds into three-dimensional spherical nanoparticles approximately 100 nm in diameter.

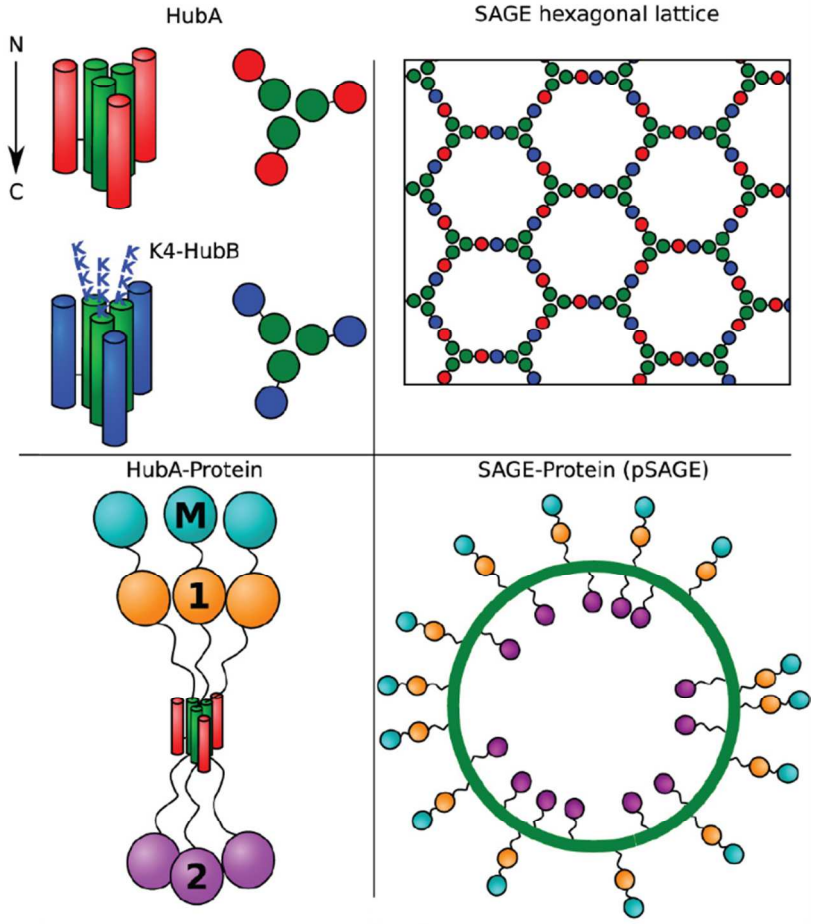


**Figure 33.** Representation of coiled coil peptide hubs with homotrimeric cores (green coils), each strand of which was bound to another acidic (red, HubA) or basic (blue, HubB) $\alpha$-helical peptide (top left panel). Some peptide hubs were synthesized with a $K_4$ *N*-terminal portion for better solubility. When coassembled in equimolar ratios, the peptide hubs form a hexagonal lattice that extend and folds into spherical nanoparticle (top right panel). Peptide/protein hubs are formed via conjugation of proteins to the

*N*- or *C*- terminus of HubA or HubB. Bottom left panel shows peptide HubA decorated on the *N*- and *C*-terminus with proteins such as GFP (1, and 2). *N*-terminally appended maltose binding proteins (light blue, M) was included in some constructs due to improved expression and solubility of the resulting proteins. Bottom right panel depicts a SAGE nanoparticle with pendent proteins displayed on either the inside or outside of the nanoparticle depending on the conjugated peptide terminus. Figure adapted with permission from F. Ross, A. Bridges, J. M. Fletcher, D. Shoemark, D. Alibhai, H. E. V. Bray, J. L. Beesley, W. M. Dawson, L. R. Hodgson, J. Mantell, P. Verkade, C. M. Edge, R. B. Sessions, D. Tew and D. N. Woolfson, *ACS Nano*, 2017, **11**, 7901–7914.[500] © 2017 American Chemical Society.

These multicomponent SAGE nanostructures could also be used to display functional proteins at the surface. The constituent coiled coil peptides could be expressed as *N*- or *C*-terminal fusions with various proteins, including GFP, mCherry, or luciferase. The $\alpha$-helical coiled coil segments of these fusions were still competent to assemble, and coassembling various ratios of these fusions facilitated the co-localized multivalent display of the cargo proteins at either the exterior or interior surface of the nanoparticles (**Figure 33** bottom left panel). The SAGEs investigated were found to tolerate display of numerous copies of fusion proteins both inside and outside of the nanoparticles as well as the simultaneous incorporation of different proteins into a single SAGE. These multi-protein decorated SAGEs are potentially useful for the modular assembly of nanomaterials for a wide variety of uses, including nanoreactors via immobilization of catalytic enzymes or for presenting antigenic proteins for vaccine development and testing. This work is an elegant demonstration of the rational design and creation of sophisticated multicomponent materials that extend beyond one-dimensional nanofibers into three-dimensional particles.

Multivalent protein display on coiled coil nanoparticles were also reported by Xu and coworkers.[506] The Xu group had developed three helix coiled coils derived from peptide-(PEG)-lipid conjugates. These three-helix coiled coil amphiphiles were shown to self-assemble into multimeric structures and stable spherical particles that have potential as biological

nanocarriers.[507,508] They subsequently designed a four-helix coiled coil conjugate that was shown to undergo effective coassembly with a three-helix conjugate to form stable spherical micelles that were less than 20 nm in diameter (**Figure 34**). By fusing additional proteins to the coiled coil motifs, they were able to create nanoparticles in which the cargo segments were displayed at the exterior face of the nanoparticles. It is noteworthy that the three- and four-helix bundles in these multicomponent structures retained their native oligomeric states upon mixing, showing no evidence for cross-oligomerization of the component coiled coil bundles. These particles, with appropriate surface functionality on the exterior face, have potential for use in tumor targeting and treatment through enhanced permeation and retention effects as well as selective ligand direction.

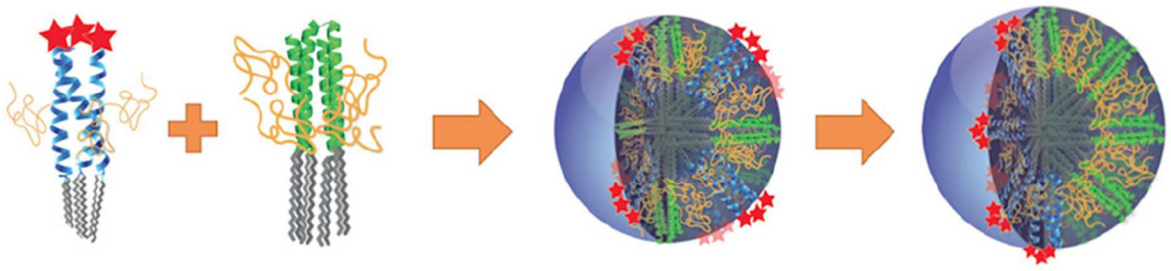

**Figure 34.** Pictorial representation of 3- and 4-helix peptide-polymer-lipid conjugates that form sub-20 nm micelles with discrete partitioning of 3- and 4-helix bundle nanodomains for local multivalent display of functional ligands. Figure reproduced with permission from J. Ang, D. Ma, B. T. Jung, S. Keten and T. Xu, *Biomacromolecules*, 2017, **18**, 3572–3580.[506] © 2017 American Chemical Society.

## Section 6. Collagen Mimetic Peptides

Collagen is a fibrous protein that is the main structural element in the extracellular matrix (ECM) and connective tissues.[509,510] Collagen is the most abundant protein in humans and is critical for structural integrity of the ECM and in bones. Proline and glycine rich sequence repeats $(X\text{-}Y\text{-}Gly)_n$, in which X and Y are often proline (P) or hydroxyproline (O) comprise the

sequence of natural collagens.[509,511] The high periodicity of rigid proline and flexible glycine residues enable self-assembly of collagen into triple helical fibrils that account for the structural rigidity of collagen. While natural collagen has been used for a variety of applications, synthetic collagen mimetics have gained attractiveness as functional materials due to their biocompatibility and ease of access.[512–516] Collagen mimetic peptides (CMPs) have also been used in coassembled multicomponent materials as will be discussed in this section.

Foundational work in the design of self-assembled CMPs enabled this synthetic architecture to be exploited for the development of hydrogels and other functional biomaterials.[517,518] Chaikof and Conticello *et al*. and Hartgerink *et al*. separately reported CMP fibrous systems that closely mimic the emergent properties of natural collagen. These CMPs have the general sequence $(PXG)_4(POG)_4(YOG)_4$ where X and Y are Arg and Glu in Chaikof's system,[519,520] and Lys and Asp in Hartgerink's system.[517,518,521] These CMPs self-assemble into triple helices stabilized by intermolecular electrostatic interactions that leave sticky ends which enable elongation in nanofibers several hundred nanometer long. In Hartgerink's example, this propagation leads to the entanglement of fibers to form a hydrogel that is degraded at rates similar to that of natural collagen.

Inspired by self-assembled triple helical CMPs, multicomponent heterotrimeric triple helical collagen mimetics have also been developed.[517] Understanding the critical noncovalent interactions that promote coassembly of CMPs into heterotrimeric helices is challenging. Investigators over the last decade have leveraged sequence variation and template assembly strategies to identify heterotrimeric CMPs.[522–529] Hartgerink *et al*. have pioneered this work with the characterization of ABC heterotrimer collagen mimetics designed to coassemble using complementary electrostatic interactions across the constituent peptide chains.[518,530–537] In an

effort to direct the selective coassembly of CMPs into heterotrimeric triple helices, neutral, negative, and positive charged CMPs were designed (**Figure 35**).[528] The three CMPs were (X-Y-Gly)$_{10}$ repeats with positive amino acids in the Y position of one peptide, negative amino acids in the X position of another peptide, with (POG)$_{10}$ used as the neutral peptide system. Mixing these peptides resulted in formation of stable heterotrimeric triple helices, with lysine-aspartate interactions providing the most significant cross-strand stabilization of the heterotrimeric assemblies.[528,531]

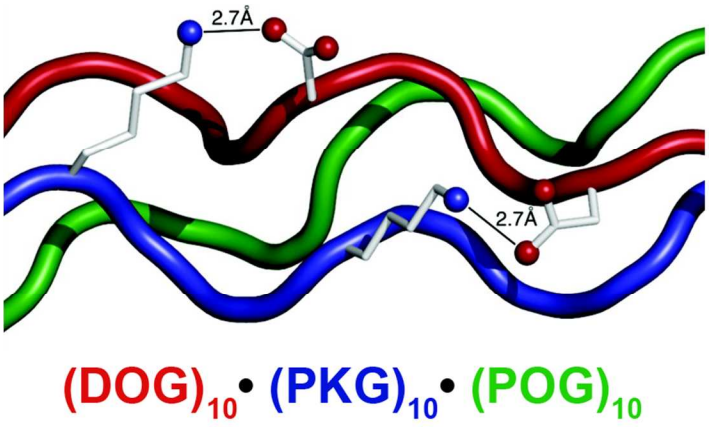


**Figure 35.** Molecular model of designed basic (red), acidic (blue), and neutral (green) CMPs for heterotrimer formation. The contact distances between Lys (blue) and Asp (red) side chains are shown. Figure adapted with permission from V. Gauba and J. D. Hartgerink, *J. Am. Chem. Soc.*, 2007, **129**, 15034–15041.[528] © 2007 American Chemical Society.

Nanda and coworkers have also exploited the charge-directed coassembly of higher order CMP structures for the development of biomaterials.[538] In an effort to rationally design CMPs, Nanda *et al.* employed computational methods to predict and design 30-residue CMPs with optimized charge pairing interactions to favor ABC heterotrimer formation in which peptides A, B, and C were composed of a different combination of five triplets: PRG, ROG, EOG, PEG, and POG.[522,539] Despite using "positive" and "negative" computational design methods to optimize

the stability and disfavor competing states respectively for the identification of an ideal ABC heterotrimer, no experimental evidence supported folding into a distinct ABC triple helix. Other heteromeric CMP species such as A:2B, 2B:C, and B:2C were experimentally observed, although it was difficult to discern between 2B:C and B:2C trimers. Further investigation of the B:C heteromixtures indicated that it was possible to alter the properties of the assemblies of the two-component systems by varying the ratio or total concentration of the mixed peptides.[539] These examples highlight the challenges associated with the rational design of heteromeric collagen systems and provide avenues for future research to deepen understanding of the fundamental principles that underlie collagen folding.

Nanda *et al*. subsequently focused on interrogating the charge contributions between designed CMPs in collagen folding processes in order to facilitate improved design of directed coassembled systems.[518–520] Mixtures of supercharged CMP peptides R6, K6, E6, and D6 (**Table 1**) were investigated to determine the difference in contributions between charged pairs to affect the higher order coassembly of triple helical CMPs.[538] Each individual peptide was tested for homotrimer formation and it was found that R6 and K6 were highly folded and E6 and D6 were only partially folded. Interestingly, mixtures of the homotrimers resulting in lateral coassembly into higher ordered microsheets, although this microsheets were only observed between R6 and either E6 or D6. Coassembly of K6 homotrimers with either of the anionic CMPs did not occur (**Figure 36**). While it was clearly evident that only arginine containing CMP triple helices participated higher ordered association with charge-complementary triple helical peptides, the reasons for this preference is unclear. It may be due in part to the higher propensity of guanidinyl nitrogens to participate in both intra- and intermolecular hydrogen bonds compared to lysine. This propensity has been observed in natural protein systems where arginine is four times more

likely to participate in complex network hydrogen bonding than lysine.[540] These studies illustrate the nuanced complexity of charge-complementary as a driving force for multicomponent coassembly of supramolecular collagen-based materials.

**Table 1.** List of cationic and anionic CMP sequences used in coassembly studies to interrogate electrostatic contributions between peptides to form heteromeric higher-ordered assemblies.[538]

| CMP | Amino Acid Sequence |
|---|---|
| **R6** | $(RRG)_3(POG)_7$ |
| **K6** | $(KKG)_3(POG)_7$ |
| **E6** | $(EEG)_3(POG)_7$ |
| **D6** | $(DDG)_3(POG)_7$ |

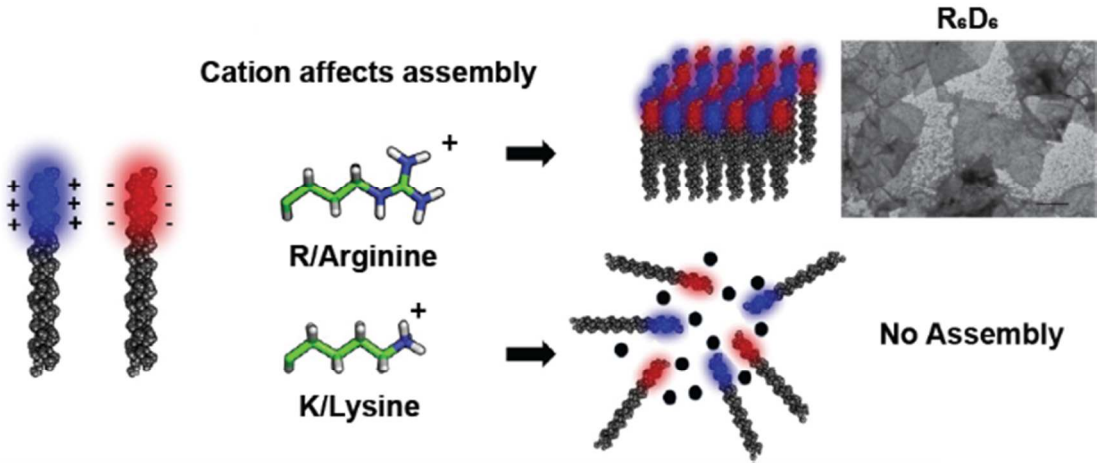


**Figure 36.** CMP triple helices with charge paired ends to facilitate coassembly. Choice of cation for the positively charged peptide affects the lateral association of triple helix coassembly into microsheet structures. Arginine triple helix CMPs ($(RRG)_3(POG)_7$) coassembled with aspartate triple helix CMPs ($(DDG)_3(POG)_7$) to provide multicomponent microsheets (top model and TEM, $R_6D_6$). When lysine

containing triple helix CMPs ($(KKG)_3(POG)_7$) were coassembled with the aspartate triple helix CMPs, $K_6D_6$ microsheets were not observed, indicating a non-equivalency in arginine and lysine for the formation of supramolecular coassembled CMP structures. Figure adapted with permission from A. S. Parmar, J. K. James, D. R. Grisham, D. H. Pike and V. Nanda, *J. Am. Chem. Soc.*, 2016, **138**, 4362–4367.[538] © 2016 American Chemical Society.

There are additional reports of coassembled multicomponent systems composed of CMPs. Nanda *et al*. initiated an additional example as an empirical study of the role of hydrophobicity in collagen assembly.[541,542] They conducted a study of CMPs by the systematic replacement of X and Y residues in the $(POG)_3(XYG)_3(POG)_4$ sequence to generate CMPs with varying degrees of hydrophobicity.[541] They identified several CMPs that self-assembled into triple helical structures with interesting higher order structures. The CMP designated as sequence H4 ($(POG)_3POGLIGLIG(POG)_4$) assembled into nanodiscs displaying a hydrophobic disc edge, whereas CMP H6 ($(POG)_3LIGLIGLIG(POG)_4$), with a longer central hydrophobic segment, formed fibers with hydrophobic ends. The hypothesis that the coassembly of these two CMPs would form a hybrid nanostructure was validated with a coassembly of 2:1 H6:H4 which produced nanostar structures in which H6 fibers were found to protrude from the hydrophobic edge of the H4 nanodiscs (**Figure 37**). They also discovered that the H4 discs coassembled with rod-shaped uni-flagellar bacilli to form structures with a disc-on-a-string (DoS) morphology by bundling of the fibrous flagella with the H4 discs.[542] This bundling effect was further studied by coassembly of H4 with a number of other systems, including fibers of $\alpha$-synuclein, collagen I, and tropomyosin, which all formed DoS structures through non-specific binding of hydrophobic regions of the fibrous proteins. These empirical studies indicate not only interesting collagen coassembly phenomena, but also the productive interface of collagen nanostructures with other supramolecular architectures.

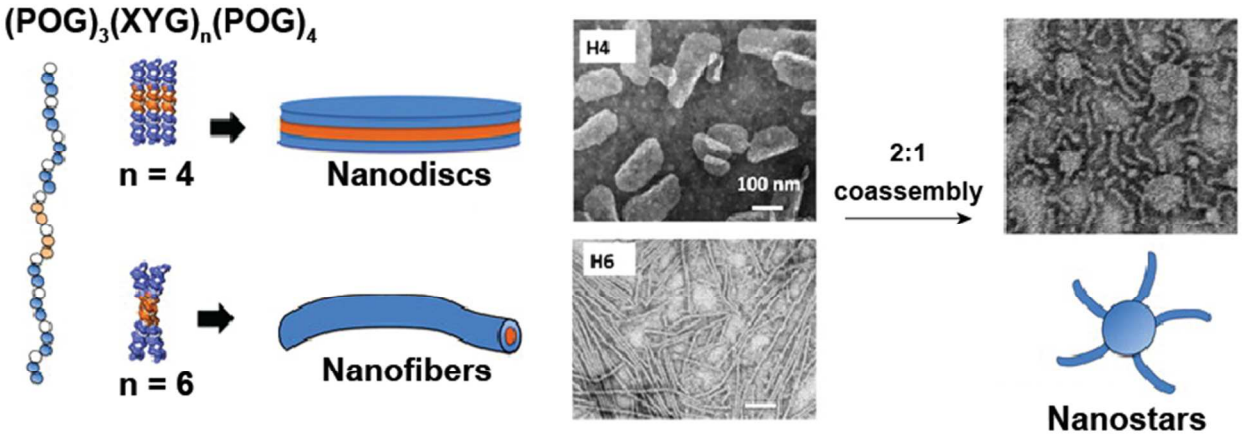


**Figure 37.** CMPs with general sequence $(POG)_3(XYG)_n(POG)_4$, where the central XYG segment varies in chain length and hydrophobicity by linking POG segments with LIG repeats. Peptide assembly with CMPs that have a shorter central hydrophobic segments results in nanodisc formation (top TEM, H4) and longer hydrophobic segments lead to fiber formation (bottom TEM, H6). A 2:1 coassembly of H6:H4 results in a combination of structures that produce nanostars where the nanofibers extend from hydrophobic nanodisc centers. Figure adapted with permission from K. McGuinness, I. J. Khan and V. Nanda, *ACS Nano*, 2014, **8**, 12514–12523.[541] © 2014 American Chemical Society.

Chmielewski *et al*. studied formation of higher order structures from CMPs in which heteromixed sequences coassemble into micro- and nanostructures through reversible metal chelation.[543] Two CMP triple helices with complementary metal binding ligands attached to the *N*- and *C*- terminus of each peptide flanking a $(POG)_9$ core were synthesized, HisCol and IdaCol, containing two histidines or an iminodiacetic acid moiety respectively (**Figure 38**). Cooperative coassembly of HisCol and IdaCol and higher order assembly into micrometer length sheets was observed only in the presence of divalent metals such as nickel, zinc, and copper. This controlled coassembly was shown to be fully reversible upon addition of EDTA. TEM images revealed a periodic banding of these structures at the nanoscale that was similar to that in natural collagen. The banding showed 9–12 nm spacing between gaps, which correlates to the computed average length of the $(POG)_9$ CMP core flanked by metal binding ligands. It was postulated that the periodic banding occurs from the linear association of metal bound triple helical CMPs which

then undergo in- or out-of-register lateral association to form higher order micro structures. The use of metal templating to direct coassembly of collagen sequences is an innovative demonstration of the versatility of multicomponent supramolecular CMP architectures.

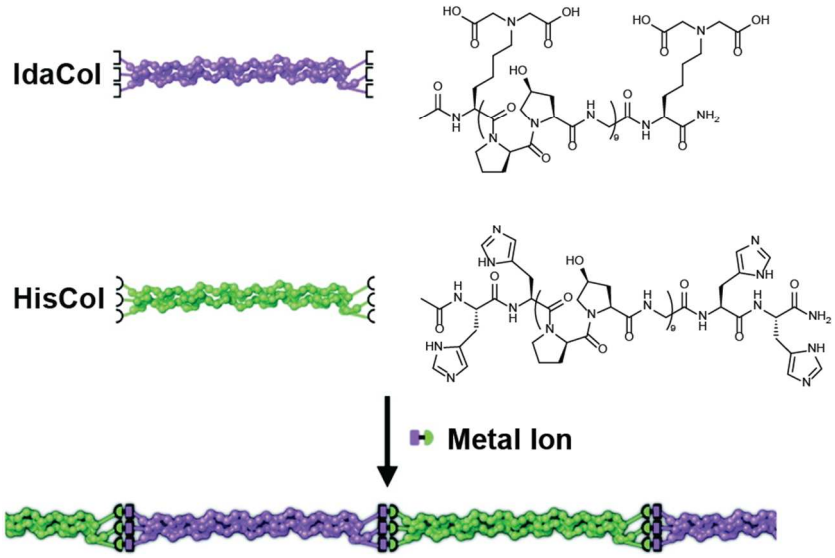


**Figure 38.** Chemical structure and three-dimensional models of IdaCol and HisCol CMPs and their coassembly via metal ion chelation using metals such as Ni, Zn, and Cu. Figure adapted with permission from M. M. Pires, D. E. Przybyla, C. M. Rubert Pérez and J. Chmielewski, *J. Am. Chem. Soc.*, 2011, **133**, 14469–14471.[543] © 2011 American Chemical Society.

## Section 7. Polydisperse Polypeptides

Polydisperse polypeptide-based hydrogels have gained attention as biomimetic materials.[544,545] "Polydisperse polypeptides" are herein defined as synthetic polypeptides synthesized by statistical polymerization of *N*-carboxyanhydride (NCA), or related, precursors as opposed to peptides prepared by solid phase peptide synthesis in which the peptide length and sequence are precisely controlled. As such, the sequence and lengths of polydisperse polypeptides are an ensemble determined by the polymerization conditions, including the numbers of amino acids and the relative concentrations of each component. These polypeptides can include any mixture of natural or nonnatural amino acid side chain functional groups,

providing highly versatile materials. Depending on the amino acid constituents, polydisperse polypeptides have been observed to be disordered[546–550] or to adopt secondary structure, including $\alpha$-helical and $\beta$-sheet conformations.[551–553] Polydisperse polypeptides, including poly(L-glutamic acid) and poly(L-lysine) (**Figure 39**), have been exploited for drug delivery,[554–556] food technologies,[557,558] tissue engineering,[559,560] and as antimicrobial agents.[561]

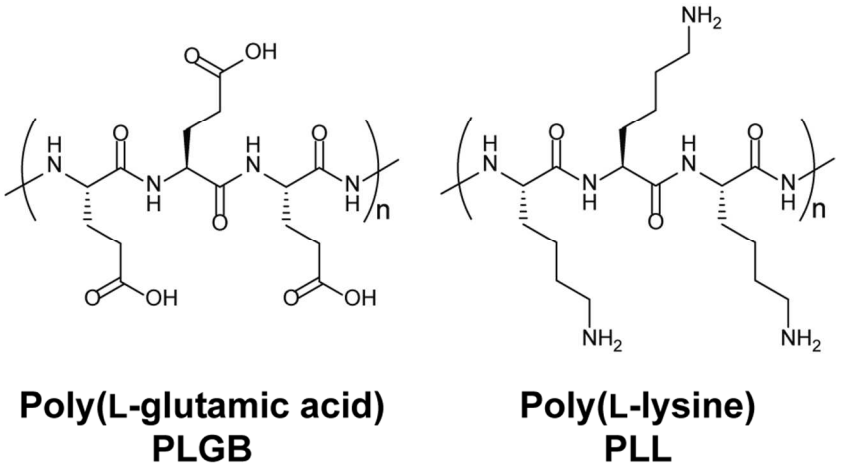


**Figure 39.** Chemical structures of poly(L-glutamic acid) and poly(L-lysine) polypeptides.

The emergent properties of polydisperse polypeptides composed of single amino acids are often not ideal for applications in water at physiological pH. For example, the charged side chains of poly(L-glutamate) at neutral pH sometimes induce interchain repulsive effects that can induce precipitation or reduce entanglement of the polypeptides into higher order networks.[562,563] To circumvent these effects for the production of stable hydrogels, Vacogne *et al.* developed the two-component poly(L-glutamate-*co*-allylglycine) polypeptide (**Scheme 2**).[563,564] Poly(γ-benzyl-L-glutamate-*co*-allylglycine) was synthesized via ring opening polymerization between NCA γ-benzyl-L-glutamate and allylglycine *N*-carboxyanhydride (NCA) precursors. Poly(γ-benzyl-L-glutamate-*co*-allylglycine) strands were then subjected to UV radiation to induce photo-

crosslinking with a 1,9-nonanedithiol linker to form fibrous gels in organic solutions (**Scheme 2**). Debenzylation of the polypeptide glutamate side chains followed by removal of solvent and subsequent reconstitution in aqueous solution resulted in a pH responsive hydrogel material. The covalent cross-linking of the polymer chains stabilized the gel network, while the glutamate side chains enable hydrogel formation at pH values of 6-10. At pH values of 6 and below, $\alpha$-helical formation dominates due to protonation of the carboxylic acids and hydrogels being to shrink.

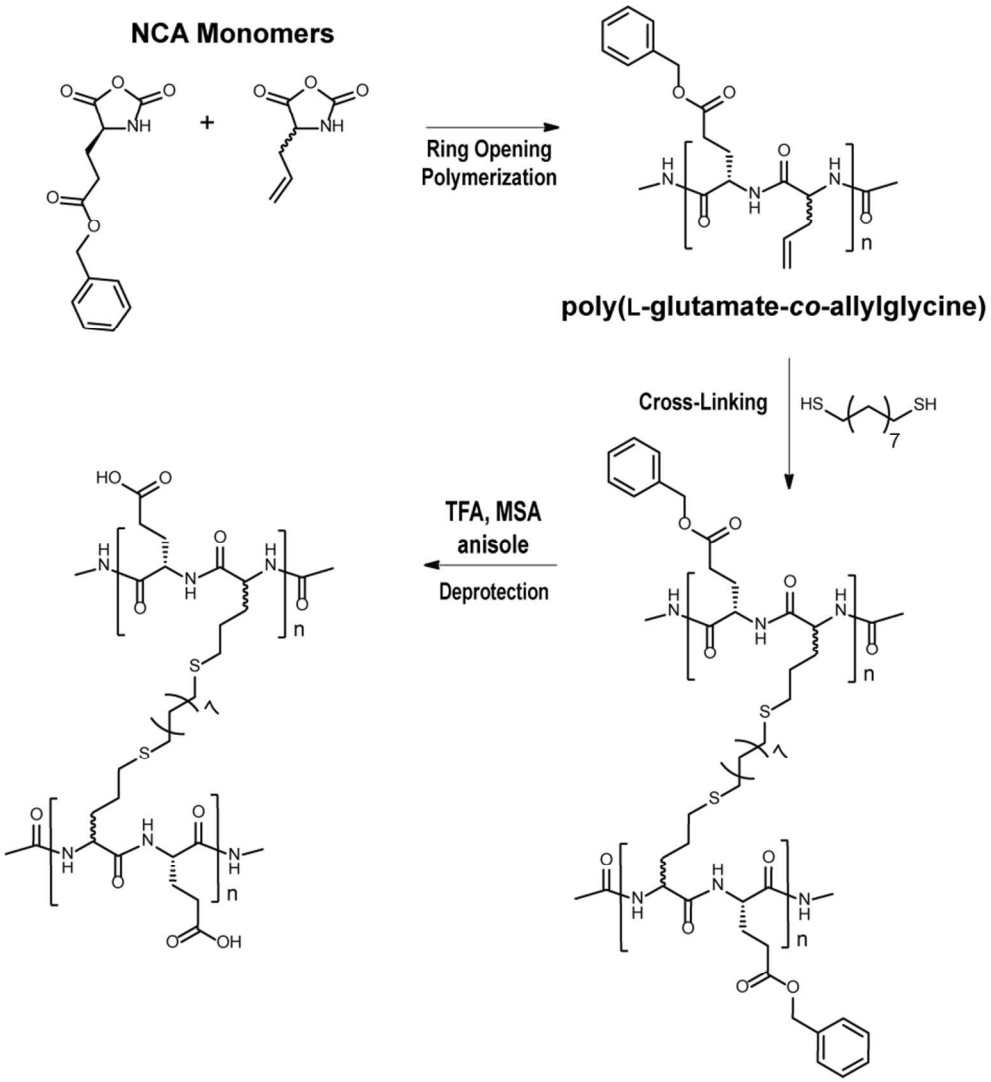


**Scheme 2.** Synthetic scheme for preparation of poly(γ-benzyl-L-glutamate-*co*-allylglycine) polypeptides by ring opening polymerization of γ-benzyl-L-glutamate and allylglycine NCA derivatives, followed by

cross-linking of peptides with 1,9-nonanedithiol, and finally deprotection of the benzyl protecting group to form water soluble polypeptides.[563]

While synthetic copolymer approaches have been used to tune the emergent properties of polydisperse polypeptides, multicomponent coassembly strategies have also been explored. Cai *et al.* employed a coassembly approach to investigate supramolecular polypeptide materials made from block copolymers that form hierarchical well-defined supramolecular structures that mimic biological multicomponent materials.[565] Supramolecular structures were observed after coassembling poly(γ-benzyl-L-glutamate) (PBLG) with poly(γ-benzyl-L-glutamate)-*block*-poly(ethylene glycol) (PBLG-*b*-PEG), which increased water solubility and altered the mechanical properties of the resulting coassembled hydrogel (**Figure 40A**). Morphological changes of the supramolecular aggregates were observed as the molecular weight of the PBLG polymers increased; spherical morphologies were observed for lower molecular weights of PBLG (PBLG molecular weight = 40,000 g $mol^{-1}$) coassembled with PBLG-*b*-PEG and long, helical rods and rings were generated in coassemblies with higher molecular weights (PBLG molecular weight = 520,000 g $mol^{-1}$) compared to small, spherical aggregates formed from the self-assembly of PBLG-*b*-PEG alone (**Figure 40B**). Increasing the water content in the coassembled mixtures from 5 wt% to 23 wt% induced a shift to super-helical structure in the aggregates, which was hypothesized to result from twisting of the PBLG rods flanked by PEG blocks in an attempt to alleviate interfacial tension between PBLG peptides (**Figure 40C**).

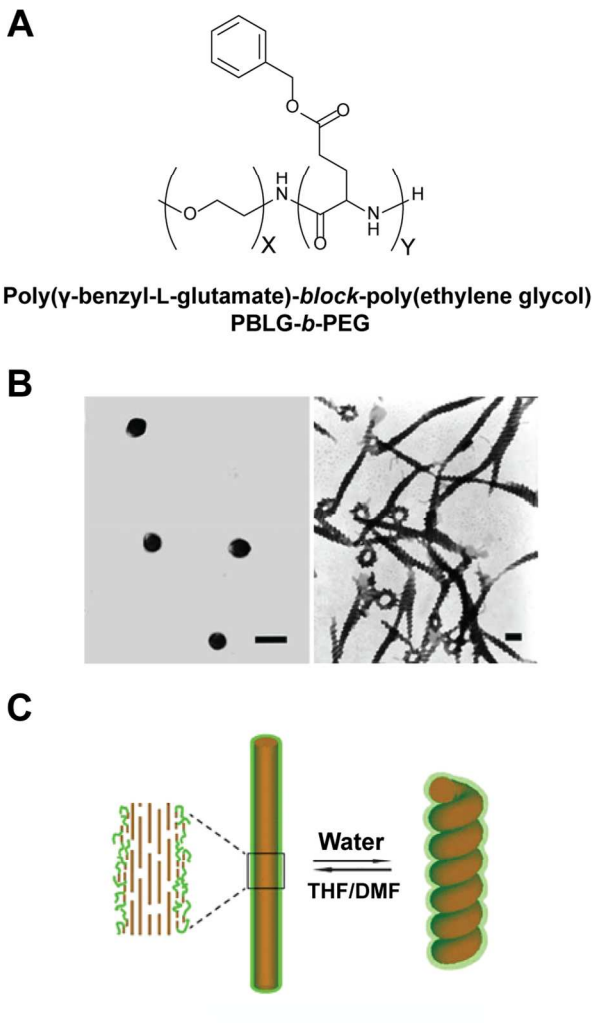


**Figure 40.** (A) Chemical structure of poly(γ-benzyl-L-glutamate)-*block*-poly(ethylene glycol). (B) TEM images of coassembled PBLG-*b*-PEG and PBLG at PBLG molecular weights of 40,000 g $mol^{-1}$ and 520,000 g $mol^{-1}$ (left and right TEM image respectively). (C) Model of predicted super-helical structure formed from twisting of PBLG rods (gold) flanked by PEG blocks (green) with increased water content in the solvent. Panels B and C reproduced from ref 565 (C. Cai, J. Lin, T. Chen, X.-S. Wang and S. Lin, *Chem. Commun.*, 2009, **0**, 2709–2711)[565] with permission from the Royal Society of Chemistry.

Based on these observations, theoretical *in silico* simulations guided selection of additional experimental coassembly formulations to increase understanding of the hierarchical assembly of these materials.[566] Varying the parameters of the coassembly conditions, including temperature, the ratio of the constituent polypeptides, and the rigidity of the polymer backbones, led to a

better understanding of supramolecular structure formation and hierarchical design of a novel morphologies including fibers, super-helices, spheres, and "balls of wool." Varying these parameters led them to deduce that interactions between PBLG segments as a function of temperature led to the formation of the super-helical and abacus-like morphologies. Investigating coassemblies of PBLG and polystyrene (PS) based polymers also gave insight into how the rigidity of the hydrophobic segments affect the supramolecular structures. Coassembly of polystyrene-*b*-poly(ethylene glycol) (PS-*b*-PEG) and PBLG homopolymers revealed fibers without helical features. These structures matched structures predicted by simulations, indicating that rigidity in the hydrophobic segment of the block copolymer is important for ordered packing in supramolecular structures. Similarly, PS homopolymers (**Figure 41A**) coassembled with PBLG-*b*-PEG block copolymers resulted in PS spherical core structures with ordered packing of PBLG segments on the outer surface of the spheres leading to striped spherical structures that resemble "balls of wool" (**Figure 41B**). Both simulations and experimentation led to rationally designed supramolecular structures that revealed insight for future hierarchical assembly processes.

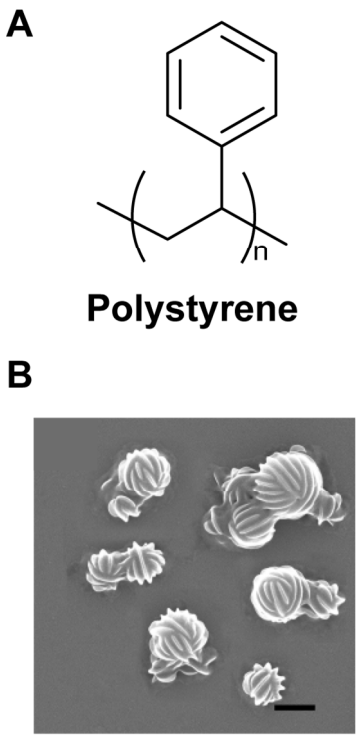


**Figure 41.** (A) Chemical structure of the polystyrene homopolymer (PS) used in coassembly with PBLG-*b*-PEG block copolymers. (B) TEM image of structures from coassembly of PBLG-*b*-PEG:PS in a weight ratio of 1.5:1 to create "balls of wool" morphologies. Panel B adapted with permission from C. Cai, Y. Li, J. Lin, L. Wang, S. Lin, X.-S. Wang and T. Jiang, *Angew. Chemie Int. Ed.*, 2013, **52**, 7732–7736.[566] 

Strategies for the directed formation of coassembled supramolecular structures from polydisperse peptides have also been investigated. Miserez *et al.* developed a system in which complementary charge was exploited to direct the coassembly of polypeptides in aqueous solutions to mimic natural glue proteins.[567] The adhesion proteins Pc-1 and Pc-2 are secreted from the sandcastle worm and are used to bind mineral particles in the construction of underwater shelter for the organism.[568,569] These proteins are post translationally modified with 3,4-dihydroxyphenylalanine (DOPA) and phosphoserine (*p*Ser). Miserez *et al.* synthesized gram scale quantities of positively and negatively charged polypeptides that mimic Pc-1 and Pc-2 adhesion proteins by NCA ring opening polymerization of precursors in ratios that matched

those found in the worm glue proteins (**Figure 42**). Serine phosphorylation was accomplished by post-polymerization phosphorylation.[570] Spherical, colloidal coacervates of the two peptides were discovered when polypeptides were mixed in a 6:4 ratio of positive:negative peptides in phosphate buffered saline solutions (pH 6.8). The pH at which coacervate initialization was observed could be altered by varying the ratio of the polypeptide components. These materials exhibited emergent properties that included low surface tension and shear thinning behavior, which was found to be similar to the adhesive properties of the natural glue proteins. These multicomponent coacervates were thus accurate models of naturally occurring bioadhesive materials.

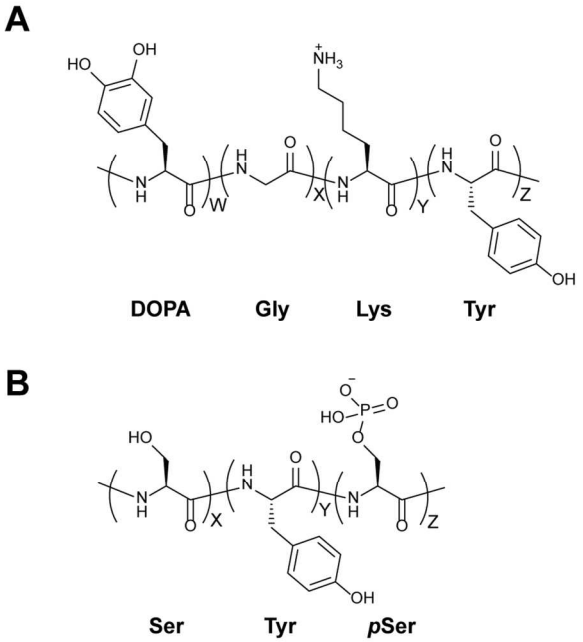


**Figure 42.** Chemical structures of positive (A) and negative (B) polypeptides that mimic adhesion proteins. The positively charged polypeptide is composed of 30 mol% DOPA, 50 mol% Gly, 10 mol% Lys, and 10 mol% Tyr and the negatively charged polypeptide is composed of 40 mol% Ser, 40 mol% *p*Ser, and 20 mol% Tyr. Each canonical and non-canonical residue is labeled beneath the chemical structure.[567]

The coassembly of polypeptides with natural proteins has also been explored in the creation of biomimetic multicomponent materials.[571–575] Resilin,[571] an insect extracellular matrix protein with low stiffness and rubber-like elasticity, has been a target for the development of biomimetic materials.[576] Rec1-resilin, a recombinant form of resilin (310 amino acids with GGRPSDSYGAPGGGN repeats), has been engineered to gel in response to external stimuli such as pH, heat, and light.[577,578] While these properties make Rec1-resilin an attractive supramolecular biomaterial, it undergoes dual-phase transition behavior at an upper and lower critical solution temperature (UCST and LCST respectively) in which phase separation occurs; unfortunately, these limits are outside of physiological temperature ranges (UCST ~6 ºC and LCST ~70 ºC). Choudhury *et al*. explored coassembly as a method to lower the upper critical solution temperature at which phase separation occurs for Rec1-resilin.[571] This was done by coassembling Rec1-resilin with polyproline-II, which has a rigid structure and relatively low molecular weight (10.7 kDa)[579] or silk fibroin (37-200 kDa).[580] Structure, morphology, and phase-transition behavior were all affected by the coassembly of these polypeptides with Rec1-resilin. Analysis of the coassembled structures indicated intermediate secondary structures and sizes of structures between that of Rec1-resilin and either of the biopolymer partners. The critical solution temperature at which assembly occurs for Rec1-resilin was lowered to 41 ºC (near physiological temperature) when coassembled with polyproline-II and 42.5 ºC when coassembled with silk fibroin. Thus, coassembly can be exploited to modify the properties of natural biomaterials to tune the emergent properties for specific application conditions.

Polydisperse peptides coassembled with proteins have also been utilized as drug delivery materials.[572,573] For example, poly(aspartic acid) (PAS), a biodegradable and water soluble negatively charged polypeptide at physiological pH, was coassembled with globular bovine

serum albumin (BSA), which contains multiple amino- and carboxylic acid groups that can be further modified after assembly with PAS and is therefore an attractive biomaterial candidate.[572] PAS/BSA coassembly was found to occur with intramolecular interactions occurring maximally at a PAS:BSA ratio of 0.54:1. Dynamic light scattering (DLS) and atomic force microscopy (AFM) studies of the coassembled material indicated complexation between polypeptide/protein particles as evidence by increased hydrodynamic radius of the particles with increasing concentrations of BSA. These polyelectrolyte/protein coassembled materials with water soluble, biocompatible components are attractive biomaterials that have abundant functionality for possible covalent attachment of bioactive molecules.

A similar multicomponent polypeptide/protein system was exploited for the encapsulation of photosensitizers for use in photodynamic antitumor therapy.[573] Yan and coworkers mixed positively charged poly(L-lysine) polypeptides (PLL) with human serum albumin (HSA) to form nanospheres (**Figure 43**) that encapsulated three different photosensitizers, chlorin e6 (Ce6), protoporphyrin IX, and verteporfin.[581] HSA was selected as the protein component since many tumors express proteinases for albumin catabolism, which could be used to trigger cargo release in the proximity of tumors *in vivo*.[582] HSA and PLL were coassembled and the resulting nanospheres were further cross-linked by treatment with dithiothreitol (DTT) to ensure disulfide bond retention in the HSA components. They demonstrated that an encapsulated photosensitizer (Ce6) was effectively released from the polypeptide/protein nanospheres in the presence of MCF-7 breast cancer tumors *in vivo*. The release of Ce6 from loaded PLL/HAS nanospheres was also triggered by changes in pH, protease degradation, and glutathione reduction. Released Ce6 could then be used in photodynamic antitumor strategies by irradiative photoexcitation. The observed tumor ablation effects of this multi-triggered release was found to be more significant

in mice bearing MCF-7 tumors than mice treated with free Ce6. These coassembled peptide/protein-based nanoparticles are promising new materials for drug delivery applications and antitumor therapy.

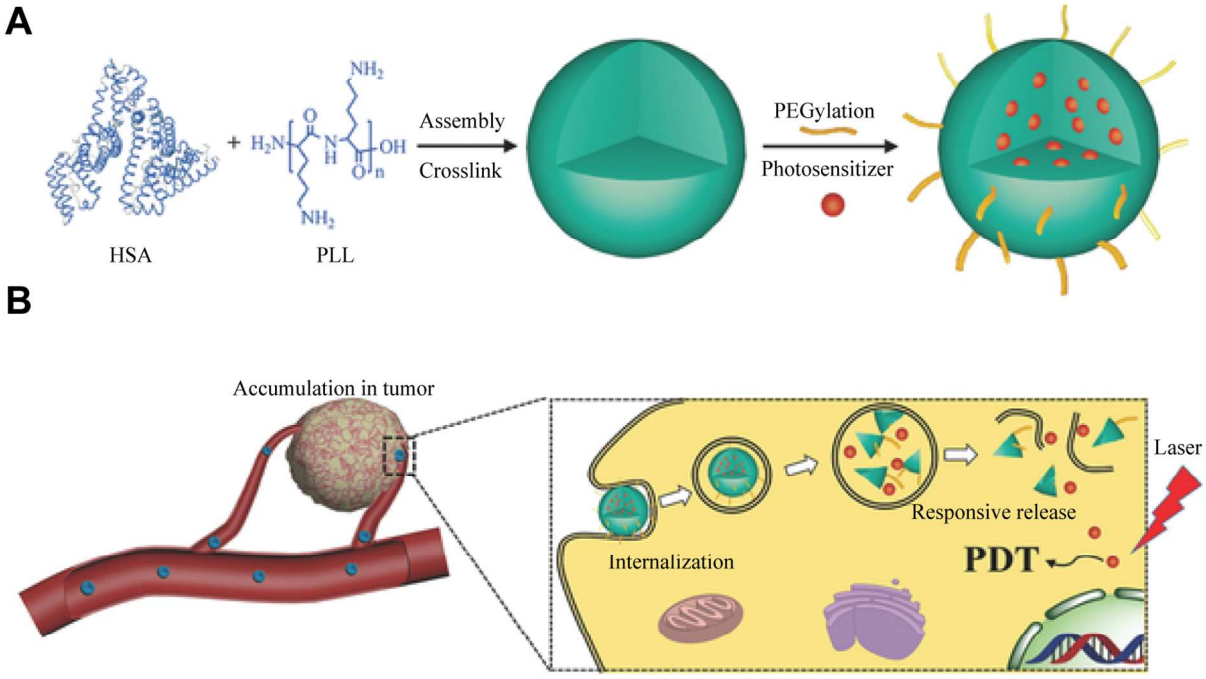


**Figure 43.** (A) Model of coassembly between human serum albumin and poly(L-lysine) to form nanospheres for surface PEG modification and encapsulation of photosensitizers. (B) Schematic representation of the *in vivo* internalization of the nanospheres at a tumor site and subsequent stimuli-responsive release of the photosensitizer for efficient photodynamic therapy. Figure reproduced with permission from N. Zhang, F. Zhao, Q. Zou, Y. Li, G. Ma and X. Yan, *Small*, 2016, **12**, 5936–5943.[573] © 2016 Wiley-VCH Verlag GmbH & Co.

Similar drug delivery vehicles were developed by Yang *et al*. to investigate targeted drug release in antitumor therapies.[574] They coassembled cholate grafted PLL (PLL-CA) with amphiphilic polyethylene glycol (PEG) doxorubicin conjugated polymers (PEG-DOX) (**Figure 44A**). Cholate was selected as hydrophobic molecule to improve tendency for vesicle formation.[583] These two polymers form micelle aggregates individually and were found to coassemble into vesicles with varying wall thickness based on the coassembly ratio of PLL-

CA:PEG-DOX (**Figure 44B**). This tunable vesicle structure, along with the use of acid labile PEG-DOX benzoic imine bonds (red in **Figure 44A**), allowed for enhanced vesicle uptake and triggered dissociation of doxorubicin with a pH drop from 7.4 to 5 in MCF-7 cancer cells *in vitro*.

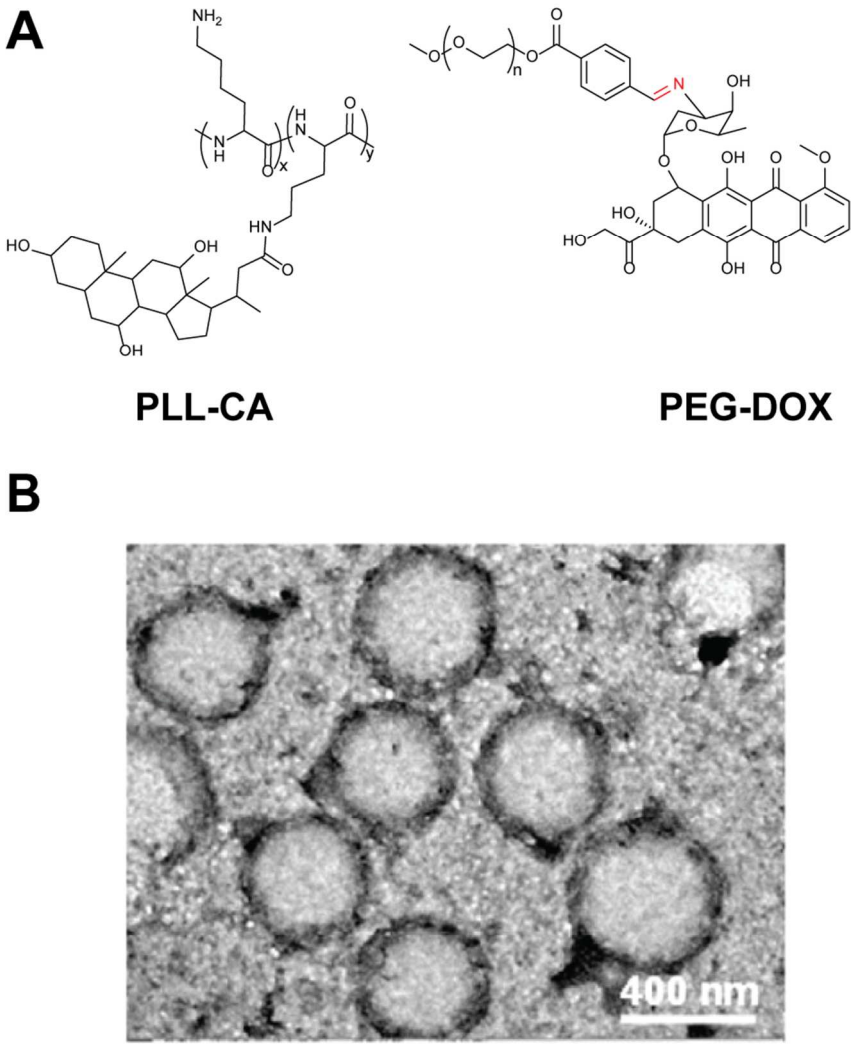


**Figure 44.** (A) Chemical structures of cholate grafted poly(L-lysine) and PEG conjugated doxorubicin. (B) TEM image of vesicles that form from the coassembly between PLL-CA7:PEG-DOX in a weight ratio of 1:2 in PBS at pH 7.4. Panel B adapted with permission from L. Zhu, L. Zhao, X. Qu and Z. Yang, *Langmuir*, 2012, **28**, 11988–11996.[574] © 2012 American Chemical Society.

**Section 8. Peptide/Biopolymer Hybrids**

Multicomponent supramolecular materials have also been developed that exploit the interaction of peptides with non-peptidic biopolymers.[32,584–592] These "hybrid" materials include mixtures of peptides with oligonucleotides,[593–596] phospholipids,[597,598] and carbohydrates.[599,600] In some cases, these materials have been created for a particular purpose, such as intracellular delivery of oligonucleotides for gene therapy.[597,601–604] In other cases, these materials have been discovered to have unique emergent properties that invoke novel applications.[605,606] While there is extensive literature devoted to hybrid materials composed of peptidic elements covalently modified with other biomolecules,[607–612] we will limit our discussion herein to selected examples of multicomponent supramolecular peptide hybrids in which the elements assemble via noncovalent interactions.

### 8.1 Peptide/Oligonucleotide Hybrids

Peptides have been shown to form supramolecular complexes with DNA or RNA oligonucleotides.[593–595,597,601–604] These hybrid materials have been designed for a variety of reasons. A major objective of many peptide/oligonucleotide hybrids has been to address the challenge of functional delivery of therapeutic oligonucleotides into cells.[613–615] Other examples have been devised that, beyond a functional application, exhibit interesting structural properties as novel materials.[606,616,617] Designed peptides for binding oligonucleotide sequences typically exploit positive charge for complementary electrostatic charge pairing with the phosphodiester backbone. Aromatic and nonpolar amino acids that can form π-π or van der Waals interactions are also found in oligonucleotide-interacting peptides. There exists a large body of work dedicated to the complexation of these designed cell penetrating peptides (CPPs) to oligonucleotides to aid in translocation across cell membranes for gene therapy

applications.[602,618–641] While CPPs coassemble with oligonucleotides to form noncovalent complexes, discussion herein will be limited to selected recent examples of peptide-based carriers for cellular oligonucleotide delivery in which the peptide/oligonucleotide nanomaterials have been characterized.[642,643]

Several groups have investigated the ability of self-assembling peptide materials to form complexes with oligonucleotide sequences through directed assembly to create artificial virus mimetics and nanocarrier systems for intracellular oligonucleotide delivery.[644–647] Lee and coworkers, for example, have shown that self-assembled $\beta$-sheet peptides with positively charged peptide segments complex with oligonucleotides to provide discreet, filamentous nanocarrier systems capable of binding and translocating siRNA and other molecular cargo into cells.[644–646] In an early study, they demonstrated that self-assembling $(FKFE)_3$ $\beta$-sheet peptides modified with a cell-penetrating peptide, $Tat_{48\text{-}60}$ (GRKKRRQRRRPPQ), encapsulated hydrophobic molecules (Nile red or pyrene) in the core of the hydrophobic nanofibril bilayer and that encapsulated molecules were transported into cells *in vitro* (**Figure 45**).[644]

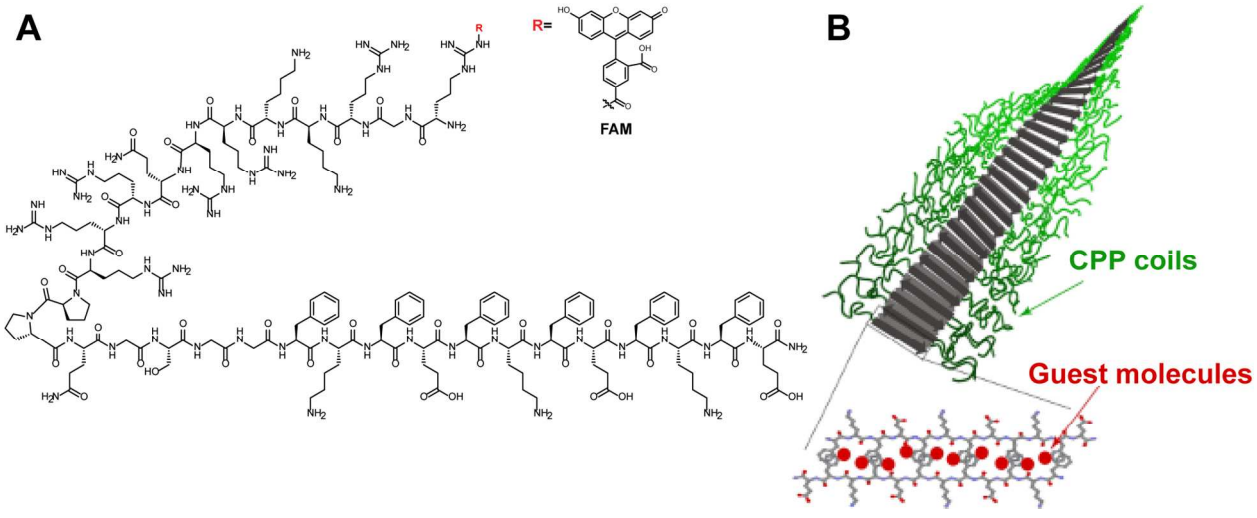


**Figure 45.** (A) Chemical structure of $Tat_{48\text{-}60}$-GSGG-$(FKFE)_3$-$NH_2$ CPP/peptide hybrid. R group labeled in red is either H or FAM (chemical structure pictured) for following cell internalization by fluorescence

microscopy. (B) Schematic of the assembly of the CPP decorated nanofibrils for guest molecule encapsulation in between the bilayer formed by the $\beta$-sheet peptide segment. Panel B reproduced with permission from Y. Lim, E. Lee and M. Lee, *Angew. Chemie Int. Ed.*, 2007, **46**, 3475–3478.[644] 

Based on these results, Lee *et al*. further developed the concept of novel filamentous nanocarrier virus mimetics for the cellular delivery of siRNA.[645] They designed and prepared an artificial virus mimetic from a multidomain self-assembly $\beta$-sheet peptide, Glu-KW (**Figure 46A**). Glu-KW (Glu-GSGSGS-KKKKKKKK-GGSGGS-$(WKWE)_3$WG) included a poly-Lys segment for siRNA binding and cell penetration, an *N*-terminal D-glucose for binding to cell surface glucose transporters in mammalian and cancerous cells, and a *C*-terminal self-assembling amphipathic sequence.[648] The peptide underwent nanofibril self-assembly in phosphate buffered saline and was also shown to bind siRNA duplexes at the surface of the peptide $\beta$-ribbon nanofibril (**Figure 46B**). They found that this designed nanocarrier system delivered siRNA into cells and elicited functional knockdown of gene targets with efficiencies near that of the Lipofectamine 2000 transfection agent.[649]

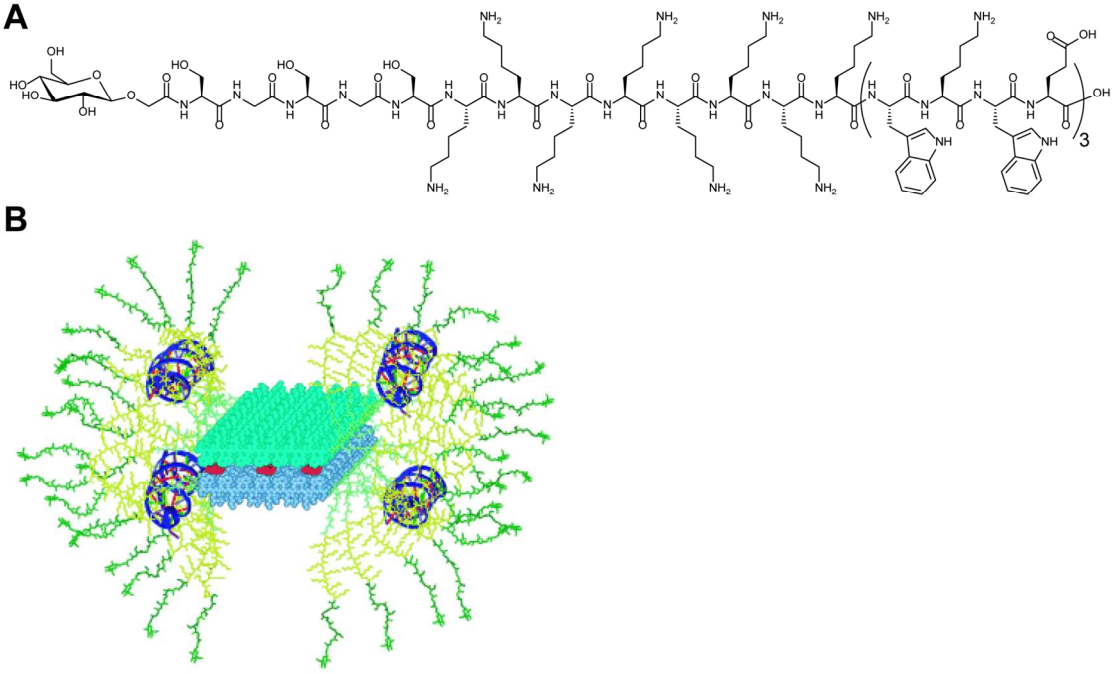


**Figure 46.** (A) Chemical structure of the Glu-KW multidomain peptide with D-glucose attached to the *N*-terminus followed by a poly-lysine segment for oligonucleotide binding, and a $\beta$-sheet $(WKWE)_3$ peptide to induce fibril formation. (B) Schematic of $\beta$-sheet formation and subsequent oligonucleotide biding (shown in dark blue) to the multivalent display of poly-lysine peptide segments on the supramolecular fibrils. Panel B reproduced with permission from Y. Lim, E. Lee, Y.-R. Yoon, M. S. Lee and M. Lee, *Angew. Chemie Int. Ed.*, 2008, **47**, 4525–4528.[645] © 2008 American Chemical Society.

Dong *et al*. have also reported similar self-assembling $\beta$-sheet multidomain peptides that mediate transport of DNA plasmids into cells.[647] They investigated several formulations of the self-assembling $\beta$-sheet peptide $(QW)_6$ in which $K_{10}$ was appended to the *N*-terminus or in which $K_5$ domains were attached to both termini. Charge distribution of the lysine domains affected both assembly and transfection efficiency of the systems. The $K_5(QW)_6K_5$ peptide failed to self-assemble, whereas the $K_{10}(QW)_6$ sequence efficiently assembled into short $\beta$-sheet nanofibrils with persistence lengths less than 50 nm. $K_{10}(QW)_6$ nanofibrils were shown to complex with the Hoechst 33258 dye[650] and facilitate its transport into HeLa cells. The $K_{10}(QW)_6$ nanofibrils bound to luciferase plasmid DNA to provide ~50 nm nanostructured complexes that invoked

luciferase expression when coincubated with HEK293 and HeLa cells, providing evidence of functional cell transport. Collectively, these studies by Lee *et al*. and Dong *et al*. demonstrate that supramolecular $\beta$-sheet assemblies can bind oligonucleotides and function as effective tranfection agents *in vitro*.

Nilsson and Dean *et al*. have developed stimuli-responsive peptide-siRNA complexes for the functional delivery of siRNA into cells.[642] Cyclic peptides were designed in which a short RNA-binding sequences was flanked with cysteine residues that facilitated cyclization by disulfide-bond formation.[651] Of these peptides, cyclic Ac-C$(WR)_4$CG-$NH_2$ was found to effectively complex with siRNA via Arg-mediated ionic interactions to form ~20 nm nanoparticles (**Figure 47A**, inset). These particles facilitated efficient delivery of siRNA into A549 lung cells *in vitro*. Highly efficient knockdown of gene targets was observed both *in vitro* and in the lungs of mouse models *in vivo*. The rationale for this delivery system is that the constraining peptide disulfide bond should be stable in the oxidizing environment of the extracellular space, giving stability to the complexes and enabling peptide-mediated delivery of the siRNA cargo to the cytosol. The peptide disulfide bonds should be reduced by cellular glutathione upon delivery to the cytosol, rendering the now-linear peptides to enzymatic proteolytic degradation and releasing the siRNA cargo to the RNA interference machinery (**Figure 47**). These multicomponent peptide-oligonucleotide supramolecular hybrids illustrate the design of functional materials through noncovalent assembly of peptides with non-peptide/protein biopolymers.

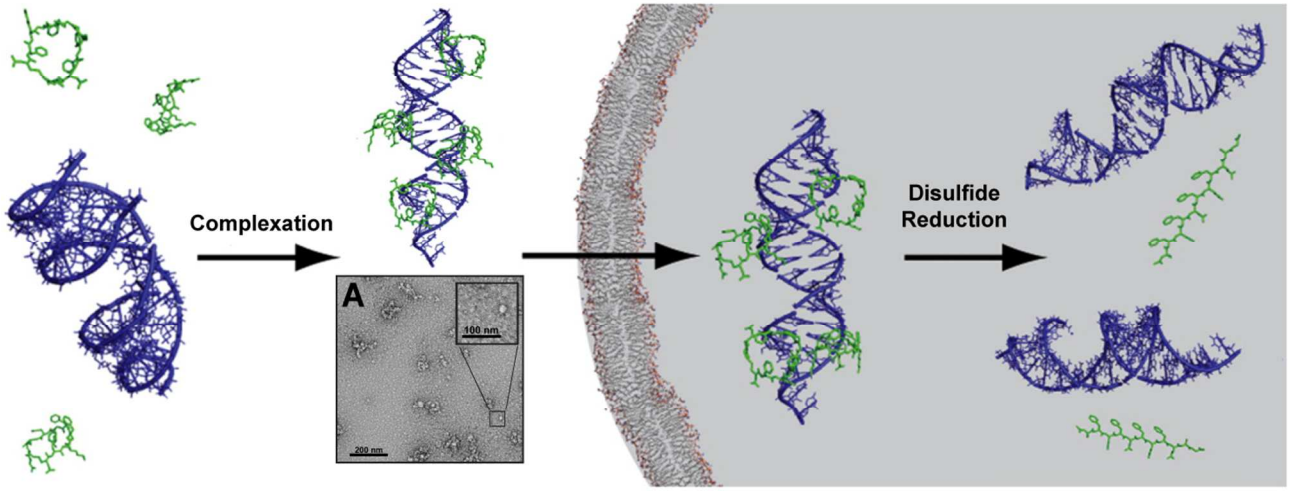


**Figure 47.** Schematic representation of siRNA complexation to positively charged, disulfide constrained peptides for facilitated entry into a cell. Upon entering the cell, reducing conditions break the disulfide bonds apart and releases siRNA. (A) Inset shows TEM image (200 nm scale bar) of peptide/siRNA nanoparticles formed in the presence of 1000-times excess peptide with a zoomed in region indicating a single nanoparticle (100 nm scale bar). Figure adapted with permission from J. J. Welch, R. J. Swanekamp, C. King, D. A. Dean and B. L. Nilsson, *ACS Med. Chem. Lett.*, 2016, **7**, 584–589.[642] © 2016 American Chemical Society.

Meier and coworkers have developed sophisticated multicomponent particles composed of self-assembling peptides that condense oligonucleotides and small molecule therapeutics for the combined stimulus-responsive cellular delivery of the cargo molecules.[643] This work was motivated by the challenges posed by multidrug resistance in cancer treatments that may be met by the codelivery of therapeutics with complementary activity profiles, including small molecule drugs and antisense oligonucleotides (AONs) that can alter the expression of proteins that enable drug resistance. Meier *et al*. had previously reported amphiphilic gramicidin-derived peptides that self-assembled into spherical micelles capable of embedding hydrophobic and hydrophilic cargo.[652–654] They adapted these peptides to include an oligonucleotide-binding tri-histidine motif attached to the assembly motif via a disulfide linker (**Figure 48**). These adapted peptides self-assembled into spherical micelles that could be loaded with hydrophobic small molecule cargo as well as AONs. These multicomponent particles were shown to effectively deliver both small

molecules and AONs into cells where reduction of the disulfide bond linker region resulted in release of the AON and small molecule cargo. This elegant design has great promise for application as a next-generation nanocarrier for the selective codelivery of therapeutic cargo molecules.

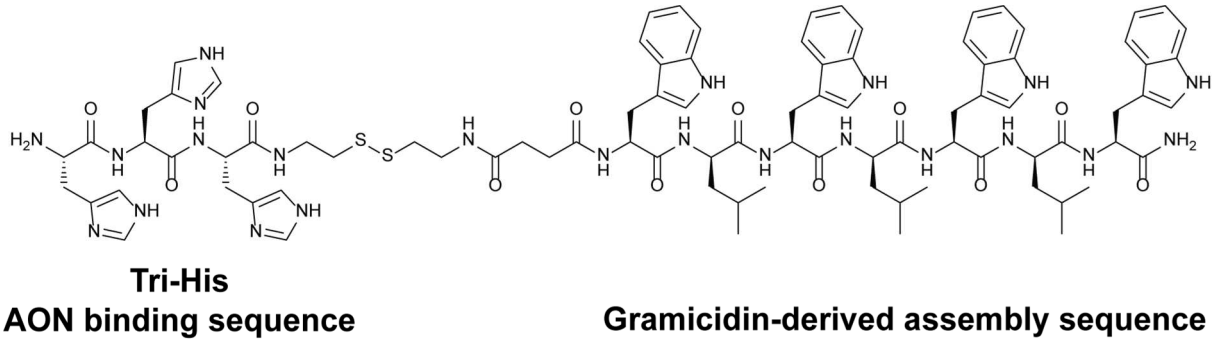


**Figure 48.** Chemical structure of Meier's amphipathic self-assembling peptides that form micelles that bind to AON and release this cargo upon disulfide bond cleavage of the tri-His sequence.[643]

Guler *et al.* investigated multicomponent peptide amphiphile (PA)/oligonucleotide sytems for intracellular delivery of AONs.[622] PAs were designed that included *N*-terminal lauryl groups attached to a $P_4$ polyproline with *C*-terminal olignoculeotide-binding/cell penetrating motifs (**Figure 49A**). These self-assembling PAs were found to form spherical particles that bound AONs at the solvent exposed exterior face (**Figure 49B**). Toxicity and AON uptake were assessed for each PA system and it was found that the KRSR-PA PA had the best toxicity/AON transport profile. Efficient transfection and release of Bcl-2 AONs in MCF-7 cells was effective for all systems except for the K-PA assembly, presumably due to poor AON binding with only a single lysine available for complementary pairing. Transport assays conducted in the presence of uptake inhibitors[655] demonstrated that AON delivery with the K-PA/AON and the $R_4$-PA/AON complexes were not inhibited by any of the assessed inhibitors, suggesting a non-endocytotic pathway for internalization. Delivery with the $R_8$-PA and KRSR-PA/AON complexes were

found to be dynamin-mediated and interestingly, coassembled $R_8$-PA/KRSR-PA/AON complexes were found to be mediated by dynamin, clathrin-mediated endocytosis, and caveolae-mediated endocytosis internalization pathways, indicating the complex effects of PA formulation on transport mechanism.

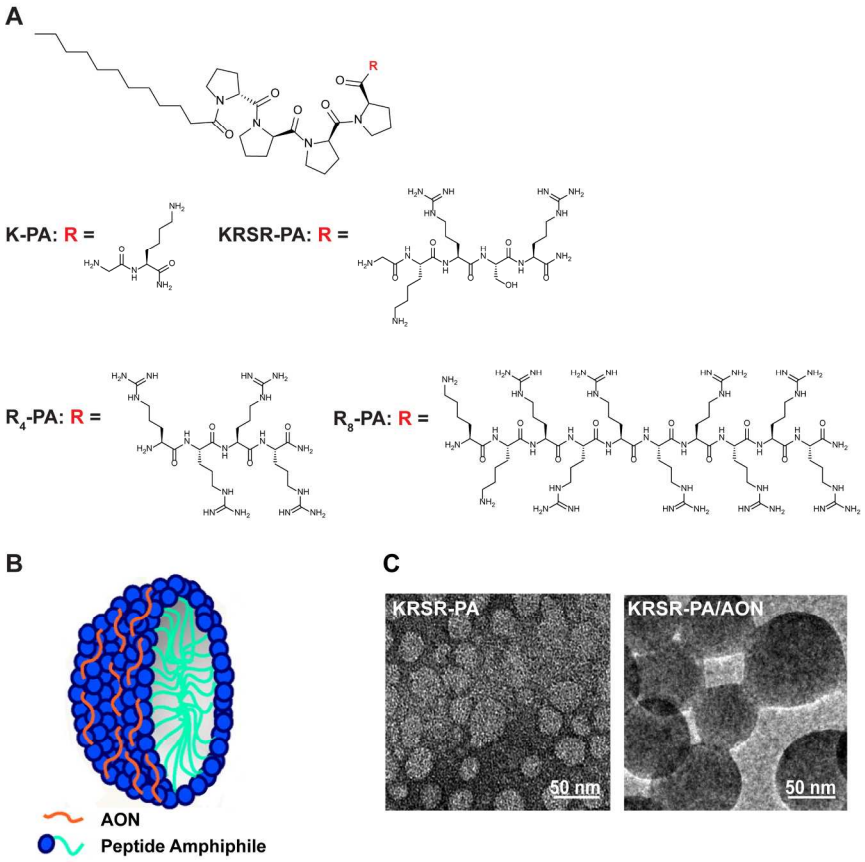


**Figure 49.** (A) Chemical structure of four peptide amphiphiles (K-PA, KRSR-PA, $R_4$-PA, and $R_8$-PA) with two different oligonucleotide binding sequences: $R_4$ or $R_8$ cell penetrating peptide segments or KRSR proteoglycan binding peptide sequence attached to a poly-proline peptide amphiphile with a $C_{11}H_{23}$ hydrophobic tail. (B) Pictorial representation of the nanoparticles formed from the complexation of K-PA derivatives with AONs. (C) TEM images of the KRSR-PA (left) and KRSR-PA/AON complexed nanoparticles (right). Increase in size from approximately 20 to 70 nm indicated AON binding to surface of the nanoparticle. Panels B and C adapted with permission from D. Mumcuoglu, M. Sardan, T. Tekinay, M. O. Guler and A. B. Tekinay, *Mol. Pharm.*, 2015, **12**, 1584–1591.[622] © 2015 American Chemical Society.

Guler *et al*. also investigated the effects that the carrier morphology has on the cellular internalization of coassembled oligonucleotides.[623] They prepared peptide amphiphiles (PAs)

with a positively charged *N*-terminal region for oligonucleotide binding, a central peptide segment consisting of either a polyproline or β-sheet peptide, and a hydrophobic tail (**Figure 50**). Each PA was also functionalized with glucose near the *N*-terminus, which facilitates multivalent glycogen display at the surface of each PA structure, a feature that can aid in tumor tissue targeting to glucose transporters that are overexpressed at the surface of cancer cells. The PAs with polyproline cores formed self-assembled nanospheres whereas the β-sheet peptide PAs self-assembled into cylindrical structures. Both of these PA nanostructures were complexed to antisense oligonucleotides (AON) and their cellular internalization was visualized *in vitro* using MCF-7 cell lines. The spherical AON carriers were internalized more rapidly than the cylindrical carriers. Cellular uptake of the spherical AON carriers was not inhibited in the presence of endocytosis inhibitors, suggesting an alternative mechanism of translocation through the cell membrane for these peptide/oligonucleotide hybrids. In contrast, translocation of the cylindrical nanocarriers into cells was significantly reduced by endocytosis inhibitors, confirming that these structures enter the cell through mediated endocytosis. These observations provide interesting insight into the design principles that underlie the development of multicomponent cellular delivery agents and also raise questions about the mechanisms of cellular transport.

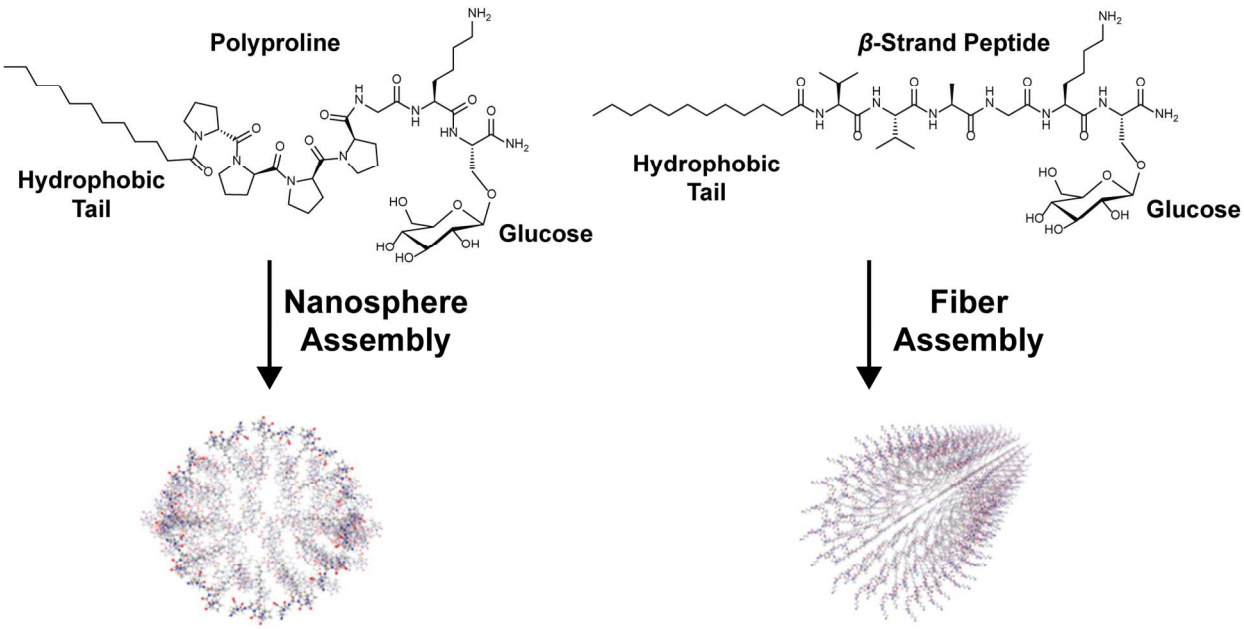


**Figure 50.** Chemical structures for Guler's peptide amphiphiles designed to form either nanospheres or fibers by incorporating a polyproline or *β*-sheet assembling peptide respectively to a hydrophobic alkyl chain tail. Each PA was also modified with glucose near a positively charged *C*-terminus for the ability to bind both oligonucleotides and cancer cell glucose receptors. Figure adapted with permission from D. Mumcuoglu, M. Sardan Ekiz, G. Gunay, T. Tekinay, A. B. Tekinay and M. O. Guler, *ACS Appl. Mater. Interfaces*, 2016, **8**, 11280–11287.[623] © 2016 American Chemical Society.

Additional peptide/oligonucleotide coassembled materials have been inspired by the structure of naturally occurring viral capsids.[616,617,656] In one example, Ni *et al*. designed peptide/DNA nanoparticles from peptides containing a hydrophobic *C*-terminal region, a central *β*-sheet peptide segment to induce self-assembly, and a cationic tail capable of binding to the phosphate backbone of DNA (**Figure 51A**).[616,656] Peptide nanococoons condensed around the DNA and produced ellipsoid-shaped nanoparticles approximately 65 × 47 nm wide (**Figure 51B**). The DNA was encapsulated inside the peptide shell, protecting it from enzymatic degradation *in vitro*. These nanococoons are similar to the structure of parapoxvirus viral capsids that encapsulate DNA inside of a striped, outer peptide barrier (**Figure 51**). Tuning the stability and morphology of the peptide/DNA mixtures was possible by altering the hydrophobic core of the

peptides and the N/P ratio (number of positive charges from peptide amines over the number of negative charges from the phosphates on DNA).[656]

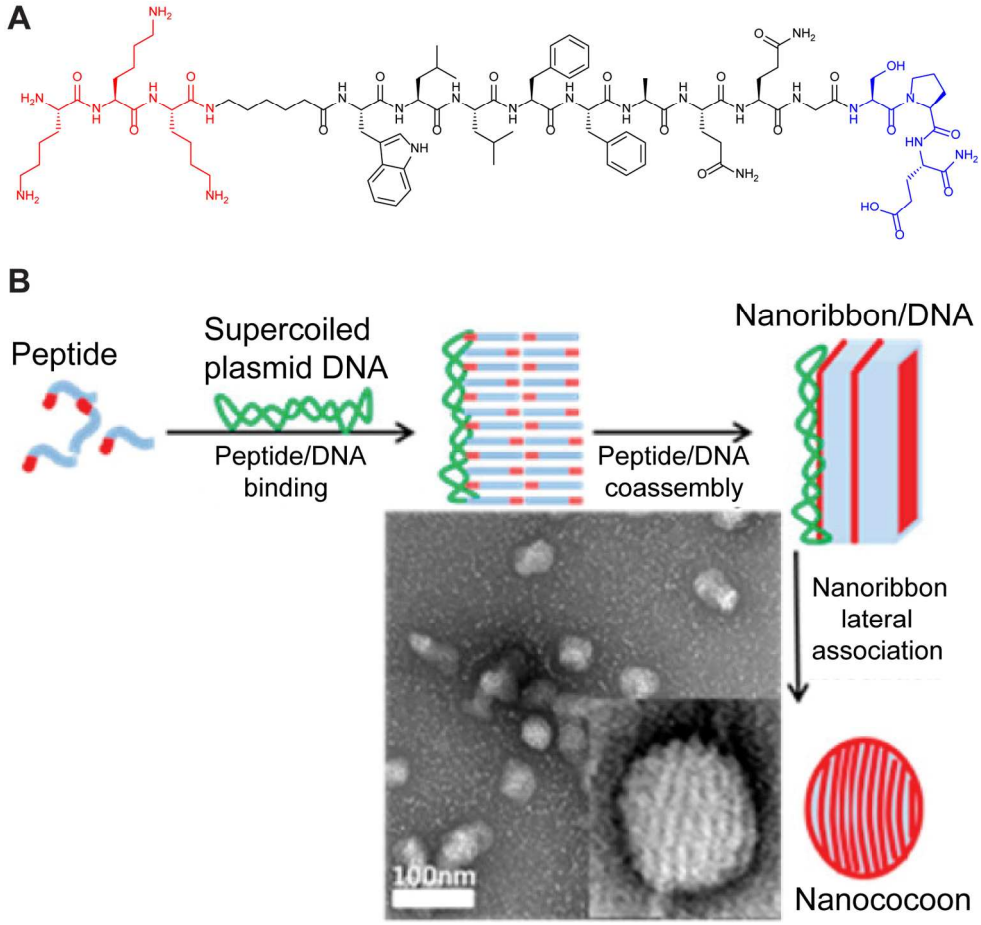


**Figure 51.** (A) Chemical structure of DNA binding peptide with a cationic (red), *β*-sheet (black), and *C*-terminal hydrophilic region (blue). (B) Schematic of peptide/DNA coassembly into nanococoon structures and a TEM image of nanococoons produced from the coassembly of these materials. Figure reproduced with permission from R. Ni and Y. Chau, *J. Am. Chem. Soc.*, 2014, **136**, 17902–17905.[616] © 2014 American Chemical Society.

Similarly, Ke *et al*. demonstrated the hybrid nanostructures formed by coassembly of collagen mimetic peptides and DNA nanosheets.[617] One dimensional banded nanowires were observed from the coassembly of the $(PRG)_3(POG)_3(PRG)_3$ collagen mimetic peptide and two layer DNA origami nanosheets (**Figure 52**). These nanowires featured a periodic coassembled structure in which the alignment of the peptide helices is perpendicular to the DNA nanosheet

faces. This allowed for the tunable control of the distances between DNA nanosheets via extension of the middle (POG) motif of the CMP. These hybrid nanostructures give a sense of the breadth of coassembled structures that are accessible by interaction of peptides with oligonucleotides.

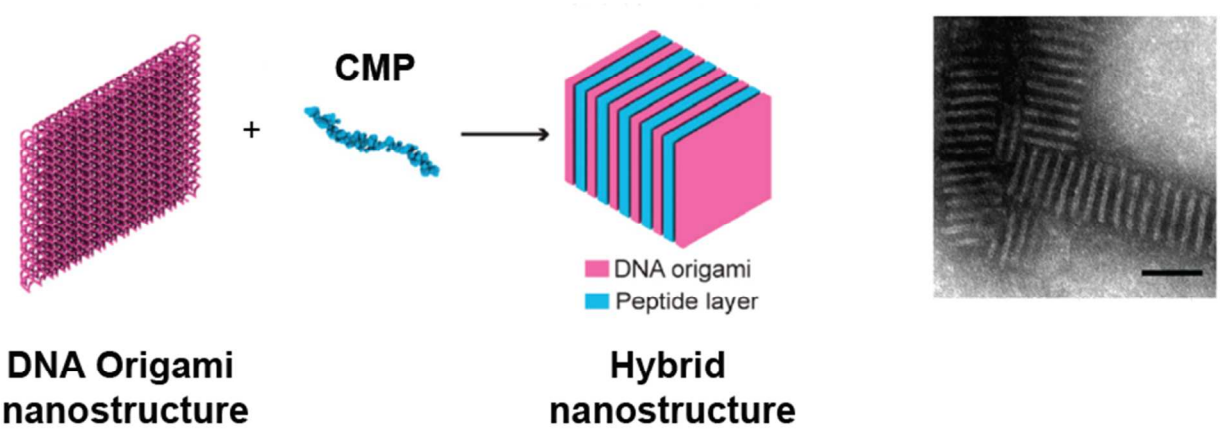


**Figure 52.** Coassembly of $(PRG)_3(POG)_3(PRG)_3$ CMP with DNA nanosheets to form one dimensional, banded nanowires. Figure reproduced with permission from T. Jiang, T. A. Meyer, C. Modlin, X. Zuo, V. P. Conticello and Y. Ke, *J. Am. Chem. Soc.*, 2017, **139**, 14025–14028.[617] © 2017 American Chemical Society.

### 8.2 Peptide/Phospholipid Hybrids

Multicomponent supramolecular peptide/phospholipid hybrid systems have been developed for applications including drug or gene delivery[597,657,658] and stabilization of membrane proteins.[598,659] In one example, Ko *et al*. developed an oligonucleotide nanoparticle delivery vehicle formed from the coassembly of the PL9R phospholipid-peptide conjugate (**Figure 53A**), with oligodeoxynucleotides (ODNs).[597] Mixtures of PL9R with ODNs formed lipid micelles with the cationic peptide segment in the interior of the micelle where the ODNs were sequestered (**Figure 53B**). ODN encapsulation was also observed by the coassembly of PL9R with unmodified phospholipids (PLs), PEGylated PLs to modify solubility, and Tat-PEG-PL

conjugates for increased cellular uptake mediated by the cell-penetrating Tat peptide (**Figure 53B**). The biocompatibility of this ODN delivery system was greater than that of a similar one assembled from PLs conjugated to polyethylenimine ODN binding cations instead of the 9R peptide, which was previously shown to encapsulate ODN but was toxic to cells above a concentration of 10 μg/mL. The PL9R system had a significantly lower toxicity threshold as indicated through a 91.4% cell viability compared to 37% of NIH 3T3 fibroblasts when treated with 50 μg/mL of the PL9R or polyethylenimine ODN delivery systems respectively. Intracellular delivery of ODNs to HeLa cells was observed with the Tat-presenting system, whereas ODNs in nanoparticles without the Tat display failed to enter the cytosol. Tumor-selective *in vivo* delivery of siRNA by Tat-nanoparticles in HeLa tumor-bearing mice was also demonstrated. These multicomponent assemblies exploit phospholipid molecules to drive assembly in nanoparticles while the peptide components are used mediate ODN encapsulation and facilitate membrane translocation and delivery of cargo.

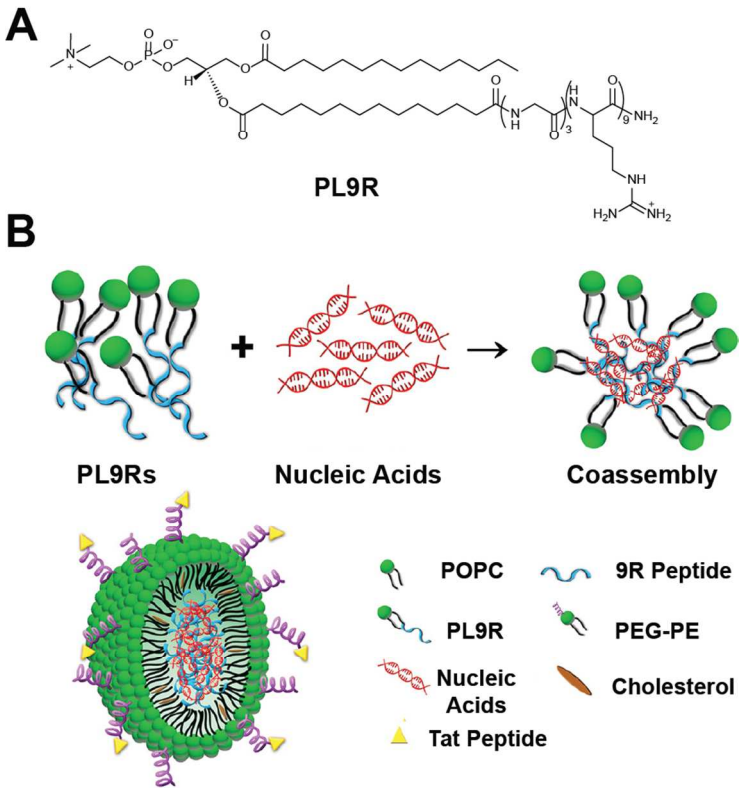


**Figure 53.** (A) Chemical structure of the PL9R phospholipid-peptide. (B) Model of the ODN nanoparticle cellular delivery system. Coassembly of phosphatidylcholine (POPC), PL9R phospholipid-peptide conjugate, a PEGylated phospholipid (PEG-PE), and cholesterol provide a delivery system capable of binding and encapsulating nucleic acids. This vesicle delivery system was surface modified for multivalent display of the Tat cell penetrating peptide for increased cellular uptake. Figure reproduced with permission from J. H. Kang, G. Battogtokh and Y. T. Ko, *Biomacromolecules*, 2017, **18**, 3733–3741.[597] © 2017 American Chemical Society.

Another coassembled vesicle system was developed by Nie *et al*. to down-regulate extracellular matrix (ECM) levels in pancreatic tumors.[657] Pancreatic tumors feature rapid proliferation of pancreatic stellate cells, which secretes ECM and presents a significant barrier to diffusion of chemotherapeutics to the tumor. The objective of this work was to create particles that encapsulate and selectively release pirfenidone (PFD) at the site of pancreatic stellate cells to down-regulate ECM formation to circumvent this barrier to tumor treatment (**Figure 54**). This objective was addressed by coassembling an amphiphilic matrix metalloproteinase-2 (MMP-2,

upregulated in many tumors) substrate peptide (GPLGIAGQ) with L-$\alpha$-phosphatidylcholine to create nanoparticles that to encapsulate pirfenidone (PFD). The MMP-2 cleavage sequence would be selectively cleaved in the tumor environment, releasing pirfenidone directly to pancreatic stellate cells. Liposomes from coassembly of the peptide and lipid components at a 1:5 ratio of peptide:lipid exhibited MMP-2 responsive release of over 80% of the encapsulated pirfenidone *in vitro*. Pancreatic tumor bearing mice were treated with the pirfenidone liposomes with 7 injections over 15 days, followed by treatment with gemcitabine, a tumor targeting chemotherapy drug, for 5 days to ablate tumor growth. A significant decrease in tumor size was seen in mice treated with the PFD vesicles compared to the control group presumably due to the down regulation of ECM at the site of the tumors from targeted pirfenidone treatment. These coassembled peptide hybrid structures are promising, sophisticated stimulus-responsive materials for tissue-specific delivery of therapeutics.

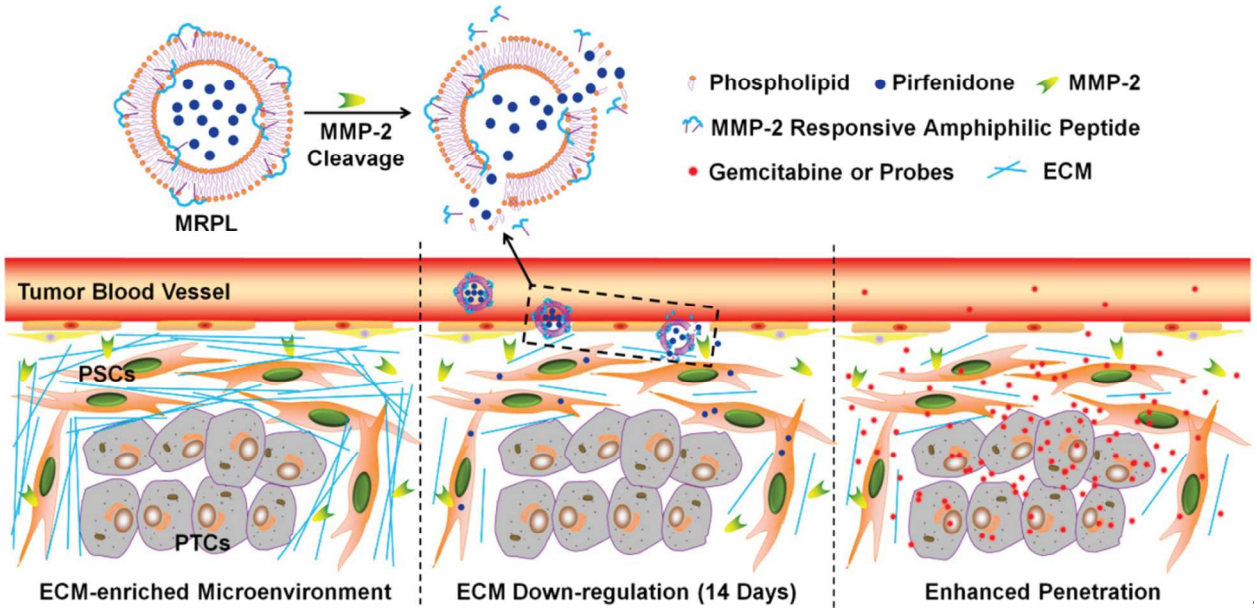


**Figure 54.** Pictorial representation of MMP-2 responsive vesicles designed to release pirfenidone *in vivo* at the site of pancreatic tumors for ECM-regulation and subsequent treatment with gemcitabine. A delivery vehicle is formed via coassembly of phospholipids with MMP-2 responsive peptide with cleavable sequence GPLGIAGQ to encapsulate pirfenidone. At tumor sites in mice, the liposomes are weakened via MMP-2 cleavage of the GPLGIAGQ peptide followed by pirfenidone release, which causes

down regulation of the extracellular matrix. The mice are then more easily treated with the antitumor drug gemcitabine to mitigate tumor growth. Figure reproduced with permission from T. Ji, J. Lang, J. Wang, R. Cai, Y. Zhang, F. Qi, L. Zhang, X. Zhao, W. Wu, J. Hao, Z. Qin, Y. Zhao and G. Nie, *ACS Nano*, 2017, **11**, 8668–8678.[657] © 2017 American Chemical Society.

Zhang *et al*. have developed an intelligent supramolecular delivery vehicle for melittin.[658] Melittin, a positively charged, 26 amino acid anticancer drug candidate (GIGAVLKVLTTGLPALISWIKRKRQQ-$NH_2$), is difficult to administer *in vivo* because it disrupts phospholipid bilayers of cell membranes and causes hemolysis as a detrimental side effect upon intravenous injection.[660] It was postulated that the charges on the $\alpha$-helical melittin peptide could be shielded during delivery in a nanoparticle via linkage to the *N*-terminus of another $\alpha$-helical peptide, FAEKFKEAVKDYFAKFWD-$NH_2$. This $\alpha$-helical peptide had previously been shown to coassemble with a peptide-phospholipid scaffold to form 20 nm core-shell lipid nanoparticles in which the inner embedded peptide retains its natural structure and function.[661] This led to the design of the hybrid $\alpha$-melittin peptide, DWFKAFYDKVAEKFKEAF-GSG-melittin, which was expected to similarly coassemble with phospholipids to embed the attached melittin peptide within the resulting nanostructure, preventing its hemolytic effects during delivery. After formation of the nanoparticle, measured zeta potentials indicated a near neutral charge of the nanoparticles, confirming effective charge shielding of the melittin. *In vitro* analysis using red blood cells indicated a significantly decreased cytotoxicity threshold for melittin nanoparticles compared to free melittin before cytotoxicity was observed. Significant tumor growth inhibition was observed by the $\alpha$-melittin nanoparticles against B16F10 melanoma when administered to tumor-bearing mice. This is yet another example of a multicomponent coassembled hybrid system that enables efficient *in vivo* delivery of a problematic drug candidate.

### 8.3 Peptide/Carbohydrate Hybrids

Peptides have been shown to coassemble with oligosaccharides as well as oligonucleotides and phospholipids. Hyaluronic acid (HA) (**Figure 55**), for example, is the most common glycosaminoglycan found in the extracellular matrix, making it an inviting material for biological applications[662–664]. In one such application, Rupenthal *et al*. developed a nanoparticle carrier system to deliver and extend the bioactivity of Cx43 MP, a peptide mimetic of a 43 kDa isoform of a connexin transmembrane protein.[665] Cx43 MP reduces inflammation, neuronal cell death, and vascular leakage after retinal injury.[666] Targeted delivery of Cx43 to the retina was accomplished by coassembling the peptide into HA-coated human serum albumin nanoparticles. Specifically, Cx43 MP was loaded into human serum albumin nanoparticles that were surface modified through conjugation of HA to provide nanoparticles that encapsulate Cx43 and display HA at the exposed surface. HA is recognized by CD4 receptors that are a widely expressed retinal glycoprotein.[667] The HA coated nanoparticles were shown to significantly increase the amount of Cx43 MP delivered to human retinal pigment epithelial cells (ARPE-19) *in vitro* compared to amount of Cx43 MP delivered by nanoparticles that were not coated with HA. The HA nanoparticles also protected Cx43 from degradation and sustained its release time in retinal cells. This is an improvement to the intravitreal delivery of the Cx43 MP using a coassembled system composed of natural components and biopolymers.[668,669]

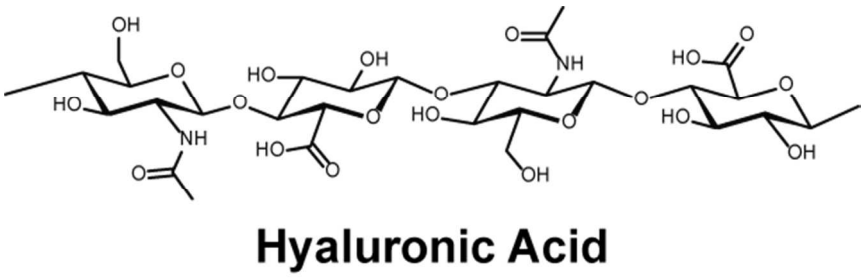


**Figure 55.** Chemical structure of hyaluronic acid.

Hong *et al*. have developed a protective film of coassembled peptide/HA components to encapsulate mesenchymal stem cells.[670] Intravenous delivery of mesenchymal stem cells (MSCs) for treatment of inflammatory diseases is plagued by challenges to MSC viability in harsh microenvironments as they are subjected to shear stress.[671] In order to increase cell survival, a coating was deposited around the MSCs using layer-by-layer coassembly of poly(L-lysine), HA, and RGD peptide building blocks to stabilize the cells with a shear thinning polymer coating (**Figure 56**). Significant increases in MSC survival rate was seen in both *in vitro* and *in vivo* experiments using protectively coated-MSCs as evidenced by the activation of the Akt protein through CD44-HA receptor binding, a key indicator for cell survival.[672] Further evidence of prolonged MSC survival was obtained using green fluorescent protein expressing MSCs (GFP(+) MSCs) with and without the multicomponent protective coating. GFP(+) MSCs were delivered intravenously to mice which were then subjected to muscle injury. The prolonged cell viability and migration of GFP(+) cells to the affected tissue was observed in 4 out of 5 mice in the group with protectively coated MSCs compared to 1 out of 5 in the control group that received injections of non-coated cells. This peptide/polymer multicomponent coating made it possible to prolong cell viability without impairing natural cell activity and provides a promising technique for cell manipulation biotechnology.

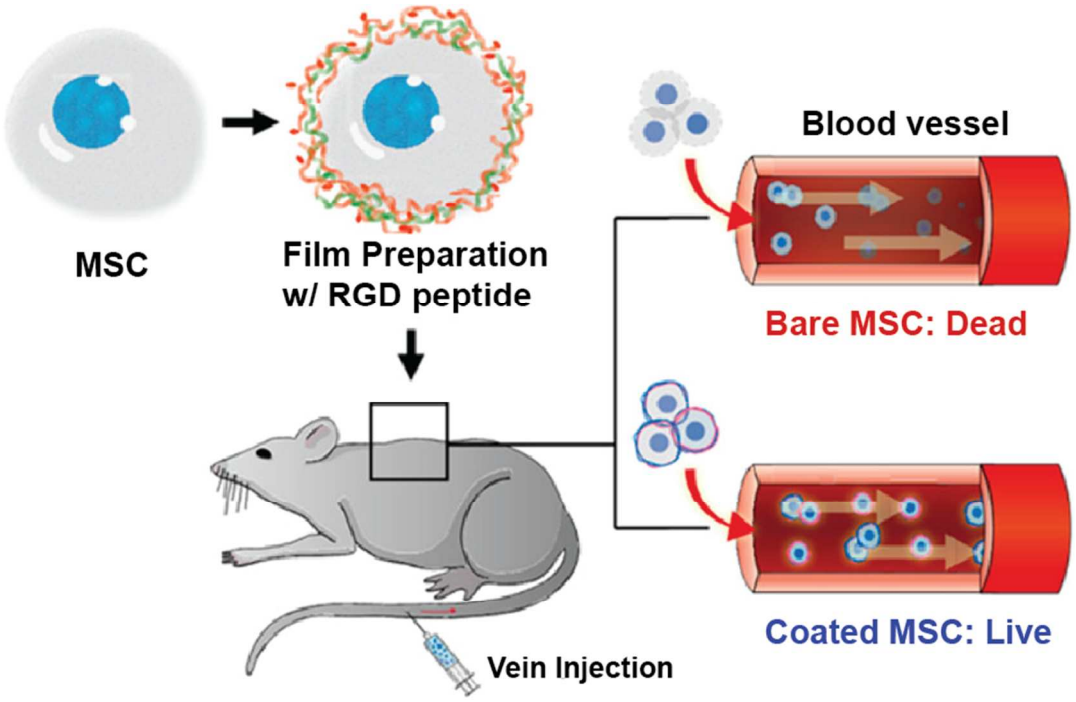


**Figure 56.** Pictorial representation of poly(L-lysine), hyaluronic acid, and RGD peptide coassembly to form a protective coating over mesenchymal stem cells. Coated cells exhibited increased survival rates upon intravenous injection in mice. Figure reproduced with permission from D. Choi, H. Lee, H. B. Kim, M. Yang, J. Heo, Y. Won, S. S. Jang, J. K. Park, Y. Son, T. I. Oh, E. Lee and J. Hong, *Chem. Mater.*, 2017, **29**, 2055–2065.[670] © 2017 American Chemical Society.

As many of the previous examples have illustrated, oftentimes a nanoparticle or vesicle structure is prepared in a solution containing negative and positively charged peptide/polymer/drug molecules that interact through complementary noncovalent interactions. The driving forces that govern the assembly and mechanical properties of the resulting structures are not well understood at the molecular level.[673,674] In order to gain insight into the fundamental principles that govern multicomponent supramolecular assembly, Stupp *et al*. investigated the relationship between osmotic pressure and membrane formation in a two-liquid multicomponent system which contained oppositely charged peptide amphiphiles (+) and HA (-) molecules (**Figure 57A**).[605,606] The addition of the higher density HA solution to a lower density solution containing a positively charged PA ($C_{16}V_3A_3K_3$-$NH_2$) led to a polymer-filled peptide sac in

which a membrane instantaneously forms at the interface of the two solutions. Osmotic swelling and inflation of the membrane were investigated to characterize the mechanical response of these peptide sacs in solutions. It was found that higher incubation times of HA drops in the PA solution led to a decrease in water permeability of the membranes. Osmotic pressure was also investigated by removing the membrane sacs from their initializing solution and placing them into pure water. Membranes were found to inflate with permanent deformation with some retention of elasticity and recoverable strain (**Figure 57B**). Interestingly, membranes formed from a solution with higher HA content or longer incubation times in the initial PA solution resulted in less permanent changes due to osmotic pressure change. Cell viability and differentiation was also demonstrated inside the PA/HA sacs by human MSC encapsulation and subsequent culture in growth media over a period of two weeks.[605] These unique peptide/polymer sacs that have both dynamic and static components exhibit interesting characteristics in a controlled coassembly between two oppositely charged biomolecules.

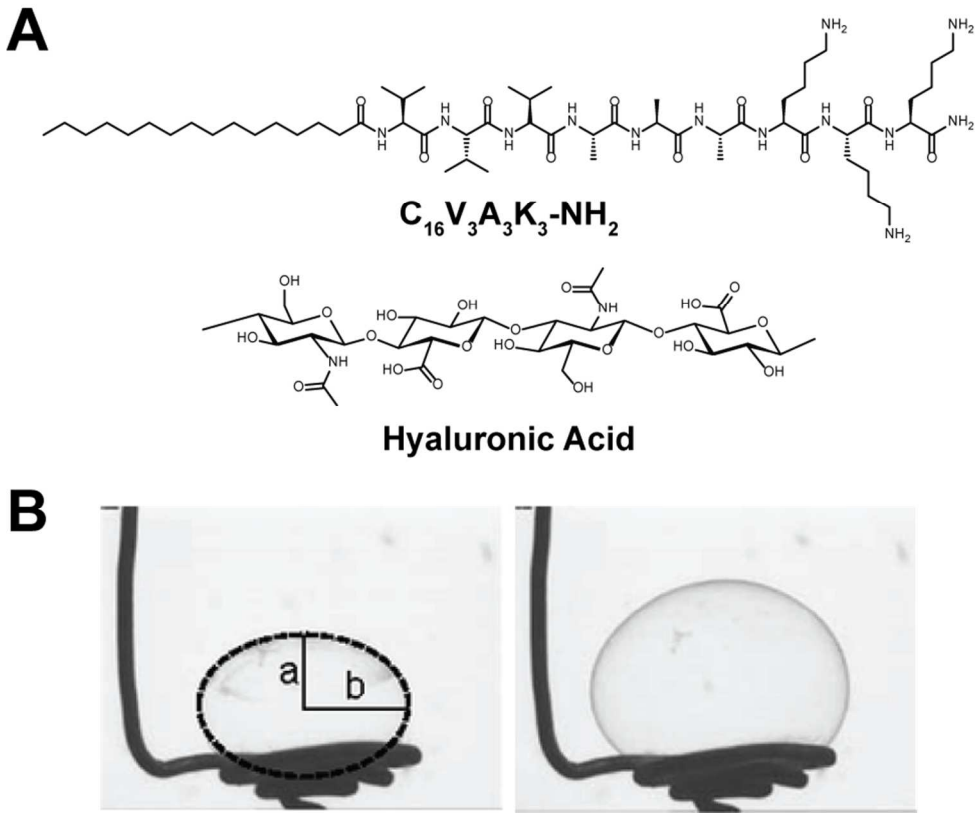


**Figure 57.** (A) Chemical structures of the $C_{16}V_3A_3K_3$-$NH_2$ PA and hyaluronic acid used to make polymer-filled peptide sacs. (B) Images of the polymer sac swelling capability in water where the initial sac is shown in the left image and the swollen sac in pure water is shown on the right. Lines **a** and **b** indicated on the left hand side are used to determine the volume of the peptide sac; **a** measures approximately 1.5 mm in this image. Panel B reproduced from ref 606 (J. Boekhoven, R. H. Zha, F. Tantakitti, E. Zhuang, R. Zandi, C. J. Newcomb and S. I. Stupp, *RSC Adv.*, 2015, **5**, 8753–8756)[606] with permission from the Royal Society of Chemistry.

Stupp *et al*. also investigated alginate-PA core-shell microparticles for drug delivery applications.[675] This alginate-PA multicomponent system was used to pioneer techniques to tune the size and diameter of PA-oligosaccharide hybrid materials. First, a sodium alginate dispersion was created and cross-linked via addition of calcium ions (**Figure 58A**). Size tunable particles were formed ranging from 600 nm to 2.3 μm in diameter. These particles were then submerged in a solution of cationic $C_{16}V_3A_3K_3$ PAs, resulting in assembly of the PA at the surface of the PA particle. In order to assess the ability to use these PA coated particles as drug carriers, the

alginate was first modified with doxorubicin through an acid cleavable hydrazone linker (**Figure 58B**), which makes it amenable to release of doxorubicin in acidic tumor microenvironments. Doxorubicin loaded particles were encapsulated within a coassembled two-component PA system unfunctionalized PA mixed with varying ratios of a second folate-functionalized PA. Folate was used to target the particles to cancer cells overexpressing folate receptors. MDA-MB-231 breast cancer cells treated with doxorubicin-loaded particles containing 10% folate-PA exhibited $IC_{50}$ values for cancer cell growth that were 60-fold lower than those treated with nanoparticles without folate-conjugated PA. These PA/oligosaccharide supramolecular particles illustrate the growing sophistication in the design of multicomponent materials informed by fundamental understanding of the chemical, material, and biological characteristics of the system components.

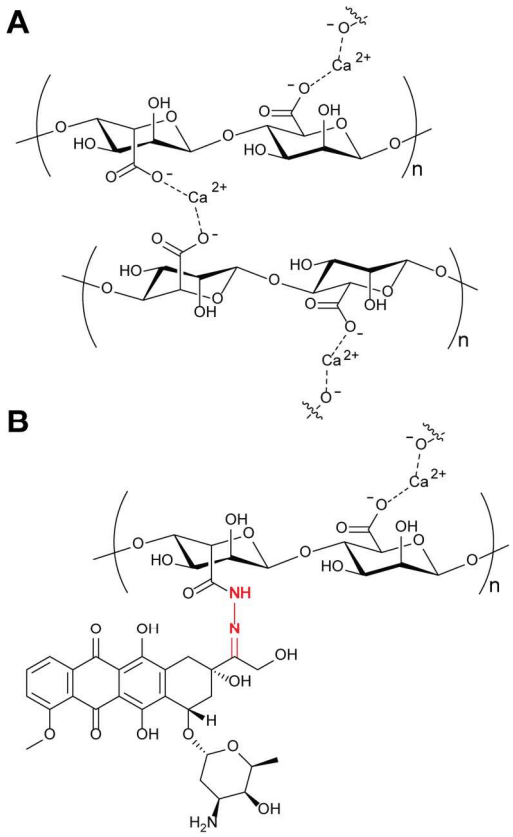

**Figure 58.** (A) Chemical structure of calcium cross-linked alginate. (B) Chemical structure of doxorubicin modified alginate with an acid cleavable hydrazone linker highlighted in red.[675]

**Section 9. Conclusion**

The design of multicomponent coassembled peptide-based materials is an emerging frontier in supramolecular chemistry and biomaterials. As has been illustrated herein, the peptide coassembly provides materials in which the emergent properties are often dramatically altered compared to the properties of the self-assembled materials of the individual components. Often, these emergent properties are difficult to predict and explain. There, there is the need and opportunity to study and understand these multicomponent materials in order to understand the fundamental kinetic, thermodynamic, and structural physicochemical principles that account for their unique characteristics. This much needed insight will enable a shift in approach from largely empirical to principle-based rational design of next-generation multicomponent peptide-based materials. This shift has already begun, as can be seen in several elegant examples of rationally designed materials discussed herein. While much of the work reported herein has involved binary mixtures of peptides, there are also examples of much more complex mixtures. The complexity of multicomponent supramolecular architectures will increase as our understanding of the fundamental principles of supramolecular chemistry deepens. Using the complex hierarchical construction of the cell as inspiration, we anticipate the future design of even more complex multicomponent structures in which peptides and other biomolecules interact in the productive generation of functional materials.

**Acknowledgements**

We acknowledge Jennifer Urban and Jade Welch for helpful comments on the manuscript. Preparation of the manuscript was supported by funding from the National Science Foundation (DMR-1148836) and the National Heart, Lung, and Blood Institute of the National Institutes of Health (R01HL138538).

1 M. Jouanne, S. Rault and A.-S. Voisin-Chiret, *Eur. J. Med. Chem.*, 2017, **139**, 153–167.

2 P. C. Ke, M.-A. Sani, F. Ding, A. Kakinen, I. Javed, F. Separovic, T. P. Davis and R. Mezzenga, *Chem. Soc. Rev.*, 2017, **46**, 6492–6531.

3 U. Keil, S. Hauptmann, A. Bonert, I. Scherping, A. Eckert and W. E. Müller, *J. Alzheimers. Dis.*, 2006, **9**, 139–146.

4 M. J. Rowan, I. Klyubin, Q. Wang, N. W. Hu and R. Anwyl, *Biochem. Soc. Trans.*, 2007, **35**, 1219–1223.

5 K. E. Marshall, R. Marchante, W.-F. Xue and L. C. Serpell, *Prion*, 2014, **8**, 192–196.

6 J. I. Clark, *Philos. Trans. R. Soc. B Biol. Sci.*, 2013, **368**, 20120104.

7 J. L. Silva, E. A. Cino, I. N. Soares, V. F. Ferreira and G. A. P. de Oliveira, *Acc. Chem. Res.*, 2018, **51**, 181–190.

8 D. F. Jarosz and V. Khurana, *Cell*, 2017, **171**, 1001–1014.

9 B. Nizynski, W. Dzwolak and K. Nieznanski, *Protein Sci.*, 2017, **26**, 2126–2150.

10 F. Di Domenico, A. Tramutola, C. Foppoli, E. Head, M. Perluigi and D. A. Butterfield, *Free Radic. Biol. Med.*, 2018, **114**, 94–101.

11 R. Ricciarelli and E. Fedele, *Curr. Neuropharmacol.*, 2017, **15**, 926–935.

12 G. G. Kovacs, V. M. Lee and J. Q. Trojanowski, *Brain Pathol.*, 2017, **27**, 675–690.

13 Q. Qian, S. K. Mitter, S. L. Pay, X. Qi, C. B. Rickman, M. B. Grant and M. E. Boulton, in

*Advances in Experimental Medicine and Biology*, Springer, New York, 2016, pp. 333–339.

14 J. W. Shay, *Curr. Opin. Cell Biol.*, 2018, **52**, 1–7.

15 J. Maciejowski and T. de Lange, *Nat. Rev. Mol. Cell Biol.*, 2017, **18**, 175–186.

16 F. Chiti and C. M. Dobson, *Annu. Rev. Biochem.*, 2006, **75**, 333–366.

17 R. O. Hynes and A. Naba, *Cold Spring Harb. Perspect. Biol.*, 2012, **4**, a004903.

18 R. P. Mecham, *Curr. Protoc. Cell Biol.*, 2001, **10**, 10.1-10.16.

19 J.-P. Jin, *Arch. Biochem. Biophys.*, 2013, **535**, 1–2.

20 R. Alfaro-Aco and S. Petry, *J. Biol. Chem.*, 2015, **290**, 17154–17162.

21 F. U. Hartl, *Annu. Rev. Biochem.*, 2017, **86**, 21–26.

22 S. K. Chaturvedi, M. K. Siddiqi, P. Alam and R. H. Khan, *Process Biochem.*, 2016, **51**, 1183–1192.

23 V. Jayawarna and R. V. Ulijn, in *Supramolecular Chemistry: From Molecules to Nanomaterials*, John Wiley & Sons, Ltd, Chichester, 2012, pp. 3525–3539.

24 S. I. Stupp, *Nano Lett.*, 2010, **10**, 4783–4786.

25 A. M. Grumezescu, *Fabrication and Self-Assembly of Nanobiomaterials*, Elsevier, Oxford, 2016.

26 C. J. Bowerman and B. L. Nilsson, *Biopolymers*, 2012, **98**, 169–184.

27 Y.-B. Lim and M. Lee, *J. Mater. Chem.*, 2008, **18**, 723–727.

28 S. Zhang, *Nat. Biotechnol.*, 2003, **21**, 1171–1178.

29 C. A. E. Hauser and S. Zhang, *Chem. Soc. Rev.*, 2010, **39**, 2780–2790.

30 M. Reches and E. Gazit, *Curr. Nanosci.*, 2006, **2**, 105–111.

31 I. W. Hamley, *Angew. Chemie Int. Ed.*, 2014, **53**, 6866–6881.

32 V. Mikhalevich, I. Craciun, M. Kyropoulou, C. G. Palivan and W. Meier, *Biomacromolecules*, 2017, **18**, 3471–3480.

33 G. Wei, Z. Su, N. P. Reynolds, P. Arosio, I. W. Hamley, E. Gazit and R. Mezzenga, *Chem. Soc. Rev.*, 2017, **46**, 4661–4708.

34 S. Eskandari, T. Guerin, I. Toth and R. J. Stephenson, *Adv. Drug Deliv. Rev.*, 2017, **110–111**, 169–187.

35 R. Ischakov, L. Adler-Abramovich, L. Buzhansky, T. Shekhter and E. Gazit, *Bioorganic Med. Chem.*, 2013, **21**, 3517–3522.

36 D. Leite, E. Barbu, G. Pilkington and A. Lalatsa, *Curr. Top. Med. Chem.*, 2015, **15**, 2277–2289.

37 P. Kondiah, Y. Choonara, P. Kondiah, T. Marimuthu, P. Kumar, L. du Toit and V. Pillay, *Molecules*, 2016, **21**, 1580–1610.

38 Y. Li, J. Rodrigues and H. Tomás, *Chem. Soc. Rev.*, 2012, **41**, 2193–2221.

39 M. Rad-Malekshahi, L. Lempsink, M. Amidi, W. E. Hennink and E. Mastrobattista, *Bioconjug. Chem.*, 2016, **27**, 3–18.

40 K. M. French, I. Somasuntharam and M. E. Davis, *Adv. Drug Deliv. Rev.*, 2016, **96**, 40–

53.

41 J. J. Panda and V. S. Chauhan, *Polym. Chem.*, 2014, **5**, 4431–4449.

42 R. Pugliese and F. Gelain, *Trends Biotechnol.*, 2017, **35**, 145–158.

43 M. J. Webber, E. J. Berns and S. I. Stupp, *Isr. J. Chem.*, 2013, **53**, 530–554.

44 T. E. Brown and K. S. Anseth, *Chem. Soc. Rev.*, 2017, **46**, 6532–6552.

45 Y. Loo, M. Goktas, A. B. Tekinay, M. O. Guler, C. A. E. Hauser and A. Mitraki, *Adv. Healthc. Mater.*, 2015, **4**, 2557–2586.

46 R. Ravichandran, M. Griffith and J. Phopase, *J. Mater. Chem. B*, 2014, **2**, 8466–8478.

47 I. El-Sherbiny and M. Yacoub, *Glob. Cardiol. Sci. Pract.*, 2013, **2013**, 316–342.

48 Z. Yu, Z. Cai, Q. Chen, M. Liu, L. Ye, J. Ren, W. Liao and S. Liu, *Biomater. Sci.*, 2016, **4**, 365–374.

49 P. D. Tatman, E. G. Muhonen, S. T. Wickers, A. O. Gee, E.-S. Kim and D.-H. Kim, *Biomater. Sci.*, 2016, **4**, 543–554.

50 M. Miotto, R. Gouveia and C. Connon, *J. Funct. Biomater.*, 2015, **6**, 687–707.

51 S. Koutsopoulos, *J. Biomed. Mater. Res. Part A*, 2016, **104**, 1002–1016.

52 B. He, X. Yuan, J. Wu, Y. Bai and D. Jiang, *Sci. Adv. Mater.*, 2015, **7**, 1221–1232.

53 S. Maude, E. Ingham and A. Aggeli, *Nanomedicine*, 2013, **8**, 823–847.

54 R. Xing, S. Li, N. Zhang, G. Shen, H. Möhwald and X. Yan, *Biomacromolecules*, 2017, **18**, 3514–3523.

55 G. A. Hudalla, J. A. Modica, Y. F. Tian, J. S. Rudra, A. S. Chong, T. Sun, M. Mrksich and J. H. Collier, *Adv. Healthc. Mater.*, 2013, **2**, 1114–1119.

56 J. S. Rudra, Y. F. Tian, J. P. Jung and J. H. Collier, *Proc. Natl. Acad. Sci.*, 2010, **107**, 622–627.

57 M. Negahdaripour, N. Golkar, N. Hajighahramani, S. Kianpour, N. Nezafat and Y. Ghasemi, *Biotechnol. Adv.*, 2017, **35**, 575–596.

58 M. Rad-Malekshahi, M. F. Fransen, M. Krawczyk, M. Mansourian, M. Bourajjaj, J. Chen, F. Ossendorp, W. E. Hennink, E. Mastrobattista and M. Amidi, *Mol. Pharm.*, 2017, **14**, 1482–1493.

59 G. Zhao, S. Chandrudu, M. Skwarczynski and I. Toth, *Eur. Polym. J.*, 2017, **93**, 670–681.

60 J. López-Sagaseta, E. Malito, R. Rappuoli and M. J. Bottomley, *Comput. Struct. Biotechnol. J.*, 2016, **14**, 58–68.

61 C. Chen, K. Liu, J. Li and X. Yan, *Adv. Colloid Interface Sci.*, 2015, **225**, 177–193.

62 Q. Zou, K. Liu, M. Abbas and X. Yan, *Adv. Mater.*, 2016, **28**, 1031–1043.

63 S. Kim, J. H. Kim, J. S. Lee and C. B. Park, *Small*, 2015, **11**, 3623–3640.

64 L. Adler-Abramovich and E. Gazit, *Chem. Soc. Rev.*, 2014, **43**, 6881–6893.

65 J.-H. Lee, J. H. Lee, Y. J. Lee and K. T. Nam, *Curr. Opin. Biotechnol.*, 2013, **24**, 599–605.

66 E. Gazit, *Chem. Isr.*, 2012, **26**, 24–31.

67 H. A. M. Ardona, E. R. Draper, F. Citossi, M. Wallace, L. C. Serpell, D. J. Adams and J.

D. Tovar, *J. Am. Chem. Soc.*, 2017, **139**, 8685–8692.

68 A. M. Sanders, T. J. Magnanelli, A. E. Bragg and J. D. Tovar, *J. Am. Chem. Soc.*, 2016, **138**, 3362–3370.

69 Y. Li, M. Qin, Y. Cao and W. Wang, *Sci. China Physics, Mech. Astron.*, 2014, **57**, 849–858.

70 A. Vedadghavami, F. Minooei, M. H. Mohammadi, S. Khetani, A. Rezaei Kolahchi, S. Mashayekhan and A. Sanati-Nezhad, *Acta Biomater.*, 2017, **62**, 42–63.

71 F. Brandl, F. Sommer and A. Goepferich, *Biomaterials*, 2007, **28**, 134–146.

72 M. Hughes, H. Xu, P. W. J. M. Frederix, A. M. Smith, N. T. Hunt, T. Tuttle, I. A. Kinloch and R. V. Ulijn, *Soft Matter*, 2011, **7**, 10032–10038.

73 H.-S. Jang, J.-H. Lee, Y.-S. Park, Y.-O. Kim, J. Park, T.-Y. Yang, K. Jin, J. Lee, S. Park, J. M. You, K.-W. Jeong, A. Shin, I.-S. Oh, M.-K. Kwon, Y.-I. Kim, H.-H. Cho, H. N. Han, Y. Kim, Y. H. Chang, S. R. Paik, K. T. Nam and Y.-S. Lee, *Nat. Commun.*, 2014, **5**, 3665–3675.

74 J. Lee, I. R. Choe, N.-K. Kim, W.-J. Kim, H.-S. Jang, Y.-S. Lee and K. T. Nam, *ACS Nano*, 2016, **10**, 8263–8270.

75 K.-S. Moon, E. Lee, Y. Lim and M. Lee, *Chem. Commun.*, 2008, **0**, 4001–4003.

76 A. S. Hoffman, *Adv. Drug Deliv. Rev.*, 2013, **65**, 10–16.

77 C. T. Huynh, M. K. Nguyen and D. S. Lee, *Macromolecules*, 2011, **44**, 6629–6636.

78 F. G. Thankam and J. Muthu, *J. Mech. Behav. Biomed. Mater.*, 2014, **35**, 111–122.

79 J. Z. Gasiorowski and J. H. Collier, *Biomacromolecules*, 2011, **12**, 3549–3558.

80 J. H. Collier, J. S. Rudra, J. Z. Gasiorowski and J. P. Jung, *Chem. Soc. Rev.*, 2010, **39**, 3413–3424.

81 O. J. G. M. Goor, S. I. S. Hendrikse, P. Y. W. Dankers and E. W. Meijer, *Chem. Soc. Rev.*, 2017, **46**, 6621–6637.

82 V. L. Sedman, X. Chen, S. Allen, C. J. Roberts, V. V. Korolkov and S. J. B. Tendler, *J. Microsc.*, 2013, **249**, 165–172.

83 J. T. M. DiMaio, T. M. Doran, D. M. Ryan, D. M. Raymond and B. L. Nilsson, *Biomacromolecules*, 2017, **18**, 3591–3599.

84 R. J. Swanekamp, J. J. Welch and B. L. Nilsson, *Chem. Commun.*, 2014, **50**, 10133–10136.

85 K. J. Nagy, M. C. Giano, A. Jin, D. J. Pochan and J. P. Schneider, *J. Am. Chem. Soc.*, 2011, **133**, 14975–14977.

86 K. Nagy-Smith, P. J. Beltramo, E. Moore, R. Tycko, E. M. Furst and J. P. Schneider, *ACS Cent. Sci.*, 2017, **3**, 586–597.

87 D. M. Ryan, T. M. Doran and B. L. Nilsson, *Chem. Commun.*, 2011, **47**, 475–477.

88 F. Taraballi, M. Campione, A. Sassella, A. Vescovi, A. Paleari, W. Hwang and F. Gelain, *Soft Matter*, 2009, **5**, 660–668.

89 X. Wang, A. Horii and S. Zhang, *Soft Matter*, 2008, **4**, 2388–2395.

90 G. Fichman and E. Gazit, *Acta Biomater.*, 2014, **10**, 1671–1682.

91 J. T. M. DiMaio, D. M. Raymond and B. L. Nilsson, *Org. Biomol. Chem.*, 2017, **15**, 5279–5283.

92 G. A. Hudalla, T. Sun, J. Z. Gasiorowski, H. Han, Y. F. Tian, A. S. Chong and J. H. Collier, *Nat. Mater.*, 2014, **13**, 829–836.

93 H.-E. Jin, J. Jang, J. Chung, H. J. Lee, E. Wang, S.-W. Lee and W.-J. Chung, *Nano Lett.*, 2015, **15**, 7138–7145.

94 J. Castillo-León, in *Micro and Nanofabrication Using Self-Assembled Biological Nanostructures*, Elsevier, Oxford, 2015, pp. 21–31.

95 K. Y. Tomizaki, S. Wakizaka, Y. Yamaguchi, A. Kobayashi and T. Imai, *Langmuir*, 2014, **30**, 846–856.

96 Y. Liang, D. G. Lynn and K. M. Berland, *J. Am. Chem. Soc.*, 2010, **132**, 6306–6308.

97 E. M. Smoak, M. P. Dabakis, M. M. Henricus, R. Tamayev and I. A. Banerjee, *J. Pept. Sci.*, 2011, **17**, 14–23.

98 D. M. Ridgley, E. C. Claunch, P. W. Lee and J. R. Barone, *Biomacromolecules*, 2014, **15**, 1240–1247.

99 S. M. M. Reddy and G. Shanmugam, *ChemPhysChem*, 2016, **17**, 2897–2907.

100 F. Gobeaux, N. Fay, C. Tarabout, C. Mériadec, F. Meneau, M. Ligeti, D.-A. Buisson, J.-C. Cintrat, K. M. H. Nguyen, L. Perrin, C. Valéry, F. Artzner and M. Paternostre, *J. Am. Chem. Soc.*, 2012, **134**, 723–733.

101 H. Robson, J. G. E. M. Fraaije and A. Kros, *Angew. Chemie Int. Ed.*, 2010, **49**, 8570–8572.

102 J. Wang, K. Liu, R. Xing and X. Yan, *Chem. Soc. Rev.*, 2016, **45**, 5589–5604.

103 G. Fichman, T. Guterman, J. Damron, L. Adler-Abramovich, J. Schmidt, E. Kesselman, L. J. W. Shimon, A. Ramamoorthy, Y. Talmon and E. Gazit, *Sci. Adv.*, 2016, **2**, e1500827.

104 Y. Tian, H. V. Zhang, K. L. Kiick, J. G. Saven and D. J. Pochan, *Org. Biomol. Chem.*, 2017, **15**, 6109–6118.

105 A. Dehsorkhi, V. Castelletto and I. W. Hamley, *J. Pept. Sci.*, 2014, **20**, 453–467.

106 B. A. Thurston, J. D. Tovar and A. L. Ferguson, *Mol. Simul.*, 2016, **42**, 955–975.

107 E. Mayans, G. Ballano, J. Sendros, M. Font-Bardia, J. L. Campos, J. Puiggalí, C. Cativiela and C. Alemán, *ChemPhysChem*, 2017, **18**, 1888–1896.

108 R. Li, C. C. Horgan, B. Long, A. L. Rodriguez, L. Mather, C. J. Barrow, D. R. Nisbet and R. J. Williams, *RSC Adv.*, 2015, **5**, 301–307.

109 C. J. Bowerman, W. Liyanage, A. J. Federation and B. L. Nilsson, *Biomacromolecules*, 2011, **12**, 2735–2745.

110 J. Kim, T. H. Han, Y. Il Kim, J. S. Park, J. Choi, D. G. Churchill, S. O. Kim and H. Ihee, *Adv. Mater.*, 2010, **22**, 583–587.

111 J. Wang, K. Liu, L. Yan, A. Wang, S. Bai and X. Yan, *ACS Nano*, 2016, **10**, 2138–2143.

112 J. Wang, C. Yuan, Y. Han, Y. Wang, X. Liu, S. Zhang and X. Yan, *Small*, 2017, **13**, 1702175.

113 T. D. Do and M. T. Bowers, *Anal. Chem.*, 2015, **87**, 4245–4252.

114 M. S. Ishikawa, C. Busch, M. Motzkus, H. Martinho and T. Buckup, *Phys. Chem. Chem.*

*Phys.*, 2017, **19**, 31647–31654.

115 N. A. Dudukovic, B. C. Hudson, A. K. Paravastu and C. F. Zukoski, *Nanoscale*, 2018, **10**, 1508–1516.

116 T. Waku and N. Tanaka, *Polym. Int.*, 2017, **66**, 277–288.

117 L. M. De Leon Rodriguez, Y. Hemar, J. Cornish and M. A. Brimble, *Chem. Soc. Rev.*, 2016, **45**, 4797–4824.

118 D. Mandal, A. Nasrolahi Shirazi and K. Parang, *Org. Biomol. Chem.*, 2014, **12**, 3544–3561.

119 M. Fändrich, *Cell. Mol. Life Sci.*, 2007, **64**, 2066–2078.

120 P. Alam, K. Siddiqi, S. K. Chturvedi and R. H. Khan, *Int. J. Biol. Macromol.*, 2017, **103**, 208–219.

121 R. Tycko and R. B. Wickner, *Acc. Chem. Res.*, 2013, **46**, 1487–1496.

122 A. Abedini and D. P. Raleigh, in *Wiley Encyclopedia of Chemical Biology*, John Wiley & Sons, Inc., Hoboken, 2009, pp. 64–70.

123 J. Hardy and G. Higgins, *Science*, 1992, **256**, 184–185.

124 S. Xu, *J. Phys. Chem. B*, 2009, **113**, 12447–12455.

125 R. Nelson, M. R. Sawaya, M. Balbirnie, A. Madsen, C. Riekel, R. Grothe and D. Eisenberg, *Nature*, 2005, **435**, 773–778.

126 E. D. Eanes and G. G. Glenner, *J. Histochem. Cytochem.*, 1968, **16**, 673–677.

127 T. L. S. Benzinger, D. M. Gregory, T. S. Burkoth, H. Miller-Auer, D. G. Lynn, R. E.

Botto and S. C. Meredith, *Proc. Natl. Acad. Sci.*, 1998, **95**, 13407–13412.

128 A. T. Petkova, G. Buntkowsky, F. Dyda, R. D. Leapman, W.-M. Yau and R. Tycko, *J. Mol. Biol.*, 2004, **335**, 247–260.

129 T. Luhrs, C. Ritter, M. Adrian, D. Riek-Loher, B. Bohrmann, H. Dobeli, D. Schubert and R. Riek, *Proc. Natl. Acad. Sci.*, 2005, **102**, 17342–17347.

130 A. T. Petkova, W.-M. Yau and R. Tycko, *Biochemistry*, 2006, **45**, 498–512.

131 R. Tycko, *Q. Rev. Biophys.*, 2006, **39**, 1–55.

132 J.-H. Lee, I.-H. Lee, Y.-J. Choe, S. Kang, H. Y. Kim, W.-P. Gai, J.-S. Hahn and S. R. Paik, *Biochem. J.*, 2009, **418**, 311–323.

133 A. W. P. Fitzpatrick, B. Falcon, S. He, A. G. Murzin, G. Murshudov, H. J. Garringer, R. A. Crowther, B. Ghetti, M. Goedert and S. H. W. Scheres, *Nature*, 2017, **547**, 185–190.

134 L. Gremer, D. Schölzel, C. Schenk, E. Reinartz, J. Labahn, R. B. G. Ravelli, M. Tusche, C. Lopez-Iglesias, W. Hoyer, H. Heise, D. Willbold and G. F. Schröder, *Science*, 2017, **358**, 116–119.

135 A. Khondker, R. J. Alsop and M. C. Rheinstädter, *Membranes*, 2017, **7**, 1–49.

136 M. Fändrich, J. Meinhardt and N. Grigorieff, *Prion*, 2009, **3**, 89–93.

137 T.-W. Lin, C.-F. Chang, Y.-J. Chang, Y.-H. Liao, H.-M. Yu and Y.-R. Chen, *PLoS One*, 2017, **12**, e0174561.

138 S. Bansal, I. K. Maurya, N. Yadav, C. K. Thota, V. Kumar, K. Tikoo, V. S. Chauhan and R. Jain, *ACS Chem. Neurosci.*, 2016, **7**, 615–623.

139 E. A. Fradinger, B. H. Monien, B. Urbanc, A. Lomakin, M. Tan, H. Li, S. M. Spring, M. M. Condron, L. Cruz, C.-W. Xie, G. B. Benedek and G. Bitan, *Proc. Natl. Acad. Sci.*, 2008, **105**, 14175–14180.

140 S. Bansal, I. K. Maurya, K. Shenmar, N. Yadav, C. K. Thota, V. Kumar, K. Tikoo, V. S. Chauhan, R. Jain, P. I. Arvidsson, G. B. Benedek, G. Bitan, G. Quinn, M. Bairu, A. Pastrak, J. D. Cedarbaum, K. Beyreuther, R. E. Tanzi and C. L. Masters, *RSC Adv.*, 2017, **7**, 4167–4173.

141 B. Neddenriep, A. Calciano, D. Conti, E. Sauve, M. Paterson, E. Bruno and D. A. Moffet, *Open Biotechnol. J.*, 2011, **5**, 39–46.

142 T. Takahashi and H. Mihara, *Acc. Chem. Res.*, 2008, **41**, 1309–1318.

143 P.-N. Cheng, C. Liu, M. Zhao, D. Eisenberg and J. S. Nowick, *Nat. Chem.*, 2012, **4**, 927–933.

144 J. Luo and J. P. Abrahams, *Chem. A Eur. J.*, 2014, **20**, 2410–2419.

145 J. Kumar and V. Sim, *Prion*, 2014, **8**, 119–124.

146 X. Zheng, C. Wu, D. Liu, H. Li, G. Bitan, J.-E. Shea and M. T. Bowers, *J. Phys. Chem. B*, 2016, **120**, 1615–1623.

147 H. Li, F. Rahimi and G. Bitan, *ACS Chem. Neurosci.*, 2016, **7**, 845–856.

148 P. Y. Cho, G. Joshi, J. A. Johnson and R. M. Murphy, *ACS Chem. Neurosci.*, 2014, **5**, 542–551.

149 Q. Wang, X. Yu, L. Li and J. Zheng, *Curr. Pharm. Des.*, 2014, **20**, 1223–1243.

150 K. Rajasekhar, S. N. Suresh, R. Manjithaya and T. Govindaraju, *Sci. Rep.*, 2015, **5**, 8139.

151 D. Goyal, S. Shuaib, S. Mann and B. Goyal, *ACS Comb. Sci.*, 2017, **19**, 55–80.

152 A. Jha, M. G. Kumar, H. N. Gopi and K. M. Paknikar, *Langmuir*, 2018, **34**, 1591–1600.

153 J. Geng, M. Li, J. Ren, E. Wang and X. Qu, *Angew. Chemie Int. Ed.*, 2011, **50**, 4184–4188.

154 Q. Nie, X. Du and M. Geng, *Acta Pharmacol. Sin.*, 2011, **32**, 545–551.

155 J. a Lemkul and D. R. Bevan, *ACS Chem. Neurosci.*, 2012, **3**, 845–856.

156 Y. S. Lee, H. Y. Kim, Y. Kim, J. H. Seo, E. J. Roh, H. Han and K. J. Shin, *Bioorg. Med. Chem.*, 2012, **20**, 4921–4935.

157 F. Belluti, A. Rampa, S. Gobbi and A. Bisi, *Expert Opin. Ther. Pat.*, 2013, **23**, 581–596.

158 B. Torok, S. Bag, M. Sarkar, S. Dasgupta and M. Torok, *Curr. Bioact. Compd.*, 2013, **9**, 37–63.

159 M. Stefani and S. Rigacci, *Int. J. Mol. Sci.*, 2013, **14**, 12411–12457.

160 A. J. Doig and P. Derreumaux, *Curr. Opin. Struct. Biol.*, 2015, **30**, 50–56.

161 A. Francioso, P. Punzi, A. Boffi, C. Lori, S. Martire, C. Giordano, M. D'Erme and L. Mosca, *Bioorg. Med. Chem.*, 2015, **23**, 1671–1683.

162 S. N. A. Bukhari and I. Jantan, *Mini Rev. Med. Chem.*, 2015, **15**, 1110–1121.

163 S. Brahmachari, A. Paul, D. Segal and E. Gazit, *Future Med. Chem.*, 2017, **9**, 797–810.

164 D. A. Sheik, S. Dewhurst and J. Yang, *Acc. Chem. Res.*, 2017, **50**, 2159–2166.

165 R. Liu, R. Su, M. Liang, R. Huang, M. Wang, W. Qi and Z. He, *Curr. Med. Chem.*, 2012, **19**, 4157–4174.

166 E. Gazit, *FEBS J.*, 2005, **272**, 5971–5978.

167 F. Prati, G. Bottegoni, M. L. Bolognesi and A. Cavalli, *J. Med. Chem.*, 2018, **61**, 619–637.

168 M. Baldassarre, C. M. Baronio, L. A. Morozova-Roche and A. Barth, *Chem. Sci.*, 2017, **8**, 8247–8254.

169 A. Jan, O. Gokce, R. Luthi-Carter and H. A. Lashuel, *J. Biol. Chem.*, 2008, **283**, 28176–28189.

170 M. Suzuki, T. Takahashi, J. Sato, M. Mie, E. Kobatake and H. Mihara, *ChemBioChem*, 2010, **11**, 1525–1530.

171 L. Niu, L. Liu, W. Xi, Q. Han, Q. Li, Y. Yu, Q. Huang, F. Qu, M. Xu, Y. Li, H. Du, R. Yang, J. Cramer, K. V. Gothelf, M. Dong, F. Besenbacher, Q. Zeng, C. Wang, G. Wei and Y. Yang, *ACS Nano*, 2016, **10**, 4143–4153.

172 L. M. Young, R. A. Mahood, J. C. Saunders, L.-H. Tu, D. P. Raleigh, S. E. Radford and A. E. Ashcroft, *Analyst*, 2015, **140**, 6990–6999.

173 G. Cinar, I. Orujalipoor, C. J. Su, U. S. Jeng, S. Ide and M. O. Guler, *Langmuir*, 2016, **32**, 6506–6514.

174 N. L. Truex, Y. Wang and J. S. Nowick, *J. Am. Chem. Soc.*, 2016, **138**, 13882–13890.

175 N. L. Truex and J. S. Nowick, *J. Am. Chem. Soc.*, 2016, **138**, 13891–13900.

176 P. Arosio, T. P. J. Knowles and S. Linse, *Phys. Chem. Chem. Phys.*, 2015, **17**, 7606–7618.

177 M. Wolff, D. Unuchek, B. Zhang, V. Gordeliy, D. Willbold and L. Nagel-Steger, *PLoS One*, 2015, **10**, e0127865.

178 R. K. Spencer, H. Li and J. S. Nowick, *J. Am. Chem. Soc.*, 2014, **136**, 5595–5598.

179 W. Hoyer, C. Gronwall, A. Jonsson, S. Stahl and T. Hard, *Proc. Natl. Acad. Sci.*, 2008, **105**, 5099–5104.

180 R. V Rughani and J. P. Schneider, *MRS Bull.*, 2008, **33**, 530–535.

181 A. Smith, in *Subcellular Biochemistry*, Springer, New York, 2012, pp. 29–51.

182 S. Zhang, T. Holmes, C. Lockshin and A. Rich, *Proc. Natl. Acad. Sci.*, 1993, **90**, 3334–3338.

183 S. Zhang, C. Lockshin, R. Cook and A. Rich, *Biopolymers*, 1994, **34**, 663–672.

184 Y. Hong, R. L. Legge, S. Zhang and P. Chen, *Biomacromolecules*, 2003, **4**, 1433–1442.

185 D. M. Marini, W. Hwang, D. A. Lauffenburger, S. Zhang and R. D. Kamm, *Nano Lett.*, 2002, **2**, 295–299.

186 W. Hwang, D. M. Marini, R. D. Kamm and S. Zhang, *J. Chem. Phys.*, 2003, **118**, 389–397.

187 Y. Sun, Y. Zhang, L. Tian, Y. Zhao, D. Wu, W. Xue, S. Ramakrishna, W. Wu and L. He, *Biomed. Mater.*, 2016, **12**, 15007.

188 H. Yokoi, T. Kinoshita and S. Zhang, *Proc. Natl. Acad. Sci.*, 2005, **102**, 8414–8419.

189 S. Sathaye, H. Zhang, C. Sonmez, J. P. Schneider, C. M. Macdermaid, C. D. Von Bargen, J. G. Saven and D. J. Pochan, *Biomacromolecules*, 2014, **15**, 3891–3900.

190 D. A. Salick, J. K. Kretsinger, D. J. Pochan and J. P. Schneider, *J. Am. Chem. Soc.*, 2007, **129**, 14793–14799.

191 L. Haines-Butterick, K. Rajagopal, M. Branco, D. Salick, R. Rughani, M. Pilarz, M. S. Lamm, D. J. Pochan and J. P. Schneider, *Proc. Natl. Acad. Sci.*, 2007, **104**, 7791–7796.

192 J. P. Jung, A. K. Nagaraj, E. K. Fox, J. S. Rudra, J. M. Devgun and J. H. Collier, *Biomaterials*, 2009, **30**, 2400–2410.

193 J. S. Rudra, T. Sun, K. C. Bird, M. D. Daniels, J. Z. Gasiorowski, A. S. Chong and J. H. Collier, *ACS Nano*, 2012, **6**, 1557–1564.

194 J. H. Collier, B. Hu, J. W. Ruberti, J. Zhang, P. Shum, D. H. Thompson and P. B. Messersmith, *J. Am. Chem. Soc.*, 2001, **123**, 9463–9464.

195 H. Dong, V. M. Yuwono and J. D. Hartgerink, in *Molecular Recognition and Polymers*, John Wiley & Sons, Inc., Hoboken, 2008, pp. 359–393.

196 M. R. Caplan, E. M. Schwartzfarb, S. Zhang, R. D. Kamm and D. A. Lauffenburger, *Biomaterials*, 2002, **23**, 219–227.

197 A. L. Sieminski, C. E. Semino, H. Gong and R. D. Kamm, *J. Biomed. Mater. Res. A*, 2008, **87**, 494–504.

198 R. J. Betush, J. M. Urban and B. L. Nilsson, *Pept. Sci.*, 2018, **110**, e23099.

199 K. J. Channon, G. L. Devlin and C. E. MacPhee, *J. Am. Chem. Soc.*, 2009, **131**, 12520–12521.

200 A. Rajbhandary and B. L. Nilsson, in *Gels Handbook: Fundamentals, Properties and Application. Volume 1: Fundamentals of Hydrogels*, Wold Scientific Publishing,

Singapore, 2016, pp. 219–250.

201 Y. Wen, S. L. Roudebush, G. A. Buckholtz, T. R. Goehring, N. Giannoukakis, E. S. Gawalt and W. S. Meng, *Biomaterials*, 2014, **35**, 5196–5205.

202 M. J. Saunders, W. Liu, C. Szent-Gyorgyi, Y. Wen, Z. Drennen, A. S. Waggoner and W. S. Meng, *Bioconjug. Chem.*, 2013, **24**, 803–810.

203 Y. Wen, H. R. Kolonich, K. M. Kruszewski, N. Giannoukakis, E. S. Gawalt and W. S. Meng, *Mol. Pharm.*, 2013, **10**, 1035–1044.

204 A. Tajima, W. Liu, I. Pradhan, S. Bertera, C. Bagia, M. Trucco, W. S. Meng and Y. Fan, *Clin. Immunol.*, 2015, **160**, 82–89.

205 H. Kodama, S. Matsumura, T. Yamashita and H. Mihara, *Chem. Commun.*, 2004, **2**, 2876–2877.

206 Y. Zheng, Y. Wen, A. M. George, A. M. Steinbach, B. E. Phillips, N. Giannoukakis, E. S. Gawalt and W. S. Meng, *Biomaterials*, 2011, **32**, 249–257.

207 F. Gelain, D. Bottai, A. Vescovi and S. Zhang, *PLoS One*, 2006, **1**, e119.

208 R. G. Ellis-Behnke, Y.-X. Liang, S.-W. You, D. K. C. Tay, S. Zhang, K.-F. So and G. E. Schneider, *Proc. Natl. Acad. Sci. U. S. A.*, 2006, **103**, 5054–5059.

209 A. Horii, X. Wang, F. Gelain and S. Zhang, *PLoS One*, 2007, **2**, e190.

210 S. Koutsopoulos and S. Zhang, *J. Control. Release*, 2012, **160**, 451–458.

211 X. Liu, X. Wang, A. Horii, X. Wang, L. Qiao, S. Zhang and F.-Z. Cui, *Nanoscale*, 2012, **4**, 2720–2727.

212 J. Wang, J. Zheng, Q. Zheng, Y. Wu, B. Wu, S. Huang, W. Fang and X. Guo, *Mater. Sci. Eng. C*, 2015, **46**, 140–147.

213 X.-C. Li, Y.-H. Wu, X.-D. Bai, W. Ji, Z.-M. Guo, C.-F. Wang, Q. He and D. Ruan, *Tissue Eng. Part A*, 2016, **22**, 1218–1228.

214 M. H. Helfrich, S. A. Nesbitt, P. T. Lakkakorpi, M. J. Barnes, S. C. Bodary, G. Shankar, W. T. Mason, D. L. Mendrick, H. K. Väänänen and M. A. Horton, *Bone*, 1996, **19**, 317–328.

215 C. G. Knight, L. F. Morton, a R. Peachey, D. S. Tuckwell, R. W. Farndale and M. J. Barnes, *J. Biol. Chem.*, 2000, **275**, 35–40.

216 J. P. Ranieri, R. Bellamkonda, E. J. Bekos, T. G. Vargo, J. A. Gardella and P. Aebischer, *J. Biomed. Mater. Res.*, 1995, **29**, 779–785.

217 J. C. Schense, J. Bloch, P. Aebischer and J. A. Hubbell, *Nat. Biotechnol.*, 2000, **18**, 415–419.

218 E. Ruoslahti and M. Pierschbacher, *Science*, 1987, **238**, 491–497.

219 Z. Greenberg, H. Gavish, A. Muhlrad, M. Chorev, A. Shteyer, M. Attar-Namdar, A. Tartakovsky and I. Bab, *J. Cell. Biochem.*, 1997, **65**, 359–367.

220 R. V. Petrov, A. A. Mikhailova and L. A. Fonina, *Biopolymers*, 1997, **43**, 139–146.

221 J. P. Jung, J. V Moyano and J. H. Collier, *Integr. Biol.*, 2011, **3**, 185–196.

222 J. S. Rudra, S. Mishra, A. S. Chong, R. A. Mitchell, E. H. Nardin, V. Nussenzweig and J. H. Collier, *Biomaterials*, 2012, **33**, 6476–6484.

223 Y. Wen, A. Waltman, H. Han and J. H. Collier, *ACS Nano*, 2016, **10**, 9274–9286.

224 S. Choi, W. Jeong, T.-H. Kim and Y. Lim, *Soft Matter*, 2011, **7**, 1675–1677.

225 Y. F. Tian, G. A. Hudalla, H. Han and J. H. Collier, *Biomater. Sci.*, 2013, **1**, 1037–1045.

226 M. A. Elsawy, A. M. Smith, N. Hodson, A. Squires, A. F. Miller and A. Saiani, *Langmuir*, 2016, **32**, 4917–4923.

227 S. Boothroyd, A. Saiani and A. F. Miller, *Biopolymers*, 2014, **101**, 669–680.

228 J. T. M. . DiMaio, D. Easterhoff, A. M. . Moore, S. Dewhurst and B. L. Nilsson, in *Proceedings of the Twenty-Third American and the Sixth International Peptide Symposium*, Prompt Scientific Publishing, San Diego, 2013, pp. 154–155.

229 H. Wang, Y. Wang, X. Zhang, Y. Hu, X. Yi, L. Ma, H. Zhou, J. Long, Q. Liu and Z. Yang, *Chem. Commun.*, 2015, **51**, 14239–14242.

230 S. Sangiambut, K. Channon, N. M. Thomson, S. Sato, T. Tsuge, Y. Doi and E. Sivaniah, *Adv. Mater.*, 2013, **25**, 2661–2665.

231 K. Pagel, T. Seri, H. von Berlepsch, J. Griebel, R. Kirmse, C. Böttcher and B. Koksch, *ChemBioChem*, 2008, **9**, 531–536.

232 E. T. Pashuck, B. J. R. Duchet, C. S. Hansel, S. A. Maynard, L. W. Chow and M. M. Stevens, *ACS Nano*, 2016, **10**, 11096–11104.

233 S. Ramachandran, J. Trewhella, Y. Tseng and Y. B. Yu, *Chem. Mater.*, 2006, **18**, 6157–6162.

234 X. D. Xu, C. S. Chen, B. Lu, S. X. Cheng, X. Z. Zhang and R. X. Zhuo, *J. Phys. Chem. B*,

2010, **114**, 2365–2372.

235 L. L. Hyland, M. B. Taraban, Y. Feng, B. Hammouda and Y. B. Yu, *Biopolymers*, 2012, **97**, 177–188.

236 I. Cohen-Erez and H. Rapaport, *Biomacromolecules*, 2015, **16**, 3827–3835.

237 K. C. Clarke and L. A. Lyon, *Macromolecules*, 2016, **49**, 5366–5373.

238 Y. Hu, R. Lin, P. Zhang, J. Fern, A. G. Cheetham, K. Patel, R. Schulman, C. Kan and H. Cui, *ACS Nano*, 2016, **10**, 880–888.

239 S. Li, A. K. Mehta, A. N. Sidorov, T. M. Orlando, Z. Jiang, N. R. Anthony and D. G. Lynn, *J. Am. Chem. Soc.*, 2016, **138**, 3579–3586.

240 D. T. Seroski, A. Restuccia, A. D. Sorrentino, K. R. Knox, S. J. Hagen and G. A. Hudalla, *Cell. Mol. Bioeng.*, 2016, **9**, 335–350.

241 L. Pauling and R. B. Corey, *Proc. Natl. Acad. Sci.*, 1953, **39**, 253–256.

242 M. Hennes, K. Wolff and H. Stark, *Phys. Rev. Lett.*, 2014, **112**, 238104.

243 R. Tugyi, K. Uray, D. Ivan, E. Fellinger, A. Perkins and F. Hudecz, *Proc. Natl. Acad. Sci.*, 2005, **102**, 413–418.

244 G. Liang, Z. Yang, R. Zhang, L. Li, Y. Fan, Y. Kuang, Y. Gao, T. Wang, W. W. Lu and B. Xu, *Langmuir*, 2009, **25**, 8419–8422.

245 M. B. Taraban, Y. Feng, B. Hammouda, L. L. Hyland and Y. B. Yu, *Chem. Mater.*, 2012, **24**, 2299–2310.

246 S. Marchesan, L. Waddington, C. D. Easton, D. A. Winkler, L. Goodall, J. Forsythe and P.

G. Hartley, *Nanoscale*, 2012, **4**, 6752–6760.

247 S. Marchesan, C. D. Easton, K. E. Styan, L. J. Waddington, F. Kushkaki, L. Goodall, K. M. McLean, J. S. Forsythe and P. G. Hartley, *Nanoscale*, 2014, **6**, 5172–5180.

248 M. Melchionna, K. Styan and S. Marchesan, *Curr. Top. Med. Chem.*, 2016, **16**, 2009–2018.

249 Y. Mitsui, Y. Iitaka and M. Tsuboi, *J. Mol. Biol.*, 1967, **24**, 15–26.

250 H. Wadai, K. I. Yamaguchi, S. Takahashi, T. Kanno, T. Kawai, H. Naiki and Y. Goto, *Biochemistry*, 2005, **44**, 157–164.

251 T. Koga, M. Matsuoka and N. Higashi, *J. Am. Chem. Soc.*, 2005, **127**, 17596–17597.

252 R. J. Swanekamp, J. T. M. Dimaio, C. J. Bowerman and B. L. Nilsson, *J. Am. Chem. Soc.*, 2012, **134**, 5556–5559.

253 K. Kar, I. Arduini, K. W. Drombosky, P. C. A. Van Der Wel and R. Wetzel, *J. Mol. Biol.*, 2014, **426**, 816–829.

254 A. Lunkes, Y. Trottier and J. L. Mandel, *Essays Biochem.*, 1998, **33**, 149–163.

255 F. O. Walker, *Lancet*, 2007, **369**, 218–228.

256 J. J. Weber, A. S. Sowa, T. Binder and J. Hübener, *Biomed Res. Int.*, 2014, **2014**, 1–22.

257 S. Dutta, A. R. Foley, C. J. A. Warner, X. Zhang, M. Rolandi, B. Abrams and J. A. Raskatov, *Angew. Chemie Int. Ed.*, 2017, **56**, 11506–11510.

258 D. J. Adams, *Macromol. Biosci.*, 2011, **11**, 160–173.

259 C. Tomasini and N. Castellucci, *Chem. Soc. Rev.*, 2013, **42**, 156–172.

260 E. K. Johnson, D. J. Adams and P. J. Cameron, *J. Mater. Chem.*, 2011, **21**, 2024–2027.

261 M. de Loos, B. L. Feringa and J. H. van Esch, *European J. Org. Chem.*, 2005, **2005**, 3615–3631.

262 A. R. Hirst, I. A. Coates, T. R. Boucheteau, J. F. Miravet, B. Escuder, V. Castelletto, I. W. Hamley and D. K. Smith, *J. Am. Chem. Soc.*, 2008, **130**, 9113–9121.

263 J. Raeburn, A. Zamith Cardoso and D. J. Adams, *Chem. Soc. Rev.*, 2013, **42**, 5143–5156.

264 A. R. Hirst, B. Escuder, J. F. Miravet and D. K. Smith, *Angew. Chemie Int. Ed.*, 2008, **47**, 8002–8018.

265 L. A. Estroff and A. D. Hamilton, *Chem. Rev.*, 2004, **104**, 1201–1217.

266 B. Xu, *Langmuir*, 2009, **25**, 8373–8374.

267 J. J. Panda, A. Mishra, A. Basu and V. S. Chauhan, *Biomacromolecules*, 2008, **9**, 2244–2250.

268 L. E. Buerkle and S. J. Rowan, *Chem. Soc. Rev.*, 2012, **41**, 6089–6102.

269 X. Yang, G. Zhang and D. Zhang, *J. Mater. Chem.*, 2012, **22**, 38–50.

270 H. Kar and S. Ghosh, *Nat. Chem.*, 2015, **7**, 765–767.

271 J. Raeburn and D. J. Adams, *Chem. Commun.*, 2015, **51**, 5170–5180.

272 C. Colquhoun, E. R. Draper, E. G. B. Eden, B. N. Cattoz, K. L. Morris, L. Chen, T. O. McDonald, A. E. Terry, P. C. Griffiths, L. C. Serpell and D. J. Adams, *Nanoscale*, 2014, **6**, 13719–13725.

273 D. M. Ryan, S. B. Anderson, F. T. Senguen, R. E. Youngman and B. L. Nilsson, *Soft*

*Matter*, 2010, **6**, 475–479.

274 D. M. Ryan and B. L. Nilsson, *Polym. Chem.*, 2012, **3**, 18–33.

275 W. Liyanage and B. L. Nilsson, *Langmuir*, 2016, **32**, 787–799.

276 D. M. Ryan, T. M. Doran, S. B. Anderson and B. L. Nilsson, *Langmuir*, 2011, **27**, 4029–4039.

277 D. M. Ryan, S. B. Anderson and B. L. Nilsson, *Soft Matter*, 2010, **6**, 3220–3231.

278 A. Rajbhandary, D. M. Raymond and B. L. Nilsson, *Langmuir*, 2017, **33**, 5803–5813.

279 T. Das, M. Häring, D. Haldar and D. Díaz Díaz, *Biomater. Sci.*, 2018, **6**, 38–59.

280 K. Tao, A. Levin, L. Adler-Abramovich and E. Gazit, *Chem. Soc. Rev.*, 2016, **45**, 3935–3953.

281 D. G. Babar and S. Sarkar, *Appl. Nanosci.*, 2017, **7**, 101–107.

282 S. Perween, B. Chandanshive, H. C. Kotamarthi and D. Khushalani, *Soft Matter*, 2013, **9**, 10141–10145.

283 P. Koley and A. Pramanik, *J. Mater. Sci.*, 2014, **49**, 2000–2012.

284 X. Yan, P. Zhu and J. Li, *Chem. Soc. Rev.*, 2010, **39**, 1877–1890.

285 M. Reches and E. Gazit, *Science*, 2003, **300**, 625–627.

286 C. H. Görbitz, *Chem. Commun.*, 2006, **0**, 2332–2334.

287 S.-Y. Qin, Y. Pei, X.-J. Liu, R.-X. Zhuo and X.-Z. Zhang, *J. Mater. Chem. B*, 2013, **1**, 668–675.

288 C. H. Görbitz, *Chem. - Eur. J.*, 2001, **7**, 5153–5159.

289 C. Henrik Görbitz, *New J. Chem.*, 2003, **27**, 1789–1793.

290 C. H. Görbitz, *Chem. - Eur. J.*, 2007, **13**, 1022–1031.

291 M. Reches and E. Gazit, *Nano Lett.*, 2004, **4**, 581–585.

292 M. Reches and E. Gazit, *Phys. Biol.*, 2006, **3**, S10–S19.

293 L. Adler-Abramovich, P. Marco, Z. A. Arnon, R. C. G. Creasey, T. C. T. Michaels, A. Levin, D. J. Scurr, C. J. Roberts, T. P. J. Knowles, S. J. B. Tendler and E. Gazit, *ACS Nano*, 2016, **10**, 7436–7442.

294 N. Kol, L. Adler-Abramovich, D. Barlam, R. Z. Shneck, E. Gazit and I. Rousso, *Nano Lett.*, 2005, **5**, 1343–1346.

295 I. Azuri, L. Adler-Abramovich, E. Gazit, O. Hod and L. Kronik, *J. Am. Chem. Soc.*, 2014, **136**, 963–969.

296 S. Khanra, K. Ghosh, F. F. Ferreira, W. A. Alves, F. Punzo, P. Yu and S. Guha, *Phys. Chem. Chem. Phys.*, 2017, **19**, 3084–3093.

297 S. Almohammed, S. O. Oladapo, K. Ryan, A. L. Kholkin, J. H. Rice and B. J. Rodriguez, *RSC Adv.*, 2016, **6**, 41809–41815.

298 Q. Li, Y. Jia, L. Dai, Y. Yang and J. Li, *ACS Nano*, 2015, **9**, 2689–2695.

299 G. Singh, A. M. Bittner, S. Loscher, N. Malinowski and K. Kern, *Adv. Mater.*, 2008, **20**, 2332–2336.

300 A. Nuraeva, S. Vasilev, D. Vasileva, P. Zelenovskiy, D. Chezganov, A. Esin, S. Kopyl, K.

Romanyuk, V. Y. Shur and A. L. Kholkin, *Cryst. Growth Des.*, 2016, **16**, 1472–1479.

301 M. Wang, L. Du, X. Wu, S. Xiong and P. K. Chu, *ACS Nano*, 2011, **5**, 4448–4454.

302 L. Adler-Abramovich, M. Reches, V. L. Sedman, S. Allen, S. J. B. Tendler and E. Gazit, *Langmuir*, 2006, **22**, 1313–1320.

303 R. Huang, W. Qi, R. Su, J. Zhao and Z. He, *Soft Matter*, 2011, **7**, 6418–6421.

304 P. Zhu, X. Yan, Y. Su, Y. Yang and J. Li, *Chem. - Eur. J.*, 2010, **16**, 3176–3183.

305 H. Ma, J. Fei, Q. Li and J. Li, *Small*, 2015, **11**, 1787–1791.

306 X. Yan, Y. Cui, Q. He, K. Wang, J. Li, W. Mu, B. Wang and Z. Ou□yang, *Chem. - Eur. J.*, 2008, **14**, 5974–5980.

307 M. Reches and E. Gazit, *Isr. J. Chem.*, 2005, **45**, 363–371.

308 N. A. Dudukovic and C. F. Zukoski, *Langmuir*, 2014, **30**, 4493–4500.

309 L. Adler-Abramovich and E. Gazit, *J. Pept. Sci.*, 2008, **14**, 217–223.

310 F.-Y. Wu, S.-M. Hsu, H. Cheng, L.-H. Hsu and H.-C. Lin, *New J. Chem.*, 2015, **39**, 4240–4243.

311 A. M. Smith, R. J. Williams, C. Tang, P. Coppo, R. F. Collins, M. L. Turner, A. Saiani and R. V. Ulijn, *Adv. Mater.*, 2008, **20**, 37–41.

312 A. Mahler, M. Reches, M. Rechter, S. Cohen and E. Gazit, *Adv. Mater.*, 2006, **18**, 1365–1370.

313 S. Fleming and R. V. Ulijn, *Chem. Soc. Rev.*, 2014, **43**, 8150–8177.

314 R. C. G. Creasey, I. Louzao, Z. A. Arnon, P. Marco, L. Adler-Abramovich, C. J. Roberts, E. Gazit and S. J. B. Tendler, *Soft Matter*, 2016, **12**, 9451–9457.

315 S. S. Rohner, J. Ruiz-Olles and D. K. Smith, *RSC Adv.*, 2015, **5**, 27190–27196.

316 S. Yuran, Y. Razvag and M. Reches, *ACS Nano*, 2012, **6**, 9559–9566.

317 C. Guo, Z. A. Arnon, R. Qi, Q. Zhang, L. Adler-Abramovich, E. Gazit and G. Wei, *ACS Nano*, 2016, **10**, 8316–8324.

318 Y. Wang, R. Huang, W. Qi, Y. Xie, M. Wang, R. Su and Z. He, *Small*, 2015, **11**, 2893–2902.

319 S. Maity, S. Nir and M. Reches, *J. Mater. Chem. B*, 2014, **2**, 2583–2591.

320 X. Yan, Q. He, K. Wang, L. Duan, Y. Cui and J. Li, *Angew. Chemie Int. Ed.*, 2007, **46**, 2431–2434.

321 M. Reches and E. Gazit, *Nat. Nanotechnol.*, 2006, **1**, 195–200.

322 P. Tamamis, L. Adler-Abramovich, M. Reches, K. Marshall, P. Sikorski, L. Serpell, E. Gazit and G. Archontis, *Biophys. J.*, 2009, **96**, 5020–5029.

323 T. H. Han, T. Ok, J. Kim, D. O. Shin, H. Ihee, H. S. Lee and S. O. Kim, *Small*, 2010, **6**, 945–951.

324 J. Adamcik and R. Mezzenga, *Curr. Opin. Colloid Interface Sci.*, 2012, **17**, 369–376.

325 Y. Li, H. Liang, H. Zhao, D. Chen, B. Liu, T. Fuhs and M. Dong, *J. Nanomater.*, 2016, **2016**, 1–18.

326 S. L. Gras, L. J. Waddington and K. N. Goldie, in *Methods in Molecular Biology*,

Springer, New York, 2011, pp. 197–214.

327 S. Gregoire, J. Irwin and I. Kwon, *Korean J. Chem. Eng.*, 2012, **29**, 693–702.

328 E. Takai, G. Ohashi, R. Ueki, Y. Yamada, J. I. Fujita and K. Shiraki, *Am. J. Biochem. Biotechnol.*, 2014, **10**, 31–39.

329 C. Goldsbury, U. Baxa, M. N. Simon, A. C. Steven, A. Engel, J. S. Wall, U. Aebi and S. A. Müller, *J. Struct. Biol.*, 2011, **173**, 1–13.

330 S. Marchesan, K. E. Styan, C. D. Easton, L. Waddington and A. V Vargiu, *J. Mater. Chem. B*, 2015, **3**, 8123–8132.

331 B. Morel, L. Varela and F. Conejero-Lara, *J. Phys. Chem. B*, 2010, **114**, 4010–4019.

332 H. LeVine, *Methods Enzymol.*, 1999, **309**, 274–284.

333 M. Biancalana and S. Koide, *Biochim. Biophys. Acta*, 2010, **1804**, 1405–1412.

334 M. R. H. Krebs, E. H. C. Bromley and A. M. Donald, *J. Struct. Biol.*, 2005, **149**, 30–37.

335 H. Wang and Z. Yang, *Nanoscale*, 2012, **4**, 5259–5267.

336 W. Y. Seow and C. A. E. Hauser, *Mater. Today*, 2014, **17**, 381–388.

337 J. J. Panda and V. S. Chauhan, *Polym. Chem.*, 2014, **5**, 4431–4449.

338 S. Marchesan, A. Vargiu and K. Styan, *Molecules*, 2015, **20**, 19775–19788.

339 J. Kopeček, *Biomaterials*, 2007, **28**, 5185–5192.

340 J. B. Matson and S. I. Stupp, *Chem. Commun.*, 2012, **48**, 26–33.

341 H. Acar, S. Srivastava, E. J. Chung, M. R. Schnorenberg, J. C. Barrett, J. L. LaBelle and

M. Tirrell, *Adv. Drug Deliv. Rev.*, 2017, **110**–**111**, 65–79.

342 S. Kyle, A. Aggeli, E. Ingham and M. J. McPherson, *Trends Biotechnol.*, 2009, **27**, 423–433.

343 S. R. Caliari and J. A. Burdick, *Nat. Methods*, 2016, **13**, 405–414.

344 J. H. Collier, *Soft Matter*, 2008, **4**, 2310–2315.

345 D. Higashi, M. Yoshida and M. Yamanaka, *Chem. - Asian J.*, 2013, **8**, 2584–2587.

346 A. C. Society, M. Id, M. Type, D. Submitted, C. List, L. D. Article, T. Minemura, T. Science, T. Yoshikawa, T. Suzuki and T. Hanabusa, *Langmuir*, 2013, **29**, 14666–14673.

347 K. Liu and J. W. Steed, *Soft Matter*, 2013, **9**, 11699–11705.

348 J. Nanda, A. Biswas and A. Banerjee, *Soft Matter*, 2013, **9**, 4198–4208.

349 M. Ghosh, M. Halperin-Sternfeld, I. Grigoriants, J. Lee, K. T. Nam and L. Adler-Abramovich, *Biomacromolecules*, 2017, **18**, 3541–3550.

350 S. Bertazzo, W. F. Zambuzzi, D. D. P. Campos, T. L. Ogeda, C. V. Ferreira and C. A. Bertran, *Colloids Surf. B*, 2010, **78**, 177–184.

351 F. Laydi, R. Rahouadj, G. Cauchois, J.-F. Stoltz and N. de Isla, *Biomed. Mater. Eng.*, 2013, **23**, 311–315.

352 R. Shu, R. McMullen, M. J. Baumann and L. R. McCabe, *J. Biomed. Mater. Res. A*, 2003, **67**, 1196–1204.

353 K. A. Bhadang, C. A. Holding, H. Thissen, K. M. McLean, J. S. Forsythe and D. R. Haynes, *Acta Biomater.*, 2010, **6**, 1575–1583.

354 D. W. Hutmacher, *Biomaterials*, 2000, **21**, 2529–2543.

355 M. Halperin-Sternfeld, M. Ghosh, R. Sevostianov, I. Grigoriants and L. Adler-Abramovich, *Chem. Commun.*, 2017, **53**, 9586–9589.

356 S.-M. Hsu, F.-Y. Wu, T.-S. Lai, Y.-C. Lin and H.-C. Lin, *RSC Adv.*, 2015, **5**, 22943–22946.

357 S. E. D'Souza, M. H. Ginsberg and E. F. Plow, *Trends Biochem. Sci.*, 1991, **16**, 246–250.

358 T. G. Kim and T. G. Park, *Tissue Eng.*, 2006, **12**, 221–233.

359 S. L. Bellis, *Biomaterials*, 2011, **32**, 4205–4210.

360 E. Garanger, D. Boturyn, J.-L. Coll, M.-C. Favrot and P. Dumy, *Org. Biomol. Chem.*, 2006, **4**, 1958–1965.

361 W. Liyanage, K. Vats, A. Rajbhandary, D. S. W. Benoit and B. L. Nilsson, *Chem. Commun.*, 2015, **51**, 11260–11263.

362 C. C. Horgan, A. L. Rodriguez, R. Li, K. F. Bruggeman, N. Stupka, J. K. Raynes, L. Day, J. W. White, R. J. Williams and D. R. Nisbet, *Acta Biomater.*, 2016, **38**, 11–22.

363 A. D. Theocharis, S. S. Skandalis, C. Gialeli and N. K. Karamanos, *Adv. Drug Deliv. Rev.*, 2016, **97**, 4–27.

364 M. Zhou, A. M. Smith, A. K. Das, N. W. Hodson, R. F. Collins, R. V. Ulijn and J. E. Gough, *Biomaterials*, 2009, **30**, 2523–2530.

365 M. Zhou, R. V Ulijn and J. E. Gough, *J. Tissue Eng.*, 2014, **5**, 204173141453159.

366 V. Jayawarna, M. Ali, T. A. Jowitt, A. F. Miller, A. Saiani, J. E. Gough and R. V. Ulijn,

*Adv. Mater.*, 2006, **18**, 611–614.

367 V. Jayawarna, S. M. Richardson, A. R. Hirst, N. W. Hodson, A. Saiani, J. E. Gough and R. V. Ulijn, *Acta Biomater.*, 2009, **5**, 934–943.

368 S. Rimmer, C. Johnson, B. Zhao, J. Collier, L. Gilmore, S. Sabnis, P. Wyman, C. Sammon, N. J. Fullwood and S. MacNeil, *Biomaterials*, 2007, **28**, 5319–5331.

369 N. Faucheux, R. Schweiss, K. Lützow, C. Werner and T. Groth, *Biomaterials*, 2004, **25**, 2721–2730.

370 A. J. Engler, S. Sen, H. L. Sweeney and D. E. Discher, *Cell*, 2006, **126**, 677–689.

371 S. Fleming, S. Debnath, P. W. J. M. Frederix, N. T. Hunt and R. V. Ulijn, *Biomacromolecules*, 2014, **15**, 1171–1184.

372 E. V. Alakpa, V. Jayawarna, A. Lampel, K. V. Burgess, C. C. West, S. C. J. Bakker, S. Roy, N. Javid, S. Fleming, D. A. Lamprou, J. Yang, A. Miller, A. J. Urquhart, P. W. J. M. Frederix, N. T. Hunt, B. Péault, R. V. Ulijn and M. J. Dalby, *Chem*, 2016, **1**, 298–319.

373 K. C. Clause, L. J. Liu and K. Tobita, *Cell Commun. Adhes.*, 2010, **17**, 48–54.

374 D. Dado, M. Sagi, S. Levenberg and A. Zemel, *Regen. Med.*, 2012, **7**, 101–116.

375 M. Crisan, S. Yap, L. Casteilla, C. W. Chen, M. Corselli, T. S. Park, G. Andriolo, B. Sun, B. Zheng, L. Zhang, C. Norotte, P. N. Teng, J. Traas, R. Schugar, B. M. Deasy, S. Badylak, H. J. Buhring, J. P. Giacobino, L. Lazzari, J. Huard and B. Péault, *Cell Stem Cell*, 2008, **3**, 301–313.

376 E. V. Alakpa, V. Jayawarna, K. E. V. Burgess, C. C. West, B. Péault, R. V. Ulijn and M. J. Dalby, *Sci. Rep.*, 2017, **7**, 6895–6905.

377 M. Wang, Y. Lv, X. Liu, W. Qi, R. Su and Z. He, *ACS Appl. Mater. Interfaces*, 2016, **8**, 14133–14141.

378 Y. Zhang, X. Liu, M. Wang, Y. Zhao, W. Qi, R. Su and Z. He, *RSC Adv.*, 2017, **7**, 15736–15741.

379 P. Das, S. Yuran, J. Yan, P. S. Lee and M. Reches, *Chem. Commun.*, 2015, **51**, 5432–5435.

380 S. K. M. Nalluri, N. Shivarova, A. L. Kanibolotsky, M. Zelzer, S. Gupta, P. W. J. M. Frederix, P. J. Skabara, H. Gleskova and R. V. Ulijn, *Langmuir*, 2014, **30**, 12429–12437.

381 G. Scott, S. Roy, Y. M. Abul-Haija, S. Fleming, S. Bai and R. V. Ulijn, *Langmuir*, 2013, **29**, 14321–14327.

382 J. Wu and G.-H. Ma, *Small*, 2016, **12**, 4633–4648.

383 Y. M. Abul-Haija, S. Roy, P. W. J. M. Frederix, N. Javid, V. Jayawarna and R. V. Ulijn, *Small*, 2014, **10**, 973–979.

384 R. J. Williams, A. M. Smith, R. Collins, N. Hodson, A. K. Das and R. V. Ulijn, *Nat. Nanotechnol.*, 2009, **4**, 19–24.

385 S. Toledano, R. J. Williams, V. Jayawarna and R. V. Ulijn, *J. Am. Chem. Soc.*, 2006, **128**, 1070–1071.

386 J. W. Sadownik, J. Leckie and R. V. Ulijn, *Chem. Commun.*, 2011, **47**, 728–730.

387 Z. Yang, H. Gu, D. Fu, P. Gao, J. K. Lam and B. Xu, *Adv. Mater.*, 2004, **16**, 1440–1444.

388 Z. Yang, G. Liang and B. Xu, *Acc. Chem. Res.*, 2008, **41**, 315–326.

389 Y. Gao, Z. Yang, Y. Kuang, M.-L. Ma, J. Li, F. Zhao and B. Xu, *Biopolymers*, 2010, **94**, 19–31.

390 J. Gao, H. Wang, L. Wang, J. Wang, D. Kong and Z. Yang, *J. Am. Chem. Soc.*, 2009, **131**, 11286–11287.

391 C. Berdugo, S. K. M. Nalluri, N. Javid, B. Escuder, J. F. Miravet and R. V. Ulijn, *ACS Appl. Mater. Interfaces*, 2015, **7**, 25946–25954.

392 P. W. J. M. Frederix, G. G. Scott, Y. M. Abul-Haija, D. Kalafatovic, C. G. Pappas, N. Javid, N. T. Hunt, R. V. Ulijn and T. Tuttle, *Nat. Chem.*, 2015, **7**, 30–37.

393 G. G. Scott, P. J. McKnight, T. Tuttle and R. V. Ulijn, *Adv. Mater.*, 2016, **28**, 1381–1386.

394 Y. M. Abul-Haija, G. G. Scott, J. K. Sahoo, T. Tuttle and R. V. Ulijn, *Chem. Commun.*, 2017, **53**, 9562–9565.

395 Y. Xie, J. Zhao, R. Huang, W. Qi, Y. Wang, R. Su and Z. He, *Nanoscale Res. Lett.*, 2016, **11**, 184–192.

396 S. Dinda, M. Ghosh and P. K. Das, *Langmuir*, 2016, **32**, 6701–6712.

397 S. R. Deka, S. Yadav, D. Kumar, S. Garg, M. Mahato and A. K. Sharma, *Colloids Surf. B*, 2017, **155**, 332–340.

398 J. Fan, R. Li, H. Wang, X. He, T. P. Nguyen, R. A. Letteri, J. Zou and K. L. Wooley, *Org. Biomol. Chem.*, 2017, **15**, 5145–5154.

399 S. Sundar, Y. Chen and Y. W. Tong, *Curr. Med. Chem.*, 2014, **21**, 2469–2479.

400 S. Parween, A. Misra, S. Ramakumar and V. S. Chauhan, *J. Mater. Chem. B*, 2014, **2**,

3096–3106.

401 M. C. Branco and J. P. Schneider, *Acta Biomater.*, 2009, **5**, 817–831.

402 C. Martin, E. Oyen, J. Mangelschots, M. Bibian, T. Ben Haddou, J. Andrade, J. Gardiner, B. Van Mele, A. Madder, R. Hoogenboom, M. Spetea and S. Ballet, *Med. Chem. Commun.*, 2016, **7**, 542–549.

403 C. Martin, E. Oyen, Y. Van Wanseele, T. Ben Haddou, H. Schmidhammer, J. Andrade, L. Waddington, A. Van Eeckhaut, B. Van Mele, J. Gardiner, R. Hoogenboom, A. Madder, M. Spetea and S. Ballet, *Mater. Today Chem.*, 2017, **3**, 49–59.

404 A. Altunbas, S. J. Lee, S. A. Rajasekaran, J. P. Schneider and D. J. Pochan, *Biomaterials*, 2011, **32**, 5906–5914.

405 X. Liu, P. Zhu, J. Fei, J. Zhao, X. Yan and J. Li, *Chem. - Eur. J.*, 2015, **21**, 9461–9467.

406 A. R. Sapala, J. Kundu, P. Chowdhury and V. Haridas, *New J. Chem.*, 2016, **40**, 9907–9911.

407 J. Lu, Y. Gao, J. Wu and Y. Ju, *RSC Adv.*, 2013, **3**, 23548–23552.

408 J. Rubio-Magnieto, M. Tena-Solsona, B. Escuder and M. Surin, *RSC Adv.*, 2017, **7**, 9562–9566.

409 W. Li, I. Park, S.-K. Kang and M. Lee, *Chem. Commun.*, 2012, **48**, 8796–8798.

410 A. W. Du and M. H. Stenzel, *Biomacromolecules*, 2014, **15**, 1097–1114.

411 Q. V. Nguyen, D. P. Huynh, J. H. Park and D. S. Lee, *Eur. Polym. J.*, 2015, **72**, 602–619.

412 S. Koutsopoulos, L. D. Unsworth, Y. Nagai and S. Zhang, *Proc. Natl. Acad. Sci.*, 2009,

**106**, 4623–4628.

413 K. Kim, B. Bae, Y. J. Kang, J. M. Nam, S. Kang and J. H. Ryu, *Biomacromolecules*, 2013, **14**, 3515–3522.

414 T. Hirakura, K. Yasugi, T. Nemoto, M. Sato, T. Shimoboji, Y. Aso, N. Morimoto and K. Akiyoshi, *J. Control. Release*, 2010, **142**, 483–489.

415 P. M. Kharkar, M. S. Rehmann, K. M. Skeens, E. Maverakis and A. M. Kloxin, *ACS Biomater. Sci. Eng.*, 2016, **2**, 165–179.

416 Z. Yu, Q. Xu, C. Dong, S. Lee, L. Gao, Y. Li, M. D'Ortenzio and J. Wu, *Curr. Pharm. Des.*, 2015, **21**, 4342–4354.

417 L. Ruan, H. Zhang, H. Luo, J. Liu, F. Tang, Y.-K. Shi and X. Zhao, *Proc. Natl. Acad. Sci.*, 2009, **106**, 5105–5110.

418 Q. Wang, J. L. Mynar, M. Yoshida, E. Lee, M. Lee, K. Okuro, K. Kinbara and T. Aida, *Nature*, 2010, **463**, 339–343.

419 L. Chen, S. Revel, K. Morris, D. G. Spiller, L. C. Serpell and D. J. Adams, *Chem. Commun.*, 2010, **46**, 6738–6740.

420 A. Brizard, M. Stuart, K. van Bommel, A. Friggeri, M. de Jong and J. van Esch, *Angew. Chemie Int. Ed.*, 2008, **47**, 2063–2066.

421 L.-P. Bergeron-Sandoval, N. Safaee and S. W. Michnick, *Cell*, 2016, **165**, 1067–1079.

422 W. M. Aumiller, B. W. Davis and C. D. Keating, *Int. Rev. Cell Mol. Biol.*, 2014, **307**, 109–149.

423 A. Aguzzi and M. Altmeyer, *Trends Cell Biol.*, 2016, **26**, 547–558.

424 B. Cornils, *Angew. Chemie Int. Ed. English*, 1997, **36**, 2057–2059.

425 M. P. Krafft, F. Giulieri, P. Fontaine and M. Goldmann, *Langmuir*, 2001, **17**, 6577–6584.

426 A. Heeres, C. van der Pol, M. Stuart, A. Friggeri, B. L. Feringa and J. van Esch, *J. Am. Chem. Soc.*, 2003, **125**, 14252–14253.

427 I. O. Shklyarevskiy, P. Jonkheijm, P. C. M. Christianen, A. P. H. J. Schenning, E. W. Meijer, O. Henze, A. F. M. Kilbinger, W. J. Feast, A. Del Guerzo, J.-P. Desvergne and J. C. Maan, *J. Am. Chem. Soc.*, 2005, **127**, 1112–1113.

428 N. Javid, S. Roy, M. Zelzer, Z. Yang, J. Sefcik and R. V. Ulijn, *Biomacromolecules*, 2013, **14**, 4368–4376.

429 T. Yuan, J. Fei, Y. Xu, X. Yang and J. Li, *Macromol. Rapid Commun.*, 2017, **38**, 1700408.

430 L. Moise, S. Beseme, R. Tassone, R. Liu, F. Kibria, F. Terry, W. Martin and A. S. De Groot, *Expert Rev. Vaccines*, 2016, **15**, 607–617.

431 E. T. Clambey, B. Davenport, J. W. Kappler, P. Marrack and D. Homann, *J. Mol. Med.*, 2014, **92**, 735–741.

432 C. Yu, J. Xi, M. Li, M. An and H. Liu, *Bioconjug. Chem.*, 2017, Article ASAP. DOI: 10.1021/acs.bioconjchem.7b00632.

433 G. Charalambidis, E. Georgilis, M. K. Panda, C. E. Anson, A. K. Powell, S. Doyle, D. Moss, T. Jochum, P. N. Horton, S. J. Coles, M. Linares, D. Beljonne, J.-V. Naubron, J. Conradt, H. Kalt, A. Mitraki, A. G. Coutsolelos and T. S. Balaban, *Nat. Commun.*, 2016,

**7**, 12657.

434 Q. Zou, L. Zhang, X. Yan, A. Wang, G. Ma, J. Li, H. Möhwald and S. Mann, *Angew. Chemie Int. Ed.*, 2014, **53**, 2366–2370.

435 K. Liu, R. Xing, C. Chen, G. Shen, L. Yan, Q. Zou, G. Ma, H. Möhwald and X. Yan, *Angew. Chemie Int. Ed.*, 2014, **54**, 500–505.

436 K. Liu, Y. Kang, G. Ma, H. Möhwald and X. Yan, *Phys. Chem. Chem. Phys.*, 2016, **18**, 16738–16747.

437 S. K. Parayil, J. Lee and M. Yoon, *Photochem. Photobiol. Sci.*, 2013, **12**, 798–804.

438 K. Liu, H. Zhang, R. Xing, Q. Zou and X. Yan, *ACS Nano*, 2017, **11**, 12840–12848.

439 K. Liu, C. Yuan, Q. Zou, Z. Xie and X. Yan, *Angew. Chemie Int. Ed.*, 2017, **56**, 7876–7880.

440 K. Tao, B. Xue, S. Frere, I. Slutsky, Y. Cao, W. Wang and E. Gazit, *Chem. Mater.*, 2017, **29**, 4454–4460.

441 H. L. Ozores, M. Amorín and J. R. Granja, *J. Am. Chem. Soc.*, 2017, **139**, 776–784.

442 K. Liu, R. Xing, Q. Zou, G. Ma, H. Möhwald and X. Yan, *Angew. Chemie Int. Ed.*, 2016, **55**, 3036–3039.

443 Q. Zou, M. Abbas, L. Zhao, S. Li, G. Shen and X. Yan, *J. Am. Chem. Soc.*, 2017, **139**, 1921–1927.

444 W. Auwärter, D. Écija, F. Klappenberger and J. V. Barth, *Nat. Chem.*, 2015, **7**, 105–120.

445 D. P. Collins and J. H. Dawson, in *Comprehensive Inorganic Chemistry II*, Elsevier, 2013,

pp. 65–102.

446 L. P. Cook, G. Brewer and W. Wong-Ng, *Crystals*, 2017, **7**, 223–244.

447 L. Zhao, R. Qu, A. Li, R. Ma and L. Shi, *Chem. Commun.*, 2016, **52**, 13543–13555.

448 F. Le Guern, T.-S. Ouk, C. Ouk, R. Vanderesse, Y. Champavier, E. Pinault and V. Sol, *ACS Med. Chem. Lett.*, 2018, **9**, 11-16.

449 R. Dondi, E. Yaghini, K. M. Tewari, L. Wang, F. Giuntini, M. Loizidou, A. J. MacRobert and I. M. Eggleston, *Org. Biomol. Chem.*, 2016, **14**, 11488–11501.

450 J. M. Ribo, *Science*, 2001, **292**, 2063–2066.

451 A. D. Schwab, D. E. Smith, C. S. Rich, E. R. Young, W. F. Smith and J. C. de Paula, *J. Phys. Chem. B*, 2003, **107**, 11339–11345.

452 J. S. Lindsey, M. Ptaszek and M. Taniguchi, *Orig. Life Evol. Biosph.*, 2009, **39**, 495–515.

453 D. Deamer and A. L. Weber, *Cold Spring Harb. Perspect. Biol.*, 2010, **2**, a004929.

454 K. Liu, R. Xing, Y. Li, Q. Zou, H. Möhwald and X. Yan, *Angew. Chemie Int. Ed.*, 2016, **55**, 12503–12507.

455 M. P. Hendricks, K. Sato, L. C. Palmer and S. I. Stupp, *Acc. Chem. Res.*, 2017, **50**, 2440–2448.

456 C. J. C. Edwards-Gayle and I. W. Hamley, *Org. Biomol. Chem.*, 2017, **15**, 5867–5876.

457 R. N. Shah, N. A. Shah, M. M. Del Rosario Lim, C. Hsieh, G. Nuber and S. I. Stupp, *Proc. Natl. Acad. Sci.*, 2010, **107**, 3293–3298.

458 D. J. Toft, T. J. Moyer, S. M. Standley, Y. Ruff, A. Ugolkov, S. I. Stupp and V. L. Cryns,

*ACS Nano*, 2012, **6**, 7956–7965.

459 P. Besenius, G. Portale, P. H. H. Bomans, H. M. Janssen, A. R. A. Palmans and E. W. Meijer, *Proc. Natl. Acad. Sci.*, 2010, **107**, 17888–17893.

460 P. Besenius, K. P. van den Hout, H. M. H. G. Albers, T. F. A. de Greef, L. L. C. Olijve, T. M. Hermans, B. F. M. de Waal, P. H. H. Bomans, N. A. J. M. Sommerdijk, G. Portale, A. R. A. Palmans, M. H. P. van Genderen, J. A. J. M. Vekemans and E. W. Meijer, *Chem. - Eur. J.*, 2011, **17**, 5193–5203.

461 P. Besenius, Y. Goedegebure, M. Driesse, M. Koay, P. H. H. Bomans, A. R. A. Palmans, P. Y. W. Dankers and E. W. Meijer, *Soft Matter*, 2011, **7**, 7980–7983.

462 H. A. M. Ardoña and J. D. Tovar, *Chem. Sci.*, 2015, **6**, 1474–1484.

463 H. A. M. Ardoña, T. S. Kale, A. Ertel and J. D. Tovar, *Langmuir*, 2017, **33**, 7435–7445.

464 G. A. Silva, C. Czeisler, K. L. Niece, E. Beniash, D. A. Harrington, J. A. Kessler and S. I. Stupp, *Science*, 2004, **303**, 1352–1355.

465 M. J. Webber, J. Tongers, C. J. Newcomb, K.-T. Marquardt, J. Bauersachs, D. W. Losordo and S. I. Stupp, *Proc. Natl. Acad. Sci.*, 2011, **108**, 13438–13443.

466 E. J. Berns, S. Sur, L. Pan, J. E. Goldberger, S. Suresh, S. Zhang, J. A. Kessler and S. I. Stupp, *Biomaterials*, 2014, **35**, 185–195.

467 C. E. Morgan, A. W. Dombrowski, C. M. R. Pérez, E. S. M. Bahnson, N. D. Tsihlis, W. Jiang, Q. Jiang, J. M. Vercammen, V. S. Prakash, T. A. Pritts, S. I. Stupp and M. R. Kibbe, *ACS Nano*, 2016, **10**, 899–909.

468 H. A. Behanna, J. J. J. M. Donners, A. C. Gordon and S. I. Stupp, *J. Am. Chem. Soc.*,

2005, **127**, 1193–1200.

469 H. A. Behanna, K. Rajangam and S. I. Stupp, *J. Am. Chem. Soc.*, 2007, **129**, 321–327.

470 M. A. Khalily, G. Bakan, B. Kucukoz, A. E. Topal, A. Karatay, H. G. Yaglioglu, A. Dana and M. O. Guler, *ACS Nano*, 2017, **11**, 6881–6892.

471 I. W. Hamley, A. Dehsorkhi and V. Castelletto, *Langmuir*, 2013, **29**, 5050–5059.

472 N. Nandi, S. Basak, S. Kirkham, I. W. Hamley and A. Banerjee, *Langmuir*, 2016, **32**, 13226–13233.

473 V. Castelletto, I. W. Hamley, J. Perez, L. Abezgauz and D. Danino, *Chem. Commun.*, 2010, **46**, 9185–9187.

474 Z. Yu, A. Erbas, F. Tantakitti, L. C. Palmer, J. A. Jackman, M. O. De La Cruz, N. J. Cho and S. I. Stupp, *J. Am. Chem. Soc.*, 2017, **139**, 7823–7830.

475 K. J. C. van Bommel, C. van der Pol, I. Muizebelt, A. Friggeri, A. Heeres, A. Meetsma, B. L. Feringa and J. van Esch, *Angew. Chemie Int. Ed.*, 2004, **43**, 1663–1667.

476 H. Frisch, J. P. Unsleber, D. Lüdeker, M. Peterlechner, G. Brunklaus, M. Waller and P. Besenius, *Angew. Chemie Int. Ed.*, 2013, **52**, 10097–10101.

477 P. Ahlers, H. Frisch and P. Besenius, *Polym. Chem.*, 2015, **6**, 7245–7250.

478 R. J. Brea, M. Eugenio Vázquez, M. Mosquera, L. Castedo and J. R. Granja, *J. Am. Chem. Soc.*, 2007, **129**, 1653–1657.

479 J. Xu, X. Li, X. Li, B. Li, L. Wu, W. Li, X. Xie and R. Xue, *Biomacromolecules*, 2017, **18**, 3524–3530.

480 J. M. Mason and K. M. Arndt, *ChemBioChem*, 2004, **5**, 170–176.

481 T. Xu and J. Shu, *Soft Matter*, 2010, **6**, 212–217.

482 H. Dong, S. E. Paramonov and J. D. Hartgerink, *J Am Chem Soc*, 2008, **130**, 13691–13695.

483 M. G. Ryadnov and D. N. Woolfson, in *Nanobiotechnology II: More Concepts and Applications*, Wiley, 2007, pp. 19–40.

484 J. Liu, Q. Zheng, Y. Deng, C.-S. Cheng, N. R. Kallenbach and M. Lu, *Proc. Natl. Acad. Sci.*, 2006, **103**, 15457–15462.

485 G. Grigoryan and A. E. Keating, *Curr. Opin. Struct. Biol.*, 2008, **18**, 477–483.

486 P. Burkhard, J. Stetefeld and S. V. Strelkov, *Trends Cell Biol.*, 2001, **11**, 82–88.

487 A. N. Lupas, M. Gruber and G. N. Phillips Jr., *Proteins*, 2005, **70**, 37–78.

488 E. Moutevelis and D. N. Woolfson, *J. Mol. Biol.*, 2009, **385**, 726–732.

489 E. K. O'Shea, K. J. Lumb and P. S. Kim, *Curr. Biol.*, 1993, **3**, 658–667.

490 R. Fairman, H. G. Chao, T. B. Lavoie, J. J. Villafranca, G. R. Matsueda and J. Novotny, *Biochemistry*, 1996, **35**, 2824–2829.

491 D. N. Woolfson, *Adv. Protein Chem.*, 2005, **70**, 79–112.

492 H. Dong and J. D. Hartgerink, *Biomacromolecules*, 2006, **7**, 691–695.

493 B. C. Root, L. D. Pellegrino, E. D. Crawford, B. Kokona and R. Fairman, *Protein Sci.*, 2009, **18**, 329–336.

494 M. Pechar, R. Pola, R. Laga, K. Ulbrich, L. Bednárová, P. Maloň, I. Sieglová, V. Král, M. Fábry and O. Vaněk, *Biomacromolecules*, 2011, **12**, 3645–3655.

495 C. Aronsson, S. Dånmark, F. Zhou, P. Öberg, K. Enander, H. Su and D. Aili, *Sci. Rep.*, 2015, **5**, 14063–14072.

496 B. Apostolovic, M. Danial and H.-A. Klok, *Chem. Soc. Rev.*, 2010, **39**, 3541–3575.

497 D. N. Woolfson, *Subcell. Biochem.*, 2017, **82**, 35–61.

498 D. Papapostolou, A. M. Smith, E. D. T. Atkins, S. J. Oliver, M. G. Ryadnov, L. C. Serpell and D. N. Woolfson, *Proc. Natl. Acad. Sci.*, 2007, **104**, 10853–10858.

499 M. G. Ryadnov and D. N. Woolfson, *J. Am. Chem. Soc.*, 2005, **127**, 12407–12415.

500 J. F. Ross, A. Bridges, J. M. Fletcher, D. Shoemark, D. Alibhai, H. E. V. Bray, J. L. Beesley, W. M. Dawson, L. R. Hodgson, J. Mantell, P. Verkade, C. M. Edge, R. B. Sessions, D. Tew and D. N. Woolfson, *ACS Nano*, 2017, **11**, 7901–7914.

501 H. Dong, S. E. Paramonov and J. D. Hartgerink, *J. Am. Chem. Soc.*, 2008, **130**, 13691–13695.

502 T. Nakaji-Hirabayashi, K. Kato and H. Iwata, *Biomacromolecules*, 2008, **9**, 1411–1416.

503 E. Brandenburg, H. von Berlepsch, U. I. M. Gerling, C. Böttcher and B. Koksch, *Chem. - Eur. J.*, 2011, **17**, 10651–10661.

504 E. Brandenburg, H. von Berlepsch, J. Leiterer, F. Emmerling and B. Koksch, *Biomacromolecules*, 2012, **13**, 3542–3551.

505 J. M. Fletcher, R. L. Harniman, F. R. H. Barnes, A. L. Boyle, A. Collins, J. Mantell, T. H.

Sharp, M. Antognozzi, P. J. Booth, N. Linden, M. J. Miles, R. B. Sessions, P. Verkade and D. N. Woolfson, *Science*, 2013, **340**, 595–599.

506 J. Ang, D. Ma, B. T. Jung, S. Keten and T. Xu, *Biomacromolecules*, 2017, **18**, 3572–3580.

507 H. Dong, J. Y. Shu, N. Dube, Y. Ma, M. V. Tirrell, K. H. Downing and T. Xu, *J. Am. Chem. Soc.*, 2012, **134**, 11807–11814.

508 J. Ang, D. Ma, R. Lund, S. Keten and T. Xu, *Biomacromolecules*, 2016, **17**, 3262–3267.

509 M. D. Shoulders and R. T. Raines, *Annu. Rev. Biochem.*, 2009, **78**, 929–958.

510 P. Fratzl, *Collagen: Structure and Mechanics*, Springer, Boston, 2008.

511 J. Engel and H. P. Bächinger, *Top. Curr. Chem.*, 2005, **247**, 7–33.

512 C. H. Lee, A. Singla and Y. Lee, *Int. J. Pharm.*, 2001, **221**, 1–22.

513 B. An, Y.-S. Lin and B. Brodsky, *Adv. Drug Deliv. Rev.*, 2016, **97**, 69–84.

514 T. Luo and K. L. Kiick, *Bioconjug. Chem.*, 2017, **28**, 816–827.

515 I. C. Tanrikulu and R. T. Raines, *J. Am. Chem. Soc.*, 2014, **136**, 13490–13493.

516 F. W. Kotch, I. A. Guzei and R. T. Raines, *J. Am. Chem. Soc.*, 2008, **130**, 2952–2953.

517 J. A. Fallas, L. E. R. O'Leary and J. D. Hartgerink, *Chem. Soc. Rev.*, 2010, **39**, 3510–3572.

518 L. E. R. O'Leary, J. A. Fallas, E. L. Bakota, M. K. Kang and J. D. Hartgerink, *Nat. Chem.*, 2011, **3**, 821–828.

519 S. Rele, Y. Song, R. P. Apkarian, Z. Qu, V. P. Conticello and E. L. Chaikof, *J. Am. Chem.*

*Soc.*, 2007, **129**, 14780–14787.

520 T. Jiang, C. Xu, Y. Liu, Z. Liu, J. S. Wall, X. Zuo, T. Lian, K. Salaita, C. Ni, D. Pochan and V. P. Conticello, *J. Am. Chem. Soc.*, 2014, **136**, 4300–4308.

521 B. Sarkar, L. E. R. Oleary and J. D. Hartgerink, *J. Am. Chem. Soc.*, 2014, **136**, 14417–14424.

522 F. Xu, L. Zhang, R. L. Koder and V. Nanda, *Biochemistry*, 2010, **49**, 2307–2316.

523 C. Byrne, P. A. McEwan, J. Emsley, P. M. Fischer and W. C. Chan, *Chem. Commun.*, 2011, **47**, 2589–2591.

524 L. T. Lebruin, S. Banerjee, B. D. O'Rourke and M. A. Case, *Biopolymers*, 2011, **95**, 792–800.

525 Y. Li, X. Mo, D. Kim and S. M. Yu, *Biopolymers*, 2011, **95**, 94–104.

526 S. W. Chang, S. J. Shefelbine and M. J. Buehler, *Biophys. J.*, 2012, **102**, 640–648.

527 A. S. Parmar, S. Zahid, S. V. Belure, R. Young, N. Hasan and V. Nanda, *J. Struct. Biol.*, 2014, **185**, 163–167.

528 V. Gauba and J. D. Hartgerink, *J. Am. Chem. Soc.*, 2007, **129**, 15034–15041.

529 A. A. Jalan, K. A. Jochim and J. D. Hartgerink, *J. Am. Chem. Soc.*, 2014, **136**, 7535–7538.

530 J. A. Hodges and R. T. Raines, *J. Am. Chem. Soc.*, 2005, **127**, 15923–15932.

531 V. Gauba and J. D. Hartgerink, *J. Am. Chem. Soc.*, 2007, **129**, 2683–2690.

532 V. Gauba and J. D. Hartgerink, *J. Am. Chem. Soc.*, 2008, **130**, 7509–7515.

533 J. A. Fallas, V. Gauba and J. D. Hartgerink, *J. Biol. Chem.*, 2009, **284**, 26851–26859.

534 L. E. Russell, J. A. Fallas and J. D. Hartgerink, *J. Am. Chem. Soc.*, 2010, **132**, 3242–3243.

535 L. E. R. Oleary, J. A. Fallas and J. D. Hartgerink, *J. Am. Chem. Soc.*, 2011, **133**, 5432–5443.

536 J. A. Fallas, M. A. Lee, A. A. Jalan and J. D. Hartgerink, *J. Am. Chem. Soc.*, 2012, **134**, 1430–1433.

537 K. A. Clements, A. M. Acevedo-Jake, D. R. Walker and J. D. Hartgerink, *Biomacromolecules*, 2017, **18**, 617–624.

538 A. S. Parmar, J. K. James, D. R. Grisham, D. H. Pike and V. Nanda, *J. Am. Chem. Soc.*, 2016, **138**, 4362–4367.

539 F. Xu, J. Li, V. Jain, R. S. Tu, Q. Huang and V. Nanda, *J. Am. Chem. Soc.*, 2012, **134**, 47–50.

540 J. E. Donald, D. W. Kulp and W. F. DeGrado, *Proteins Struct. Funct. Bioinf.*, 2011, **79**, 898–915.

541 K. McGuinness, I. J. Khan and V. Nanda, *ACS Nano*, 2014, **8**, 12514–12523.

542 K. McGuinness and V. Nanda, *Org. Biomol. Chem.*, 2017, **15**, 5893–5898.

543 M. M. Pires, D. E. Przybyla, C. M. Rubert Pérez and J. Chmielewski, *J. Am. Chem. Soc.*, 2011, **133**, 14469–14471.

544 Z. Song, Z. Han, S. Lv, C. Chen, L. Chen, L. Yin and J. Cheng, *Chem. Soc. Rev.*, 2017, **46**, 6570–6599.

545 T. Saxena, L. Karumbaiah and C. M. Valmikinathan, in *Natural and Synthetic Biomedical Polymers*, Elsevier, San Diego, 2014, pp. 43–65.

546 A. Norouzy, K. I. Assaf, S. Zhang, M. H. Jacob and W. M. Nau, *J. Phys. Chem. B*, 2015, **119**, 33–43.

547 V. N. Uversky, *Int. J. Biochem. Cell Biol.*, 2011, **43**, 1090–1103.

548 A. Abedini and D. P. Raleigh, *Protein Eng. Des. Sel.*, 2009, **22**, 453–459.

549 G. H. Zerze, J. Mittal and R. B. Best, *Phys. Rev. Lett.*, 2016, **116**, 68102.

550 L. X. Chen, H. L. Strauss and R. G. Snyder, *Biophys. J.*, 1993, **64**, 1533–1541.

551 P. Urnes and P. Doty, *Adv. Protein Chem.*, 1962, **16**, 401–544.

552 P. K. Sarkar and P. Doty, *Proc. Natl. Acad. Sci.*, 1966, **55**, 981–989.

553 G. Holzwarth and P. Doty, *J. Am. Chem. Soc.*, 1965, **87**, 218–228.

554 C. Li, *Adv. Drug Deliv. Rev.*, 2002, **54**, 695–713.

555 A. Richard and A. Margaritis, *Crit. Rev. Biotechnol.*, 2001, **21**, 219–232.

556 H. Yuan, K. Luo, Y. Lai, Y. Pu, B. He, G. Wang, Y. Wu and Z. Gu, *Mol. Pharm.*, 2010, **7**, 953–962.

557 A. Ogunleye, V. U. Irorere, C. Williams, D. Hill, A. Bhat and I. Radecka, *Microbiology*, 2015, **161**, 1–17.

558 I. Bajaj and R. Singhal, *Bioresour. Technol.*, 2011, **102**, 5551–5561.

559 S. R. Lyu, Y. C. Kuo, H. F. Ku and W. H. Hsieh, *Colloids Surf. B*, 2013, **103**, 304–309.

560 W. Shen, in *Biomaterials for Tissue Engineering Applications*, Springer, Vienna, 2011, pp. 243–275.

561 L. Vidal, V. Thuault, A. Mangas, R. Coveñas, A. Thienpont and M. Geffard, *J. Amino Acids*, 2014, **2014**, 1–10.

562 K. S. Krannig and H. Schlaad, *J. Am. Chem. Soc.*, 2012, **134**, 18542–18545.

563 C. D. Vacogne, S. M. Brosnan, A. Masic and H. Schlaad, *Polym. Chem.*, 2015, **6**, 5040–5052.

564 C. D. Vacogne, M. Schopferer and H. Schlaad, *Biomacromolecules*, 2016, **17**, 2384–2391.

565 C. Cai, J. Lin, T. Chen, X.-S. Wang and S. Lin, *Chem. Commun.*, 2009, **0**, 2709–2711.

566 C. Cai, Y. Li, J. Lin, L. Wang, S. Lin, X.-S. Wang and T. Jiang, *Angew. Chemie Int. Ed.*, 2013, **52**, 7732–7736.

567 L. Zhang, V. Lipik and A. Miserez, *J. Mater. Chem. B*, 2016, **4**, 1544–1556.

568 C. J. Sun, A. Srivastava, J. R. Reifert and J. H. Waite, *J. Adhes.*, 2009, **85**, 126–138.

569 C. S. Wang and R. J. Stewart, *J. Exp. Biol.*, 2012, **215**, 351–361.

570 V. Lipik, L. Zhang and A. Miserez, *Polym. Chem.*, 2014, **5**, 1351–1361.

571 J. L. Whittaker, N. K. Dutta, R. Knott, G. McPhee, N. H. Voelcker, C. Elvin, A. Hill and N. R. Choudhury, *Langmuir*, 2015, **31**, 8882–8891.

572 L. E. Nita, A. P. Chiriac, M. Bercea, M. Asandulesa and B. A. Wolf, *Int. J. Biol. Macromol.*, 2017, **95**, 412–420.

573 N. Zhang, F. Zhao, Q. Zou, Y. Li, G. Ma and X. Yan, *Small*, 2016, **12**, 5936–5943.

574 L. Zhu, L. Zhao, X. Qu and Z. Yang, *Langmuir*, 2012, **28**, 11988–11996.

575 J. P. Dhandhukia, P. Shi, S. Peddi, Z. Li, S. Aluri, Y. Ju, D. Brill, W. Wang, S. M. Janib, Y. A. Lin, S. Liu, H. Cui and J. A. Mackay, *Bioconjug. Chem.*, 2017, **28**, 2715–2728.

576 L. Li and K. L. Kiick, *ACS Macro Lett.*, 2013, **2**, 635–640.

577 C. M. Elvin, A. G. Carr, M. G. Huson, J. M. Maxwell, R. D. Pearson, T. Vuocolo, N. E. Liyou, D. C. C. Wong, D. J. Merritt and N. E. Dixon, *Nature*, 2005, **437**, 999–1002.

578 N. K. Dutta, M. Y. Truong, S. Mayavan, N. Roy Choudhury, C. M. Elvin, M. Kim, R. Knott, K. M. Nairn and A. J. Hill, *Angew. Chemie - Int. Ed.*, 2011, **50**, 4428–4431.

579 A. A. Adzhubei, M. J. E. Sternberg and A. A. Makarov, *J. Mol. Biol.*, 2013, **425**, 2100–2132.

580 L.-D. Koh, Y. Cheng, C.-P. Teng, Y.-W. Khin, X.-J. Loh, S.-Y. Tee, M. Low, E. Ye, H.-D. Yu, Y.-W. Zhang and M.-Y. Han, *Prog. Polym. Sci.*, 2015, **46**, 86–110.

581 J. P. Celli, B. Q. Spring, I. Rizvi, C. L. Evans, K. S. Samkoe, S. Verma, B. W. Pogue and T. Hasan, *Chem. Rev.*, 2010, **110**, 2795–2838.

582 G. Stehle, H. Sinn, A. Wunder, H. H. Schrenk, J. C. M. Stewart, G. Hartung, W. Maier-Borst and D. L. Heene, *Crit. Rev. Oncol. Hematol.*, 1997, **26**, 77–100.

583 I. F. Uchegbu, S. Anderson, A. Brownlie and X. Qu, in *Lipsome Technology: Liposome Preparation and Related Techniques*, CRC Press, New York, 2006, pp. 197–208.

584 S. Kessel, A. Thomas and H. G. Börner, *Angew. Chemie Int. Ed.*, 2007, **46**, 9023–9026.

585 N. Dube, A. D. Presley, J. Y. Shu and T. Xu, *Macromol. Rapid Commun.*, 2011, **32**, 344–

353.

586 K. Matsuura, *Trends Glycosci. Glycotechnol.*, 2013, **25**, 227–239.

587 C. Deng, J. Wu, R. Cheng, F. Meng, H.-A. Klok and Z. Zhong, *Prog. Polym. Sci.*, 2014, **39**, 330–364.

588 P. Sukthankar, S. K. Whitaker, M. Garcia, A. Herrera, M. Boatwright, O. Prakash and J. M. Tomich, *Langmuir*, 2015, **31**, 2946–2955.

589 P. Wilson, *Macromol. Chem. Phys.*, 2017, **218**, 1600595.

590 X. Yan and H. Möhwald, *Biomacromolecules*, 2017, **18**, 3469–3470.

591 A. Parisi-Amon, D. D. Lo, D. T. Montoro, R. E. Dewi, M. T. Longaker and S. C. Heilshorn, *ACS Biomater. Sci. Eng.*, 2017, **3**, 750–756.

592 Y. Zhou, B. Li, S. Li, H. A. M. Ardoña, W. L. Wilson, J. D. Tovar and C. M. Schroeder, *ACS Cent. Sci.*, 2017, **3**, 986–994.

593 V. Marchán, L. Debéthune, E. Pedroso and A. Grandas, *Tetrahedron*, 2004, **60**, 5461–5469.

594 C. Lou, N. J. Christensen, M. C. Martos-Maldonado, S. R. Midtgaard, M. Ejlersen, P. W. Thulstrup, K. K. Sørensen, K. J. Jensen and J. Wengel, *Chem. - Eur. J.*, 2017, **23**, 9297–9305.

595 M. O. Guler, J. K. Pokorski, D. H. Appella and S. I. Stupp, *Bioconjug. Chem.*, 2005, **16**, 501–503.

596 N. Gour, D. Kedracki, I. Safir, K. X. Ngo and C. Vebert-Nardin, *Chem. Commun.*, 2012,

**48**, 5440–5442.

597 J. H. Kang, G. Battogtokh and Y. T. Ko, *Biomacromolecules*, 2017, **18**, 3733–3741.

598 K. Ikeda, A. Horiuchi, A. Egawa, H. Tamaki, T. Fujiwara and M. Nakano, *ACS Omega*, 2017, **2**, 2935–2944.

599 J. Borges, M. P. Sousa, G. Cinar, S. G. Caridade, M. O. Guler and J. F. Mano, *Adv. Funct. Mater.*, 2017, **27**, 1605122.

600 Y. Lim, S. Park, E. Lee, H. Jeong, J.-H. Ryu, M. S. Lee and M. Lee, *Biomacromolecules*, 2007, **8**, 1404–1408.

601 T. Pierce, A. White, G. Tregear and P. Sexton, *Mini-Reviews Med. Chem.*, 2005, **5**, 41–55.

602 S. Bulut, T. S. Erkal, S. Toksoz, A. B. Tekinay, T. Tekinay and M. O. Guler, *Biomacromolecules*, 2011, **12**, 3007–3014.

603 J. H. Jeong, S. W. Kim and T. G. Park, *Bioconjug. Chem.*, 2003, **14**, 473–479.

604 J. Fabre and L. Collins, *Curr. Gene Ther.*, 2006, **6**, 459–480.

605 R. M. Capito, H. S. Azevedo, Y. S. Velichko, A. Mata and S. I. Stupp, *Science*, 2008, **319**, 1812–1816.

606 D. Carvajal, R. Bitton, J. R. Mantei, Y. S. Velichko, S. I. Stupp and K. R. Shull, *Soft Matter*, 2010, **6**, 1816–1823.

607 S. S. Santos, R. V. Gonzaga, J. V. Silva, D. F. Savino, D. Prieto, J. M. Shikay, R. S. Silva, L. H. A. Paulo, E. I. Ferreira and J. Giarolla, *Can. J. Chem.*, 2017, **95**, 907–916.

608 C. Ding and Z. Li, *Mater. Sci. Eng. C*, 2017, **76**, 1440–1453.

609 K. C. F. Leung, H. P. Ho, Y. W. Kwan and S. K. Kong, *Expert Rev. Mol. Diagn.*, 2010, **10**, 863–867.

610 L. Baltzer, in *Creative Chemical Sensor Systems*, Springer, Berlin, 2007, pp. 89–106.

611 B. Albada and N. Metzler-Nolte, *Acc. Chem. Res.*, 2017, **50**, 2510–2518.

612 M. Taskova, C. S. Madsen, K. J. Jensen, L. H. Hansen, B. Vester and K. Astakhova, *Bioconjug. Chem.*, 2017, **28**, 768–774.

613 T. C. Roberts, K. Ezzat, S. EL Andaloussi and M. S. Weinberg, in *Methods in Molecular Biology*, Springer, New York, 2016, pp. 291–310.

614 C. Scholz and E. Wagner, *J. Control. Release*, 2012, **161**, 554–565.

615 K. Gavrilov and W. M. Saltzman, *Yale J. Biol. Med.*, 2012, **85**, 187–200.

616 R. Ni and Y. Chau, *J. Am. Chem. Soc.*, 2014, **136**, 17902–17905.

617 T. Jiang, T. A. Meyer, C. Modlin, X. Zuo, V. P. Conticello and Y. Ke, *J. Am. Chem. Soc.*, 2017, **139**, 14025–14028.

618 S. H. Lee, Y. Y. Kang, H.-E. Jang and H. Mok, *Adv. Drug Deliv. Rev.*, 2016, **104**, 78–92.

619 T. Lehto, K. Ezzat, M. J. A. Wood and S. EL Andaloussi, *Adv. Drug Deliv. Rev.*, 2016, **106**, 172–182.

620 W. Tai and X. Gao, *Adv. Drug Deliv. Rev.*, 2017, **110–111**, 157–168.

621 H. Zeng, M. E. Johnson, N. J. Oldenhuis, T. N. Tiambeng and Z. Guan, *ACS Cent. Sci.*, 2015, **1**, 303–312.

622 D. Mumcuoglu, M. Sardan, T. Tekinay, M. O. Guler and A. B. Tekinay, *Mol. Pharm.*,

2015, **12**, 1584–1591.

623 D. Mumcuoglu, M. Sardan Ekiz, G. Gunay, T. Tekinay, A. B. Tekinay and M. O. Guler, *ACS Appl. Mater. Interfaces*, 2016, **8**, 11280–11287.

624 L. H. Tostanoski, Y.-C. Chiu, J. I. Andorko, M. Guo, X. Zeng, P. Zhang, W. Royal and C. M. Jewell, *ACS Nano*, 2016, **10**, 9334–9345.

625 Z. Tai, X. Wang, J. Tian, Y. Gao, L. Zhang, C. Yao, X. Wu, W. Zhang, Q. Zhu and S. Gao, *Biomacromolecules*, 2015, **16**, 1119–1130.

626 L. Crombez, G. Aldrian-Herrada, K. Konate, Q. N. Nguyen, G. K. McMaster, R. Brasseur, F. Heitz and G. Divita, *Mol. Ther.*, 2009, **17**, 95–103.

627 R. H. Mo, J. L. Zaro and W.-C. Shen, *Mol. Pharm.*, 2012, **9**, 299–309.

628 T. Asai, T. Tsuzuku, S. Takahashi, A. Okamoto, T. Dewa, M. Nango, K. Hyodo, H. Ishihara, H. Kikuchi and N. Oku, *Biochem. Biophys. Res. Commun.*, 2014, **444**, 599–604.

629 K. Tanaka, T. Kanazawa, S. Horiuchi, T. Ando, K. Sugawara, Y. Takashima, Y. Seta and H. Okada, *Int. J. Pharm.*, 2013, **455**, 40–47.

630 W. Xu, R. Pan, D. Zhao, D. Chu, Y. Wu, R. Wang, B. Chen, Y. Ding, P. Sadatmousavi, Y. Yuan and P. Chen, *Mol. Pharm.*, 2015, **12**, 56–65.

631 K. Tanaka, T. Kanazawa, T. Ogawa, Y. Takashima, T. Fukuda and H. Okada, *Int. J. Pharm.*, 2010, **398**, 219–224.

632 R. Pan, W. Xu, F. Yuan, D. Chu, Y. Ding, B. Chen, M. Jafari, Y. Yuan and P. Chen, *Acta Biomater.*, 2015, **21**, 74–84.

633 F. Simeoni, *Nucleic Acids Res.*, 2003, **31**, 2717–2724.

634 P. Arukuusk, L. Pärnaste, N. Oskolkov, D.-M. Copolovici, H. Margus, K. Padari, K. Möll, J. Maslovskaja, R. Tegova, G. Kivi, A. Tover, M. Pooga, M. Ustav and Ü. Langel, *Biochim. Biophys. Acta - Biomembr.*, 2013, **1828**, 1365–1373.

635 S. EL Andaloussi, T. Lehto, I. Mäger, K. Rosenthal-Aizman, I. I. Oprea, O. E. Simonson, H. Sork, K. Ezzat, D. M. Copolovici, K. Kurrikoff, J. R. Viola, E. M. Zaghloul, R. Sillard, H. J. Johansson, F. Said Hassane, P. Guterstam, J. Suhorutšenko, P. M. D. Moreno, N. Oskolkov, J. Hälldin, U. Tedebark, A. Metspalu, B. Lebleu, J. Lehtiö, C. I. E. Smith and Ü. Langel, *Nucleic Acids Res.*, 2011, **39**, 3972–3987.

636 K. Ezzat, S. EL Andaloussi, E. M. Zaghloul, T. Lehto, S. Lindberg, P. M. D. Moreno, J. R. Viola, T. Magdy, R. Abdo, P. Guterstam, R. Sillard, S. M. Hammond, M. J. A. Wood, A. A. Arzumanov, M. J. Gait, C. I. E. Smith, M. Hällbrink and Ü. Langel, *Nucleic Acids Res.*, 2011, **39**, 5284–5298.

637 H. Wang, W. Chen, H. Xie, X. Wei, S. Yin, L. Zhou, X. Xu and S. Zheng, *Chem. Commun.*, 2014, **50**, 7806–7809.

638 I. Nakase, G. Tanaka and S. Futaki, *Mol. Biosyst.*, 2013, **9**, 855–861.

639 H. Margus, K. Padari and M. Pooga, *Mol. Ther.*, 2012, **20**, 525–533.

640 A. Vaissière, G. Aldrian, K. Konate, M. F. Lindberg, C. Jourdan, A. Telmar, Q. Seisel, F. Fernandez, V. Viguier, C. Genevois, F. Couillaud, P. Boisguerin and S. Deshayes, *J. Nanobiotechnology*, 2017, **15**, 34–51.

641 M. Alkotaji, A. Pluen, E. Zindy, Z. Hamrang and H. Aojula, *J. Pharm. Sci.*, 2014, **103**,

293–304.

642 J. J. Welch, R. J. Swanekamp, C. King, D. A. Dean and B. L. Nilsson, *ACS Med. Chem. Lett.*, 2016, **7**, 584–589.

643 S. J. Sigg, V. Postupalenko, J. T. Duskey, C. G. Palivan and W. Meier, *Biomacromolecules*, 2016, **17**, 935–945.

644 Y. Lim, E. Lee and M. Lee, *Angew. Chemie Int. Ed.*, 2007, **46**, 3475–3478.

645 Y. Lim, E. Lee, Y.-R. Yoon, M. S. Lee and M. Lee, *Angew. Chemie Int. Ed.*, 2008, **47**, 4525–4528.

646 S. Han, D. Kim, S. Han, N. H. Kim, S. H. Kim and Y. Lim, *J. Am. Chem. Soc.*, 2012, **134**, 16047–16053.

647 D. Xu, D. Dustin, L. Jiang, D. S. K. Samways and H. Dong, *Chem. Commun.*, 2015, **51**, 11757–11760.

648 M. L. Macheda, S. Rogers and J. D. Best, *J. Cell. Physiol.*, 2005, **202**, 654–662.

649 B. Dalby, *Methods*, 2004, **33**, 95–103.

650 B. Weisblum and E. Haenssler, *Chromosoma*, 1974, **46**, 255–260.

651 C. J. Bowerman and B. L. Nilsson, *J. Am. Chem. Soc.*, 2010, **132**, 9526–9527.

652 T. B. Schuster, D. de Bruyn Ouboter, C. G. Palivan and W. Meier, *Langmuir*, 2011, **27**, 4578–4584.

653 T. B. Schuster, D. de Bruyn Ouboter, E. Bordignon, G. Jeschke and W. Meier, *Soft Matter*, 2010, **6**, 5596–5604.

654 D. de Bruyn Ouboter, T. B. Schuster, S. J. Sigg and W. P. Meier, *Colloids Surf. B*, 2013, **112**, 542–547.

655 A. P. Malefyt, S. P. Walton and C. Chan, *Nano Life*, 2012, **2**, 1241005.

656 R. Ni and Y. Chau, *Angew. Chemie Int. Ed.*, 2017, **56**, 9356–9360.

657 T. Ji, J. Lang, J. Wang, R. Cai, Y. Zhang, F. Qi, L. Zhang, X. Zhao, W. Wu, J. Hao, Z. Qin, Y. Zhao and G. Nie, *ACS Nano*, 2017, **11**, 8668–8678.

658 C. Huang, H. Jin, Y. Qian, S. Qi, H. Luo, Q. Luo and Z. Zhang, *ACS Nano*, 2013, **7**, 5791–5800.

659 S. R. Midtgaard, M. C. Pedersen, J. J. K. Kirkensgaard, K. K. Sørensen, K. Mortensen, K. J. Jensen and L. Arleth, *Soft Matter*, 2014, **10**, 738–752.

660 H. Raghuraman and A. Chattopadhyay, *Biosci. Rep.*, 2007, **27**, 189–223.

661 Z. Zhang, W. Cao, H. Jin, J. Lovell, M. Yang, L. Ding, J. Chen, I. Corbin, Q. Luo and G. Zheng, *Angew. Chemie Int. Ed.*, 2009, **48**, 9171–9175.

662 Y. Jiao, X. Pang and G. Zhai, *Curr. Drug Targets*, 2016, **17**, 720–730.

663 L. K. Widjaja, M. Bora, P. N. P. H. Chan, V. Lipik, T. T. L. Wong and S. S. Venkatraman, *J. Biomed. Mater. Res. Part A*, 2014, **102**, 3056–3065.

664 F. Dosio, S. Arpicco, B. Stella and E. Fattal, *Adv. Drug Deliv. Rev.*, 2016, **97**, 204–236.

665 D. Huang, Y.-S. Chen and I. D. Rupenthal, *Mol. Pharm.*, 2017, **14**, 533–545.

666 H. V. Danesh-Meyer, J. Zhang, M. L. Acosta, I. D. Rupenthal and C. R. Green, *Prog. Retin. Eye Res.*, 2016, **51**, 41–68.

667 H. Ponta, L. Sherman and P. A. Herrlich, *Nat. Rev. Mol. Cell Biol.*, 2003, **4**, 33–45.

668 Y.-S. Chen, I. Toth, H. V. Danesh-Meyer, C. R. Green and I. D. Rupenthal, *J. Pharm. Sci.*, 2013, **102**, 2322–2331.

669 R. D. Jager, L. P. Aiello, S. C. Patel and E. T. Cunningham, *Retina*, 2004, **24**, 676–698.

670 D. Choi, H. Lee, H. B. Kim, M. Yang, J. Heo, Y. Won, S. S. Jang, J. K. Park, Y. Son, T. I. Oh, E. Lee and J. Hong, *Chem. Mater.*, 2017, **29**, 2055–2065.

671 M. S. Shive, M. L. Salloum and J. M. Anderson, *Proc. Natl. Acad. Sci.*, 2000, **97**, 6710–6715.

672 Y. Kim, Y.-S. Lee, J. Choe, H. Lee, Y.-M. Kim and D. Jeoung, *J. Biol. Chem.*, 2008, **283**, 22513–22528.

673 K. J. M. Bishop, C. E. Wilmer, S. Soh and B. A. Grzybowski, *Small*, 2009, **5**, 1600–1630.

674 K. Ariga, J. P. Hill, M. V. Lee, A. Vinu, R. Charvet and S. Acharya, *Sci. Technol. Adv. Mater.*, 2008, **9**, 14109.

675 J. Boekhoven, R. H. Zha, F. Tantakitti, E. Zhuang, R. Zandi, C. J. Newcomb and S. I. Stupp, *RSC Adv.*, 2015, **5**, 8753–8756.

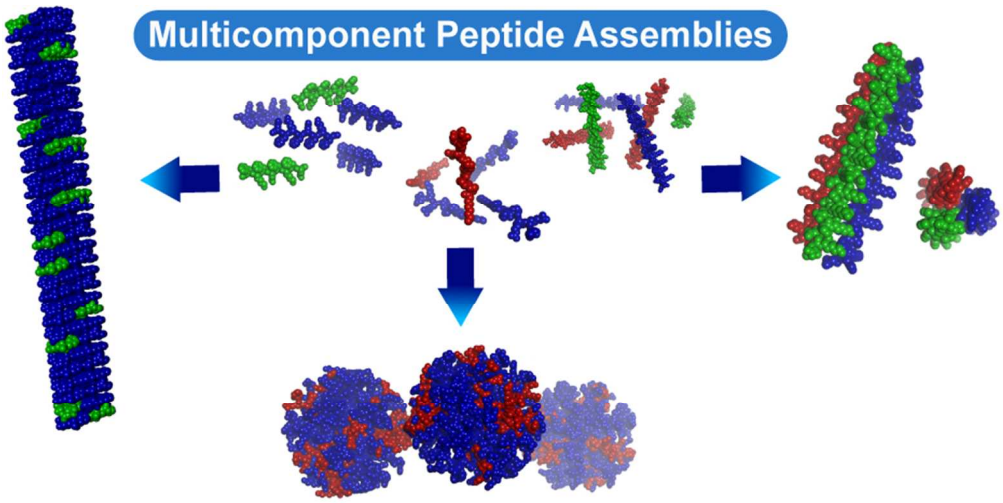


78x39mm (300 x 300 DPI)

# Multicomponent Peptide Assemblies

*Danielle M. Raymond and Bradley L. Nilsson**

Department of Chemistry, University of Rochester, Rochester, NY, 14627-0216, USA.

E-mail: nilsson@chem.rochester.edu

Fax: +1 585 276-0205; Tel. +1 585 276-3053

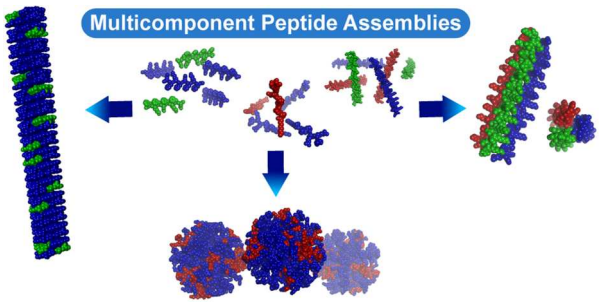


This review presents recent efforts in the development of multicomponent supramolecular peptide assemblies with a focus on multicomponent assemblies derived from $\beta$-sheet peptides, low molecular weight peptides, peptide amphiphiles, coiled coil peptides, collagen, and related systems.